

LABORATORY INVESTIGATION OF SHEAR BEHAVIOR OF ROCK
DISCONTINUITIES BASED ON SHEAR RATE, SIZE AND ROUGHNESS
CHARACTERISTICS

A THESIS SUBMITTED TO
THE GRADUATE SCHOOL OF NATURAL AND APPLIED SCIENCES
OF
MIDDLE EAST TECHNICAL UNIVERSITY

BY

ERGİN İŞLEYEN

IN PARTIAL FULFILLMENT OF THE REQUIREMENTS
FOR
THE DEGREE OF MASTER OF SCIENCE
IN
MINING ENGINEERING

SEPTEMBER 2017

Approval of the thesis:

**LABORATORY INVESTIGATION OF SHEAR BEHAVIOR OF ROCK
DISCONTINUITIES BASED ON SHEAR RATE, SIZE AND ROUGHNESS
CHARACTERISTICS**

submitted by **ERGİN İŞLEYEN** in partial fulfillment of the requirements for the degree of **Master of Science in Mining Engineering Department, Middle East Technical University** by,

Prof. Dr. Gülbin Dural Ünver
Dean, Graduate School of **Natural and Applied Sciences** _____

Prof. Dr. Celal Karpuz
Head of Department, **Mining Engineering Department** _____

Prof. Dr. H. Şebnem Düzgün
Supervisor, **Mining Engineering Department, METU** _____

Examining Committee Members:

Prof. Dr. Candan Gökçeoğlu
Geological Engineering Department, Hacettepe University _____

Prof. Dr. H. Şebnem Düzgün
Mining Engineering Department, METU _____

Prof. Dr. Bahtiyar Ünver
Mining Engineering Department, Hacettepe University _____

Assoc. Prof. Dr. Mehmet Ali Hindistan
Mining Engineering Department, Hacettepe University _____

Assist. Prof. Dr. Nejan Huvaj Sarıhan
Civil Engineering Department, METU _____

Date: 05/09/2017

I hereby declare that all information in this document has been obtained and presented in accordance with academic rules and ethical conduct. I also declare that, as required by these rules and conduct, I have fully cited and referenced all material and results that are not original to this work.

Name, Last Name :Ergin İşleyen

Signature :

ABSTRACT

LABORATORY INVESTIGATION OF SHEAR BEHAVIOR OF ROCK DISCONTINUITIES BASED ON SHEAR RATE, SIZE AND ROUGHNESS CHARACTERISTICS

İşleyen, Ergin

M.S., Department of Mining Engineering

Supervisor: Prof. Dr. H. Şebnem Düzgün

September 2017, 190 pages

Rock mass characteristics are significantly influenced by the presence of discontinuities. In order to develop safe rock engineering designs, factors affecting shear behavior of rock discontinuities should be carefully analyzed. In this study, effects of shear rate, sample size, roughness characteristics and co-dependency of these effects are investigated on rock discontinuity sample replicas.

3D models of the rock discontinuities are generated with close-range digital photogrammetry. Then, discontinuity models are obtained with a 3D printer, to be used as a mould to produce concrete discontinuity sample replicas for direct shear test. The suggested rock discontinuity sample replication methodology in the literature is adopted and found to be successful with accurate representation of intended roughness level of the sample.

The direct shear tests are conducted under three different constant normal load conditions with three different shear rates on two different sample sizes. The roughness degree of the samples are measured in terms of Z_2 , and it changes between 0.115 – 0.420.

Experimental results indicated that, shear strength increases with increasing degree of roughness. Moreover, it's revealed that effect of shear rate is a normal stress dependent property and it differs for high and low normal stress levels. Investigation of sample size effect showed contradictory results with the previous studies in the literature. It is observed that the shear strength of the small size samples is lower than the shear strength of the larger samples, even though the roughness is higher in the small samples. In addition, it's revealed that the shear rate effect is co-dependent with the effect of the roughness and the effect of sample size. The shear rate effect becomes greater as the roughness degree decreases and the sample size decreases.

Keywords: Rock discontinuity, Roughness effect, Shear rate effect, Sample size effect.

ÖZ

KAYA SÜREKSİZLİKLERİNİN MAKASLAMA DAVRANIŞLARININ MAKASLAMA HIZI, BOYUT VE PÜRÜZLÜLÜK KARAKTERİSTİKLERİNE DAYALI LABORATUVAR İNCELEMESİ

İşleyen, Ergin

Yüksek Lisans, Maden Mühendisliği Bölümü

Tez Yöneticisi: Prof. Dr. H. Şebnem Düzgün

Eylül 2017, 190 sayfa

Kaya kütlelerinin özellikleri süreksizliklerin varlığından önemli ölçüde etkilenir. Güvenilir kaya yapıları tasarlayabilmek için, kaya süreksizliklerinin davranışlarını etkileyen faktörler dikkatle analiz edilmelidir. Bu çalışmada, kaya süreksizliklerinin davranışları üzerindeki pürüzlülük, makaslama hızı, numune boyutu etkileri ve bu etkilerin birbiri üzerindeki bağımlılığı araştırılmıştır.

Kaya süreksizliklerinin 3 boyutlu modelleri yakın mesafe dijital fotogrametri yöntemiyle üretilmiştir. Ardından, süreksizlik modelleri 3B yazıcı ile elde edilip, doğrudan kesme deneylerinde kullanılacak beton numuneleri üretmek amacıyla kalıp olarak kullanılmıştır. Literatürde önerilen kaya süreksizliği numunesi replikasyon metodolojisinin başarısı, numune üzerindeki pürüzlülüğün hedeflenen düzeye yakın oluşunun gösterilmesiyle kanıtlanmıştır.

Doğrudan kesme deneyleri, üç farklı sabit normal yük durumu altında, üç farklı makaslama hızı ile, iki farklı numune boyutunda yapılmıştır. Numuneler pürüzlülük dereceleri Z_2 parametresi cinsinden belirlenmiş olup, 0,115 – 0,420 aralığında değişmektedir.

Deney sonuçları, beklendiği gibi, makaslama dayanımının pürüzlülük derecesi ile birlikte arttığını göstermektedir. Ayrıca, makaslama hızı etkisinin, normal yüke bağlı bir özellik olduğu ve etkinin yüksek ve alçak normal yük seviyelerinde farklılık gösterdiği belirlenmiştir. Buna ek olarak, numune boyutu etkisinin incelenmesi, literatürde daha önce karşılaşılmamış sonuçlar göstermiştir. Küçük boyutlu numunelerin pürüzlülük seviyeleri daha yüksek olmasına rağmen, makaslama dayanımları, büyük boyutlu numunelerin makaslama dayanımlarından düşüktür. Bunların yanı sıra, makaslama hızı etkisinin, pürüzlülük derecesi ve numune boyutu ile birbirine bağımlı olduğu tespit edilmiştir. Makaslama hızının etkisi, pürüzlülük seviyesi azaldıkça ve numune boyutu azaldıkça, artmaktadır.

Anahtar Kelimeler: Kaya süreksizliği, Pürüzlülük etkisi, Makaslama hızı etkisi, Numune boyutu etkisi.

ACKNOWLEDGEMENTS

I would like to express my profound gratitude to my supervisor, Prof. Dr. Şebnem Düzgün for her invaluable guidance, kind attitude, support, criticism and trust. It's been an honor and a privilege working with her. Also, I'd like to thank to jury members, Prof. Dr. Candan Gökçeoğlu, Prof. Dr. Bahtiyar Ünver, Assoc. Prof. Dr. Mehmet Ali Hindistan and Asst. Prof. Dr. Nejan Huvaj Sarihan, for their contributions.

I wish to thank Tahsin Işıksal, Hakan Uysal and my colleague, Res. Asst. Ahmet Güneş Yardımcı for their helps during laboratory studies of this research.

I would also like to thank my officemate Öznur Önel for her continuing friendship.

I owe my sincere gratitude to my parents, Hacer İşleyen and Adnan İşleyen and my brother, Engin İşleyen for their unconditional love and encouragement at all stages of my life.

Finally, my heartfelt thanks goes to Özge Akçay. Her endless love, understanding and supportive attitude made it possible for me to overcome every difficulty. Thank you for being a source of inspiration.

TABLE OF CONTENTS

ABSTRACT.....	v
ÖZ.....	vii
ACKNOWLEDGEMENTS.....	ix
TABLE OF CONTENT.....	x
LIST OF TABLES.....	xii
LIST OF FIGURES.....	xiii
CHAPTERS	
1.INTRODUCTION.....	1
1.1.Problem Statement.....	3
1.2.Objectives of the Study.....	4
1.3.Organisation of the Thesis.....	4
2.OVERVIEW OF THE FACTORS AFFECTING THE SHEAR BEHAVIOR OF ROCK DISCONTINUITIES.....	7
2.1. Effect of Roughness.....	7
2.2.Effect of Shear Rate.....	12
2.3. Effect of Sample Size.....	15
3. RESEARCH METHODOLOGY.....	19
4.3D MODELING OF DISCONTINUITY SURFACES WITH CLOSE-RANGE DIGITAL PHOTOGRAMMETRY.....	23
4.1.Overview of Photogrammetry of Discontinuity Surface Modeling.....	23
4.2.Photogrammetric Analysis of Rock Discontinuity Samples.....	25
4.3.Preparation of Rock Discontinuity Replicas.....	34

5.3D PRINTING AND ROUGHNESS MEASUREMENT OF ROCK DISCONTINUITY REPLICAS.....	37
5.1.Overview of 3D Printing Applications in Rock Mechanics.....	37
5.2. 3D Printing of Rock Discontinuity Surface Replicas	39
5.3. Dilation Angle of Rock Discontinuity Replicas.....	41
5.4. Roughness Characterization of the 3D Models of Discontinuity Surfaces.....	44
5.5. Roughness Characterization of the PLA Moulds and the Concrete Samples .	53
6.THE EXPERIMENTAL SETUP	61
6.1.The Sample Preparation	62
6.2. Direct Shear Test of the Specimens	70
6.3. Investigation of Material Properties for the Replicas	73
6.3.1. Uniaxial Compressive Strength Tests	74
6.3.2.Indirect Tensile Strength Tests (Brazilian Tests).....	77
6.3.3. The Joint Wall Compressive Strength (JCS)	78
7.RESULTS AND DISCUSSIONS	83
7.1.Results of Rock Discontinuity Replica Production Methodology	83
7.2.Direct Shear Test Results	85
7.3.Discussion of Co-Dependency of Roughness and Shear Rate on Shear Strength	115
7.4.Discussion of Co-dependency of Sample Size and Shear Rate on Shear Strength	124
7.5.Comparion of the Results and the Findings of the Previous Studies	135
8.CONCLUSION AND RECOMMENDATIONS.....	139
REFERENCES.....	145
APPENDICES	153
A. PHOTOGRAPHS OF THE SPECIMENS AFTER THE EXPERIMENTS...	153
B. ORIGINAL PLOTS OF THE TEST RESULTS.....	181

LIST OF TABLES

TABLES

Table 5.1. Descriptive statistics of dilation angles for Discontinuity A	43
Table 5.2. Descriptive statistics of dilation angle for Discontinuity B	44
Table 5.3. Z_2 and JRC values of Discontinuity A &B	52
Table 5.4. Z_2 and JRC values of small size samples of Discontinuity B.....	52
Table 5.5. Z_2 and JRC values of PLA moulds of Discontinuities A and B.....	58
Table 5.6. Z_2 and JRC values of concrete samples of Discontinuities A and B	58
Table 5.7. Z_2 and JRC values of PLA moulds of Discontinuities B10-1, B10-2, B10-3, B10-4.....	59
Table 5.8. Z_2 and JRC values of concrete samples of Discontinuities B10-1, B10-2, B10-3, B10-4.....	60
Table 6.1. Experiment list	71
Table 6.2. Properties of UCS & Brazilian Test Samples	74
Table 6.3. UCS test results	76
Table 6.4. Brazilian Test Results	78
Table 6.5. Joint wall compressive strengths (JCS).....	81
Table 7.1. Z_2 parameters of the models.....	84
Table 7.2. Experimental results.....	104
Table 7.3. Friction angles and cohesions	115
Table 7.4. Results of Previous Studies.....	137

LIST OF FIGURES

FIGURES

Figure 2.1. Standard roughness profiles proposed by Barton & Choubey (1977).....	9
Figure 2.2. Shear behavior with different specimen sizes, Bandis (1979).....	16
Figure 3.1. Flowchart of the proposed methodology	20
Figure 4.1: Rock discontinuity specimens A and B.....	25
Figure 4.2. Four of the eight fixed points marked on specimen B.....	26
Figure 4.3. Photogrammetric processing workflow	26
Figure 4.4. The masked areas and the markers	27
Figure 4.5. Sparse point clouds of specimens; (a) specimen A, (b) specimen B.....	28
Figure 4.6. Dense clouds of specimens; (a) specimen A, (b) specimen B.....	30
Figure 4.7. Digital elevation models of specimens; (a) specimen A, (b) specimen B.....	31
Figure 4.8. 3D models of specimens; (a) specimen A, (b) specimen B.....	32
Figure 4.9. Exported 3D models (STL); (a) specimen A, (b) specimen B	33
Figure 4.10. Modelled parts of the rock joint samples.....	34
Figure 4.11. Replicated rock discontinuity surface models; (a) discontinuity A, (b) discontinuity B	35
Figure 5.1. Fused deposition modelling (FDM) method in 3D printing.....	39
Figure 5.2. 3D printed rock discontinuity surface replicas	40
Figure 5.3. Dilation angle (i).....	41
Figure 5.4. Position of crosssections along the discontinuity replicas (plan view).....	41
Figure 5.5. Angle measurement at SketchUp using protractor tool.....	42
Figure 5.6. Workflow of Z_2 and JRC determination.....	45
Figure 5.8. TIN of Discontinuity A.....	47
Figure 5.9. TIN of Discontinuity B.....	47
Figure 5.10. TIN of small size samples of Discontinuity B.....	48
Figure 5.11. Digital Elevation Model of Discontinuity A	49
Figure 5.12. Digital Elevation Model of Discontinuity B.....	49
Figure 5.13. DEM of small size samples of Discontinuity B.....	50

Figure 5.14. Profile Locations on Digital Elevation Models	51
Figure 5.15. The dense clouds, (a): The PLA of Discontinuity A, (b): The concrete sample of Discontinuity A, (c): The PLA of Discontinuity B, (d): The concrete sample of Discontinuity B	53
Figure 5.16. The DEM of the Discontinuity A,(a):PLA mould,(b):Concrete test sample	54
Figure 5.17: The DEM of the Discontinuity B, (a): PLA mould, (b) Concrete test sample.....	55
Figure 5.18. The DEM's for the PLA moulds, (a): B10-1, (b): B10-2, (c): B10-3, (d): B10-4.....	56
Figure 5.19. The DEM's for the concrete test samples, (a): B10-1, (b): B10-2, (c): B10-3, (d): B10-4	57
Figure 6.1. Arrangement of a direct shear test equipment	62
Figure 6.2. Concrete mould casting procedure	63
Figure 6.3. Concrete sample casting procedure	65
Figure 6.4. Casting 10 cm x 10 cm size specimens.....	66
Figure 6.5. A20 sample (Before the experiment).....	67
Figure 6.6. B20 sample (Before the experiment).....	67
Figure 6.7. B10-1 sample (Before the experiment).....	68
Figure 6.8. B10-2 sample (Before the experiment).....	68
Figure 6.9. B10-3 sample (Before the experiment).....	69
Figure 6.10. B10-4 sample (Before the experiment).....	69
Figure 6.11: Direct Shear Test Equipment.....	70
Figure 6.12: Coring	73
Figure 6.13. Test samples;(A)Uniaxial compressive strength test,(B)Brazilian test .	74
Figure 6.14. Specimens after the UCS test.....	75
Figure 6.15. UCS test specimens after the test.....	75
Figure 6.16. Axial stress- axial strain curves	76
Figure 6.17. Brazilian test	77
Figure 6.18. Brazilian test specimens after the test.....	78
Figure 6.19. Application of schmidt hammer	79
Figure 6.20. Correlation chart for schmidt hammer.....	80

Figure 7.1. Evolution of Z_2 values	84
Figure 7.2. Test results (A20, $V=10 \times 10^{-4}$ mm/sec).....	85
Figure 7.3. Test results (B20, $V=10 \times 10^{-4}$ mm/sec).....	86
Figure 7.4. Test results (A20, $V=7.5 \times 10^{-4}$ mm/sec).....	87
Figure 7.5. Test results (B20, $V=7.5 \times 10^{-4}$ mm/sec).....	87
Figure 7.6. Test results (A20, $V=5 \times 10^{-4}$ mm/sec).....	88
Figure 7.7. Test results (B20, $V=5 \times 10^{-4}$ mm/sec).....	88
Figure 7.8. Test results (B10-1, $V=10 \times 10^{-4}$ mm/sec)	89
Figure 7.9. Test results (B10-2, $V=10 \times 10^{-4}$ mm/sec)	89
Figure 7.10. Test results (B10-3, $V=10 \times 10^{-4}$ mm/sec)	90
Figure 7.11. Test results (B10-4, $V=10 \times 10^{-4}$ mm/sec)	90
Figure 7.12. Test results (B10-1, $V=7.5 \times 10^{-4}$ mm/sec)	91
Figure 7.13. Test results (B10-2, $V=7.5 \times 10^{-4}$ mm/sec)	91
Figure 7.14. Test results (B10-3, $V=7.5 \times 10^{-4}$ mm/sec)	92
Figure 7.15. Test results (B10-4, $V=7.5 \times 10^{-4}$ mm/sec)	92
Figure 7.16. Test results (B10-1, $V=5 \times 10^{-4}$ mm/sec)	93
Figure 7.17. Test results (B10-2, $V=5 \times 10^{-4}$ mm/sec)	93
Figure 7.18. Test results (B10-3, $V=5 \times 10^{-4}$ mm/sec)	94
Figure 7.19. Test results (B10-4, $V=5 \times 10^{-4}$ mm/sec)	94
Figure 7.20. Test results (A20, $N=1.5$ MPa).....	95
Figure 7.21. Test results (B20, $N=1.5$ MPa).....	95
Figure 7.22. Test results (A20, $N=1.2$ MPa).....	96
Figure 7.23. Test results (B20, $N=1.2$ MPa).....	96
Figure 7.24. Test results (A20, $N=0.8$ MPa).....	97
Figure 7.25. Test results (B20, $N=0.8$ MPa).....	97
Figure 7.26. Test results (B10-1, $N=1.5$ MPa).....	98
Figure 7.27. Test results (B10-2, $N=1.5$ MPa).....	98
Figure 7.28. Test results (B10-3, $N=1.5$ MPa).....	99
Figure 7.29. Test results (B10-4, $N=1.5$ MPa).....	99
Figure 7.30. Test results (B10-1, $N=1.2$ MPa).....	100
Figure 7.31. Test results (B10-2, $N=1.2$ MPa).....	100
Figure 7.32. Test results (B10-3, $N=1.2$ MPa).....	101

Figure 7.33. Test results (B10-4, N=1.2 MPa).....	101
Figure 7.34. Test results (B10-1, N=0.8 MPa).....	102
Figure 7.35. Test results (B10-2, N=0.8 MPa).....	102
Figure 7.36. Test results (B10-3, N=0.8 MPa).....	103
Figure 7.37. Test results (B10-4, N=0.8 MPa).....	103
Figure 7.38. Shear stress-normal stress graph (A20, $V=10 \times 10^{-4}$ mm/sec)	106
Figure 7.39. Shear stress-normal stress graph (B20, $V=10 \times 10^{-4}$ mm/sec).....	106
Figure 7.40. Shear stress-normal stress graph (A20, $V=7.5 \times 10^{-4}$ mm/sec)	107
Figure 7.41. Shear stress-normal stress graph (B20, $V=7.5 \times 10^{-4}$ mm/sec).....	107
Figure 7.42. Shear stress-normal stress graph (A20, $V=5 \times 10^{-4}$ mm/sec)	108
Figure 7.43. Shear stress-normal stress graph (B20, $V=5 \times 10^{-4}$ mm/sec).....	108
Figure 7.44. Shear stress-normal stress graph (B10-1, $V=10 \times 10^{-4}$ mm/sec)	109
Figure 7.45. Shear stress-normal stress graph (B10-2, $V=10 \times 10^{-4}$ mm/sec)	109
Figure 7.46. Shear stress-normal stress graph (B10-3, $V=10 \times 10^{-4}$ mm/sec)	110
Figure 7.47. Shear stress-normal stress graph (B10-4, $V=10 \times 10^{-4}$ mm/sec)	110
Figure 7.48. Shear stress-normal stress graph (B10-1, $V=7.5 \times 10^{-4}$ mm/sec)	111
Figure 7.49. Shear stress-normal stress graph (B10-2, $V=7.5 \times 10^{-4}$ mm/sec)	111
Figure 7.50. Shear stress-normal stress graph (B10-3, $V=7.5 \times 10^{-4}$ mm/sec)	112
Figure 7.51. Shear stress-normal stress graph (B10-4, $V=7.5 \times 10^{-4}$ mm/sec)	112
Figure 7.52. Shear stress-normal stress graph (B10-1, $V=5 \times 10^{-4}$ mm/sec)	113
Figure 7.53. Shear stress-normal stress graph (B10-2, $V=5 \times 10^{-4}$ mm/sec)	113
Figure 7.54. Shear stress-normal stress graph (B10-3, $V=5 \times 10^{-4}$ mm/sec)	114
Figure 7.55. Shear stress-normal stress graph (B10-4, $V=5 \times 10^{-4}$ mm/sec)	114
Figure 7.56. Normal displacement-shear displacement graph (A20-N=1.5 MPa)...	117
Figure 7.57. Normal displacement-shear displacement graph (A20-N=0.8 MPa)...	117
Figure 7.58. Normal displacement-shear displacement graph (B20-N=1.5 MPa)...	118
Figure 7.59. Normal displacement-shear displacement graph (B20-N=0.8 MPa)...	118
Figure 7.60. Roughness-shear rate effect, A20-B20 peak shear strengths, N=1.5 Mpa.....	119
Figure 7.61. Roughness-shear rate effect, A20-B20 peak shear strengths, N=1.2 MPa.....	120
Figure 7.62. Roughness-shear rate effect, A20-B20 peak shear strengths, N=0.8 MPa.....	120

Figure 7.63. Roughness-shear rate effect, A20-B20 residual shear strengths, N=1.5 MPa.....	121
Figure 7.64. Roughness-shear rate effect, A20-B20 residual shear strengths, N=1.2 MPa.....	121
Figure 7.65. Roughness-shear rate effect, A20-B20 residual shear strengths, N=0.8 MPa.....	122
Figure 7.66. Roughness-shear rate effect - Percent changes in peak shear strength	123
Figure 7.67. Roughness-shear rate effect - Percent changes in residual shear strength	124
Figure 7.68. Size-shear rate effect, B10-B20 peak shear strengths, N=1.5 MPa.....	126
Figure 7.69. Size-shear rate effect, B10-B20 peak shear strengths, N=1.2 MPa	126
Figure 7.70. Size-shear rate effect, B10-B20 peak shear strengths, N=0.8 MPa	127
Figure 7.71. Size-shear rate effect, B10-B20 residual shear strengths, N=1.5 MPa.. ..	128
Figure 7.72. Size-shear rate effect, B10-B20 residual shear strengths, N=1.2 MPa	128
Figure 7.73. Size-shear rate effect, B10-B20 residual shear strengths, N=0.8 MPa	129
Figure 7.74. Size-shear rate effect, Average B10-B20 peak shear strengths, N=1.5 MPa	130
Figure 7.75. Size-shear rate effect, Average B10-B20 peak shear strengths, N=1.2 MPa	130
Figure 7.76. Size-shear rate effect, Average B10-B20 peak shear strengths, N=0.8MPa	131
Figure 7.77. Size-shear rate effect, Average B10-B20 residual shear strengths, N=1.5 MPa	131
Figure 7.78. Size-shear rate effect, Average B10-B20 residual shear strengths, N=1.2 MPa	132

Figure 7.79. Size-shear rate effect, Average B10-B20 residual shear strengths, N=0.8 MPa	132
Figure 7.80. Size-shear rate effect – Percent changes in peak shear strength.....	133
Figure 7.81. Size-shear rate effect - Percent changes in residual shear strength	134

CHAPTER 1

INTRODUCTION

Rock masses are not continuous and contain weakness zones such as faults, joints, bedding planes, fractures and schistosity. These geological features are generally called discontinuities. Presence of the discontinuities significantly effect the behavior of the rock masses. Especially at shallow depths, where the confining pressures are low, failure problem is not usually attributed to the intact rock, but to the sliding along the discontinuities (Hoek, 2007). Therefore, it's important to understand frictional characteristics of the rock discontinuities where the behavior of the rock mass is controlled by the failure of the discontinuity, in order to develop safe rock engineering designs.

Parameters related to the frictional behavior of rock discontinuities, such as peak and residual values of shear strength, friction angle and cohesion, can be determined by direct shear test. Although there are some variations, generally direct shear test devices incorporate; a stiff testing system on which loading devices can act, a specimen holder (shear box), loading devices to apply shear and normal loads, devices to measure loads and displacements. Specimens used in the direct shear test may be of any shape or size as long as the surface area can be determined accurately. Usually, the specimens are obtained from borehole drillings or as discontinuity samples acquired in the field (Muralha et al., 2014). Consequently, the direct shear test can be applied only once on a specimen and it's not possible to repeat the test with varying conditions on the same discontinuity plane.

Relationship between shear strength and normal stress is frequently represented by Mohr-Coulomb equation (Eqn. 1):

$$\tau = c + \sigma_n \tan\phi \quad (1)$$

where;

τ : Shear Strength

c : Cohesion

σ_n : Normal Stress

ϕ : Friction Angle

However, Barton (1971, 1973) investigated the shearing behavior of natural rock discontinuities and showed that the relationship between the shear strength and normal stress is nonlinear, therefore Mohr-Coulomb equation fails to accurately depict the true nature of shearing behavior. Barton and Choubey (1977) proposed the following empirical criterion (Eqn. 2) for rock discontinuities by conducting direct shear tests on 130 samples.

$$\tau = \sigma_n \tan(\phi_r + JRC \log_{10}(JCS/ \sigma_n)) \quad (2)$$

where;

JRC: Joint Roughness Coefficient

JCS: Jointwall Compressive Strength

The shearing behavior of rock discontinuities are effected by several factors like roughness, normal load, shear rate, scale, infilling material and presence of water.

Rock discontinuity surfaces contain varying degrees of irregularity which accounts for the roughness effect. Shearing along rough surfaces require overriding and crushing of small scale asperities or large scale undulations which in turn increases the shear strength. The roughness effect on shear behavior of the rock discontinuities are verified by several researchers in the past. One way of characterizing the roughness degree is the determination of dilation angle and it was shown that higher dilation angle leads to

a higher shear strength (Barton, 1971; Sfondrini and Sterlacchini, 1996; Yang et al., 2010). Roughness levels are frequently represented by the JRC and the shearing tests indicated that the shear strength is higher for surfaces with a higher JRC (Kimura et al., 1993; Yang et al., 2010). In addition, since the JRC is subjective parameter, it's attempted to replace the JRC with statistical parameters (Sfondrini and Sterlacchini, 1996).

Shear rate is another factor that has significant effect on shearing characteristics. The effect is attributed to the change in contact area between surfaces with changing displacement velocity. Several authors published different outcomes of the shear rate effect due to the dependence on normal stress, material type etc. Several studies concluded that increased shear rate leads to the higher shear strength values (Dieterich, 1972; Schneider, 1977; Crawford and Curran, 1981; Lockner et al., 1986; Lajtai and Gadi, 1989; Atapour and Moosavi, 2013). Conversely, studies indicating that decreased shear rate leads to the higher shear strength values, are also numerous (Crawford and Curran, 1981; Atapour and Moosavi, 2013; Kleepmak et al., 2016). In addition, there are other studies that states no significant shear rate effect (Crawford and Curran, 1981; Olsson, 1974).

Size of the samples used in direct shear test has been known to effect the outcome of the experiments. Small size sample surfaces contains only smaller and steeper asperities, whereas large size samples also contain large scale and more moderately inclined undulations. This causes a difference between roughness levels of large and small size samples of the same discontinuity surface, which in turn leads to differences in the shear strength. Effect of sample size on the shear strength of rock discontinuities has been investigated by several researchers. Several studies showed that decreasing the sample size leads to the higher shear strength values (Bandis et al., 1981; Yoshinaka et al., 1991; Ueng et al., 2010). However, there are several other studies indicating no significant sample size effect (Hencher et al., 1993; Tatone & Grasselli, 2012; Johansson, 2016).

1.1.Problem Statement

In the direct shear test of the rock discontinuities, due to the nature of the experiment, specimens can only be used once. Therefore, experiments are generally conducted on

different specimens from the same discontinuity. It's also possible to use the same specimen as long as each test is under a lower normal stress condition than the following one. However, performing experiments in these manners, increases the error margin of the results, since the surfaces show differences in each test or they get gradually deformed with repeated tests. In addition, obtaining discontinuity samples in the field or from the boreholes is not always easy, thereby limiting the number of tests that can be performed. For these reasons, replicating discontinuity samples that accurately reflects roughness levels with a material that shows rock characteristics, is an important step towards decreasing the uncertainties associated with the direct shear tests.

Conditions effecting the shear strength of rock discontinuities have been investigated by many researchers. However, these conditions are also co-dependent. In other words, effects of a condition (such as shear rate) might increase or decrease depending on another (such as roughness and sample size). Understanding the co-dependency of these conditions is important for predicting insitu shear strength of the rock discontinuities.

1.2.Objectives of the Study

The main objective of this study is to understand the effects of the discontinuity roughness, the shear rate and the sample size on the shear strength of the rock discontinuities, so that the co-dependency of these conditions can be investigated and underlying reasons for the effect can be identified.

For this purpose, it is aimed at developing a low-cost and practical methodology to replicate discontinuity samples with sufficient accuracy to preserve roughness degree. Close range digital photogrammetry and 3D printing technology are used for developing the methodology.

1.3.Organisation of the Thesis

This thesis involves eight chapters. An introduction is presented in Chapter I. Chapter II provides the overview of parameters effecting shear behavior of rock discontinuities. Research methodology is described in Chapter III. In Chapter IV, 3D modelling of rock discontinuities are presented. In Chapter V, roughness characterization of rock

discontinuities are explained. In Chapter VI, experimental setup is presented. Experimental results and discussions are given in Chapter VII. Conclusions and recommendations are presented in Chapter VIII.

CHAPTER 2

OVERVIEW OF THE FACTORS AFFECTING THE SHEAR BEHAVIOR OF ROCK DISCONTINUITIES

Shearing characteristics of rock discontinuities depends on several factors, namely surface roughness, applied normal stress, shear rate, scale, infilling, water, etc. In this study; effects of roughness, shear rate and sample size on the shear strength are further investigated. For this purpose, a literature survey on these effects is presented in the following subsections.

2.1. Effect of Roughness

The shear strength measured with direct shear test heavily depends on the roughness degree of the rock discontinuity. Influence of roughness arises from the amount, extent and strength of individual asperities, since shearing motion comprises overriding and breaking of the asperities. Barton (1971) revealed the relationship between peak dilation angle and discontinuity peak shear strength. Barton (1971) also offered an analogy to estimate peak shear strength for any range of normal stresses based on the recording of joint roughness profiles. In this section, firstly previous studies investigating roughness effect on shear strength are given. Then, studies relating roughness levels to Z_2 , fractal dimension and other statistical parameters are presented, respectively.

The effect of roughness characteristics on the shear strength is one of the intensely studied subsections in the literature. Reeves (1985) developed the relation between friction angle and statistical parameters of roughness level of a rock discontinuity surface, in order to replace laborious direct shear tests with a roughness data

acquisition process. Kimura et al. (1993) investigated the shearing behavior of rock joints with different roughness levels. After direct shearing of joints, authors observed the increase in area of damaged asperities under increasing normal stress on the joint. Sfondrini and Sterlacchini (1996) analyzed the effect of the discontinuity roughness levels on the shear strength by performing direct shear tests on discontinuity replicates produced with epoxy resins. Authors represented roughness levels with primary and secondary dilatation angles (i), and observed an increase in shear strength with increasing dilatation angles.

Yang et al. (2010) conducted direct shear tests on the discontinuity samples at two different roughness levels and investigated the effects of the roughness degree on the discontinuity shear behavior. Experimental samples were produced using molds produced by the layered object manufacturing method. As a result of the tests, it was determined that the peak shear strength is higher in the sample with high roughness. It has been determined that the roughness also affects Mohr-Coulomb parameters such as cohesion and friction angle. The increased roughness caused an increase in both parameters, more significant in cohesion. Finally, there was not any difference between the residual shear strength of different roughness levels.

Barton and Choubey (1977) proposed an empirical equation of shear strength (Eqn. 3) that accurately describes the nonlinear behavior of rock joints.

$$\tau = \sigma_n \tan [\text{JRC} \log_{10} (\text{JCS} / \sigma_n) + \varphi_b] \quad (3)$$

where τ = peak shear strength

σ_n = effective normal stress

JRC = joint roughness coefficient

JCS = joint wall compressive strength

φ_b = basic friction angle

Based on Equation 3, Barton and Choubey (1977) offered ten standard joint roughness profiles in order to quantify roughness levels, by back-calculating the equation for selected rock discontinuity samples. Figure 2.1 presents the standard roughness profiles with associated JRC values.

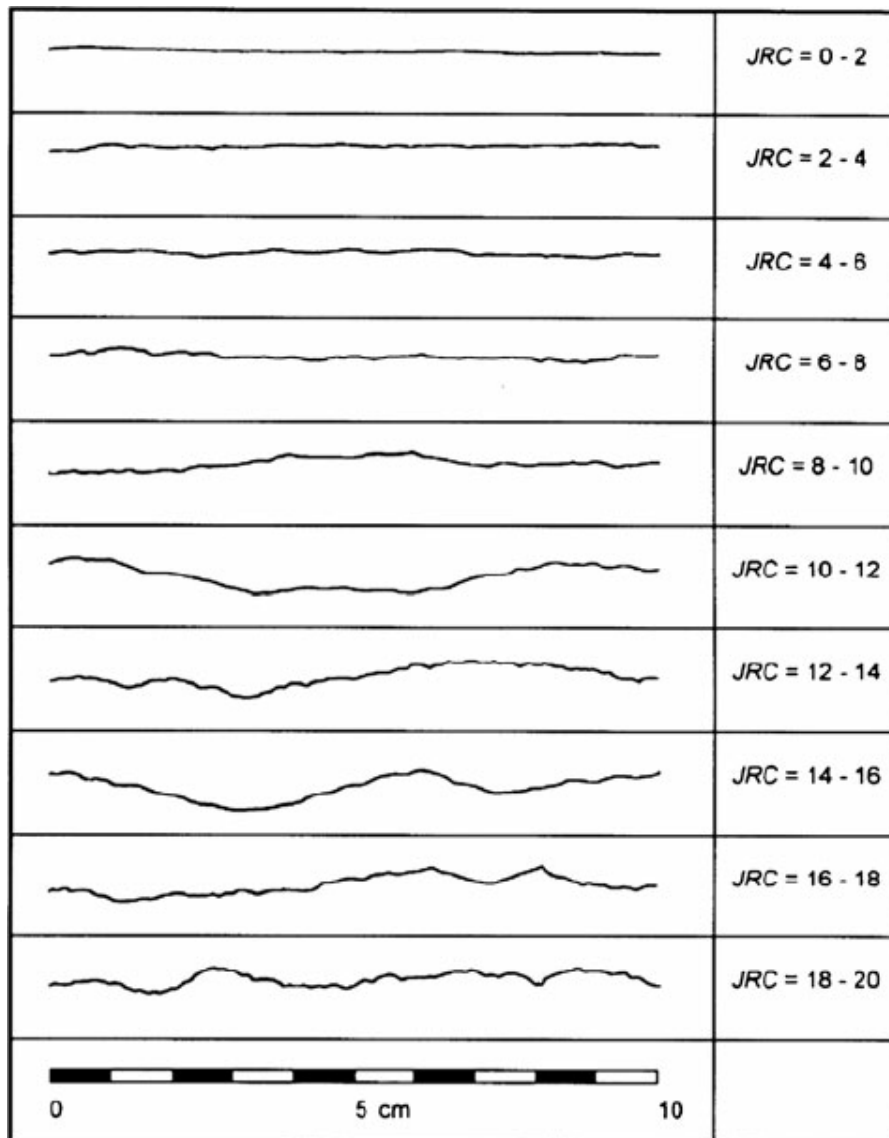


Figure 2.1. Standard roughness profiles proposed by Barton & Choubey (1977)

The standard joint roughness profiles have been used extensively to determine JRC values. However, since this approach is based on visual comparison, it becomes subjective. Therefore, many researchers attempted to develop statistical models for characterizing the roughness of the discontinuities.

Tse and Cruden (1979) developed an empirical equation, relating the Z_2 (root mean square of the first derivative of the profiles) and JRC, using linear regression, based on ten standard roughness profiles proposed by Barton and Choubey (1977). Standard profiles were enlarged 2.5 times and amplitude readings were taken at 1.27 mm intervals. Tse and Cruden (1979) expressed the Z_2 in discrete form as in Equation 4.

$$Z_2 = \left[\frac{1}{M(Dx)^2} \sum_{i=1}^M (y_{i+1} - y_i)^2 \right]^{1/2} \quad (4)$$

Where M= Number of intervals

Dx= Constant distance between two adjacent amplitude readings

y= Amplitude of the roughness about the centreline

Tse & Cruden (1979) offered the Equation 5 for correlation between Z_2 and JRC.

$$\text{JRC} = 32.2 + 32.47 \log (z_2) \quad (5)$$

Yu and Vayssade (1991) investigated the effect of sampling interval on Z_2 parameter, concluding that Z_2 is indeed sensitive to sampling interval and the Equation 4 proposed by Tse and Cruden (1979) would be meaningless if a sampling interval different from the their's is used. Yang et al. (2001) argued that scaling up the original joint profiles without changing the JRC value was an erroneous concept employed in Tse and Cruden (1979). Therefore, Yang et al. (2001) proposed a new formula using the original scale joint profiles, and also advised the use of self-affinity transformation approach when changing the original length of a joint profile which uses different scaling factors for perpendicular directions to preserve similarity. Jang et al. (2014) discussed the relationships between JRC and statistical roughness parameters such as Z_2 , SF (structure function) and R_p (roughness profile indexes). These parameters showed good correlation between each other and JRC. Dependency of JRC to sampling interval is also pointed out. Li and Zhang (2015) reviewed all previous studies that relates JRC to mentioned statistical parameters and discussed the limitations of each. Combining available roughness profiles in the literature, authors developed new empirical equations for quantitative JRC determination.

Grasselli et al. (2002) defined some roughness parameters corresponding to maximum possible contact area, maximum dip angle and degree of roughness parameter. They used these parameters to relate roughness to shear strength and trace the evolution of roughness and surface characteristics under shearing.

Kliche (1991) attempted to quantify the roughness of rock discontinuities using fractal dimension and proposed a relationship between JRC and fractal dimension in order to

determine the peak shear strength of a discontinuity without the need for subjective roughness determination. Odling (1994) analyzed the relationship between JRC and fractal dimension of natural rock discontinuities. Results of the study revealed that JRC increases with increasing amplitude and decreases with increasing fractal dimension. Xu et al. (2012) considered natural rock discontinuity surfaces as fractal curves, and developed an empirical relation with high accuracy, between JRC and fractal dimension of joints. Li and Huang (2015) reviewed the existing empirical methods for JRC determination from fractal dimension and showed variability between these methods. Li and Huang (2015) proposed a new empirical equation for JRC determination with fractal dimension, using large number of discontinuity roughness profiles, reducing the variability between individual profiles.

Belem et al. (2000) argued that roughness is a combination of primary and secondary parameters, and quantifying roughness with linear parameters based on the roughness profiles, causes underestimation of the roughness and thus increases the error margin. The statistical parameters described by Belem et al. (2000) are as follows: primary roughness parameter; degree of apparent anisotropy, secondary roughness parameters; mean surface angle, Z_2 and surface roughness coefficient defined by (El Soudani, 1978).

Jiang et al. (2006) analyzed the change in roughness condition of a rock joint using fractal dimension methods, with shearing by conducting direct shear tests under both constant normal stress and constant normal stiffness conditions. They used the results of the experiments to understand mechanical behaviour of rock joints under different boundary conditions.

Ge et al. (2014) reviewed joint roughness quantification techniques, and discussed the advantages of fractal dimension based methods. Evaluation and comparison of four fractal dimension based roughness quantification methods, are presented by authors.

Kulatilake et al. (2006) discussed variability of roughness of a rock joint surface due to anisotropy and introduced a new scale dependent fractal parameter K_v . They proposed the $K_v \times D$ (D : Fractal dimension) as an overall roughness parameter, alternative to subjective JRC.

Tatone and Grasselli (2009) developed a new methodology for 3D surface roughness characterization using optical measurement devices. The method also made it possible to determine surface anisotropy at the same time. Quantitative roughness values obtained with the methodology shown consistency with the observations. Tatone and Grasselli (2010) improved the previous study and introduced a new 2D roughness parameter using 3D models by Tatone and Grasselli (2009). The new 2D roughness parameter appeared to be in good agreement with 3D roughness values. Also, a new empirical equation is developed between 2D roughness parameter and JRC.

Zhang et al. (2014) proposed a new 2D roughness coefficient (λ) which considers dilation angle, asperity magnitude and direction. A function is generated that relates JRC to the new coefficient. Agreement between the new roughness coefficient and JRC is verified with conducted direct shearing experiments.

Hong et al. (2008) argued that roughness values were underestimated in previous studies in this field, especially for relatively rough joint surfaces. They showed difference in JRC values for the estimated values in previous studies and back-calculated values from direct shear tests with artificial surfaces. Employing at least two roughness parameters while estimating a statistical roughness parameter, is suggested as a solution for the problem.

2.2.Effect of Shear Rate

The rock discontinuities may show different shearing behavior under different shearing velocities. Dieterich (1972) conducted direct shear tests on different rock types and found that the static friction coefficient is the result of time-dependent behavior due to accumulation of rock gouge on the slip surface. The device used for testing in this study is a direct shear test device which is frequently used in the field of rock mechanics. The time intervals used in the experiments were 1 sec. to 24 h. and the normal stress was varied from 2 to 85 MPa. The study concluded that the main parameter controlling the frictional behavior of rock discontinuities is surface characteristics. Additionally, it is stated that the rock type has a weak effect on this behavior. This study also draws attention to the obvious effect of time-dependent change of friction coefficient on rock slope failure.

Olsson (1974) analyzed the effects of displacement rate along with temperature and pressure on frictional behavior of a fault in limestone. Results suggested a weak correlation between the displacement rate and frictional resistance.

Schneider (1977) conducted deformation controlled direct shear tests under 1.9 MPa normal stress. The shear displacement rate was changed between 0.01 and 200 mm/min. Each cycle amounts to 2 sec to 16 hours. As a result of this study, it was determined that the frictional resistance of the discontinuity surface increases linearly, however the resistance evolves into nonlinear behavior toward the maximum value.

Crawford and Curran (1981) revealed that shearing characteristics of rock joints depend on the velocity of the shearing. They investigated the effect by conducting direct shear tests on different rock types and different normal stress conditions. They concluded that dependence of frictional resistance of the rock joints on shear displacement rate shows variance according to several conditions. For hard rocks, frictional resistance decreases with increasing shear rate that is greater than a critical value. For soft rocks, frictional resistance increases with increasing shear rate up to a critical rate, than it remains constant. Under low normal stress condition (0.65 MPa), generally resistance increases up to certain shear rate where it remains constant afterwards, whereas under high normal stress condition (2.5 MPa), generally resistance remains constant up to a certain shear rate where it starts to decrease (Crawford and Curran, 1981).

Bowden and Curran (1984) studied the time-dependent shear behavior of the discontinuities and investigated the role of adhesion and the ratio of applied shear stress to the shear strength of the discontinuity. A large-scale direct shear test equipment was constructed to investigate the creep behavior of schists discontinuities. The dimension of the shear box was 200 mm x 300 mm. The duration of the direct shear tests was 4-5 days. Normal and shear stresses were kept constant. They stated that the applied shear stress becomes more pronounced in the schist discontinuities if the ratio of the discontinuity to the shear strength is greater than 0.9. In addition, they pointed out that, presence of clay minerals in the schist produces an adhesive force between the particles and affect the behavior of the discontinuity during shearing.

Crawford and Curran (1986) stated that the shear creep is significant on discontinuity at shear stresses close to the shear strength. They developed a numerical method to model time-dependent behavior of rocks. Empirical viscoelastic model was used because of the small number of experimental discontinuity creep data. As a result of the numerical experiments, it was determined that the shear creep becomes important when the displacement is not prevented on the discontinuity surfaces.

Lockner et al. (1986) investigated the effects of sliding rate and temperature on frictional behavior of granite surfaces. They compared friction coefficients and identified a correlation between sliding rate and frictional resistance.

Lajtai and Gadi (1989) conducted direct shear tests on a granite-granite interface in order to follow the development of the frictional resistance as displacement and surface wear grows. In this study, the friction angle of the surface was observed during shearing by 25 mm displacement steps of the same surface. The normal stress was varied from 0.2 MPa to 8 MPa. As a result of this study, the findings of Dieterich (1972) were confirmed and it was determined that the displacement ratio, time and stationary contact between the surfaces increased the friction angle.

Malan (1998) developed a direct shear test machine to model the time-dependent behavior of rock discontinuities. Experiments were carried out on filled and unfilled discontinuities. The applied normal stresses were 0.5 MPa, 1.0 MPa and 1.5 MPa. The duration of the experiments varied from 4 to 48 hours. As a result, it was shown that the magnitude of the shear creep depends on the shear stress to shear strength ratio, as mentioned in previous studies. In addition, experiments were carried out on the discontinuities with different filling thicknesses, and the effect of the filling thickness was also investigated. It was determined that the creep changes linearly with filling thickness and the creep velocity increases as the filling thickness increases.

Li et al. (2012) evaluated the shear rate dependency of rock fractures. Experimental results suggested that there is a weak relation between peak shear strength and shear rate especially at low shear rates. However, at residual stage, strength increases with increasing shear rate.

Atapour and Moosavi (2013) studied the shear rate effect on behavior of artificial joints. Artificial joints were prepared with plaster and concrete. Direct shear tests were conducted with different shear rates. They concluded that shear strength of artificial joints is dependent on the shearing velocity and the extent of this effect depends on material type, normal stress and roughness levels.

Klempmek et al. (2016) conducted triaxial shear tests to investigate the effects of shear rate on the shear strengths of smooth surfaces on different rock types. Results showed that the shear rate effect on the shear strength is more prevalent in competent rocks with relatively rough surfaces. The shear strength and dilation rates increased with increasing confining pressure. They proposed an empirical relationship between the shear rate and the shear strengths of rock fractures based on the obtained experimental results.

2.3. Effect of Sample Size

In direct shear test of rock discontinuities, specimen size has significant effect on the shear strength. The roughness level of rock discontinuity is a value that is determined for a fixed length of joint specimen. As the length of the joint specimen increases, generally, JRC value decreases. Consequently, longer discontinuity samples have lower peak shear strength. Barton and Bandis (1980) explained this effect as stating that the longer joint samples jump over smaller steep asperities, therefore only the longer and more gently inclined asperities comes into contact which controls the large scale shear strength. Figure 2.2 shows the results of the experimental study explaining the relation between the specimen size and the shear strength, conducted by Bandis (1979). Barton and Bandis (1982) introduced empirical scale correction factors for JRC and JCS in the Barton-Bandis shear strength criterion (Equations 6 and 7).

$$JRC_n = JRC_0 \left(\frac{L_n}{L_0} \right)^{-0.02 JRC_0} \quad (6)$$

$$JCS_n = JCS_0 \left(\frac{L_n}{L_0} \right)^{-0.03 JCS_0} \quad (7)$$

Where; JRC_0, JCS_0, L_0 indicates the values of the laboratory sample.

JRC_n, JCS_n indicates the insitu values.

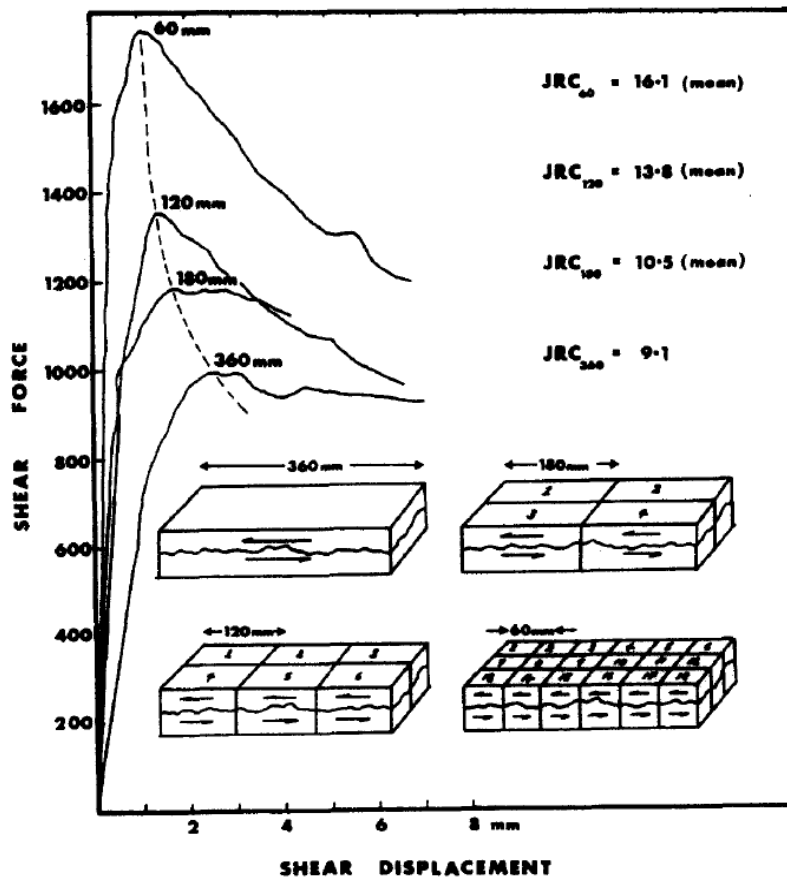


Figure 2.2. Shear behavior with different specimen sizes, Bandis (1979).

Bandis et al. (1981) studied the scale effect on rock joints by conducting direct shear tests on different size specimens. Results showed that, shear strength is a scale dependent property and peak shear strength increases as the block size decreases. They concluded that scale effect is more prevalent for rough, undulating discontinuity surfaces and almost ignorable for smooth, planar surfaces.

Yoshinaka et al. (1991) presented experimental results obtained from the investigation of the size on shear strength of rock joints. Direct shear tests were conducted on a wide range of joint lengths. They detected strong inverse correlation between the increasing shearing area and shear strength.

Hencher et al. (1993) conducted direct shear tests on different sizes of rock joint specimens and compared the results with that of Bandis (1980). Joint lengths were varied between 88 and 354 mm. Results implied insignificant size dependency of shear strength, as opposed to what was proposed by Bandis (1980).

Fardin et al. (2001) investigated the size dependency of rock discontinuity surface roughness. Authors replicated a natural joint surface with the size of 1000 mm x 1000 mm but using digitized surface. Fractal parameters of the discontinuity were calculated with 10 different sampling windows changing from 100 mm x 100 mm to 1000 mm x 1000 mm. They stated that the surface roughness is a scale dependent property that increases with decreasing size. However, it reaches a threshold where the roughness value is stabilized despite the increasing size of the rock joint.

Fardin et al. (2004) used 3D scanner technology to transfer the texture of a rock discontinuity surface with a size of 6 m x 4 m to the computer environment to investigate the size effect on roughness. Four sample surfaces ranging from 1000 mm x 1000 mm to 4000 mm x 4000 mm were selected and the roughnesses were compared by assigning the amplitude values of the surfaces. As a result of the study, it was observed that the roughness decreases with decreasing scale and that roughness value was fixed at 3000 mm x 3000 mm dimension.

Ueng et al. (2010) investigated the size effect on shear behaviour of artificial joints of two different roughness characteristics with sizes ranging from 75 mm to 300 mm in length. The average of the specimens cut from the larger dimension was higher than that of the original discontinuity. They also concluded that joint surface geometry configuration is mainly responsible for the size effect rather than the length of the specimen.

Tatone and Grasselli (2012) studied size effect on shear strength of rock joint by performing numerical direct shear test with 2-dimensional finite-discrete element method. Models with 400, 200, 100 and 50 mm joint lengths were constructed. Results did not show any significant sample size effect on the shear strength. However, size dependency of shear stiffness was identified.

Tatone and Grasselli (2013) argued that large scale surface roughness components were neglected in previous studies since the investigations were restricted to small joint surfaces ($< 1 \text{ m}^2$). Therefore, they studied the roughness scale effect by digitizing large scale surfaces (2 m x 3 m and 2 m x 2 m) and digitizing small scale samples (100 mm x 100 mm) from the same surfaces. Results showed increasing roughness with increasing sample size, contrary to many previous studies.

CHAPTER 3

RESEARCH METHODOLOGY

In this thesis, a methodology is developed to investigate the effects of shear rate, sample size and roughness characteristics on shear behavior of rock discontinuities. For this purpose, close-range digital photogrammetry and 3D printing technology is utilized to produce rock discontinuity sample replicas. Then, direct shear tests are conducted on the produced replicas to investigate the forementioned effects.

It is aimed at developing a low-cost and practical rock discontinuity replica production methodology that will accurately reflect the roughness degree of the original discontinuity. Developments in digital photogrammetry softwares and 3D printing technologies offer a promising way to achieve this. In order to decrease the error margin of the direct shear test results, experiments are conducted on discontinuity replicas with the same surface and material properties. Flowchart of the proposed methodology is given in Figure 3.1.

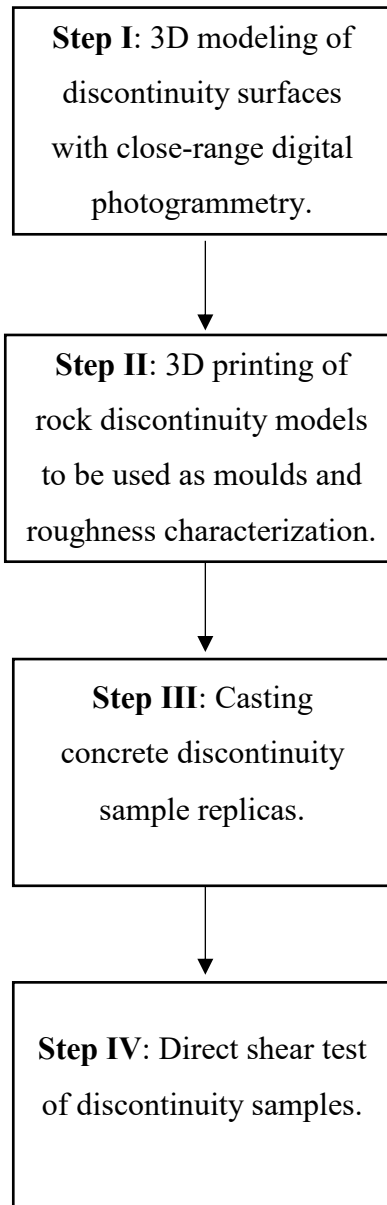


Figure 3.1. Flowchart of the proposed methodology

Step I: In the first step, 3D models of two selected rock discontinuity samples with defined roughness levels are generated with close-range digital photogrammetry. Agisoft Photoscan software is used to produce sparse point cloud, dense point cloud, digital elevation models and 3D models, respectively. Lastly, the 3D models are enlarged and re-scaled to generate 20 cm x 20 cm discontinuity models. Roughness degree of the 3D models are identified in terms of Z_2 parameter.

Step II: In the second step, generated 3D models are printed-out as solid objects by using a 3D printer. Polylactic acid (PLA) is used as the raw material. The discontinuity models are used as moulds in the next steps. At the end of step II, two 20 cm x 20 cm PLA moulds, each corresponding to a different roughness level, are obtained. Roughness degree of the PLA moulds are again identified in terms of Z_2 parameter.

Step III: In the third step, discontinuity sample replicas are cast. By using the PLA moulds and a cement mixture, concrete discontinuity samples are obtained. At first, two set of 20 cm x 20 cm replicas are cast, corresponding to two different roughness levels. Then, in order to investigate sample size effect, discontinuity replicas with higher roughness level are cut into four equal parts. Thus, four set of 10 cm x 10 cm replicas are obtained. Roughness degree of the concrete test samples are identified in terms of Z_2 parameter. Then, Z_2 of the 3D models, the PLA moulds and the concrete test samples are compared to evaluate the change in the roughness degree through the steps of discontinuity sample replication procedure. The comparison is used for evaluating the success of the proposed methodology.

Step IV: In the fourth step, direct shear tests are conducted on produced discontinuity samples. Experiments are conducted under three normal load conditions, at three shear rates (10×10^{-4} – 7.5×10^{-4} - 5×10^{-4} mm/sec), on two sample sizes (20 cm x 20 cm – 10 cm x 10 cm). Experimental results are evaluated to identify the effects of shear rate, sample size and roughness characteristics on shearing behavior. Then, co-dependency of these effects are investigated.

CHAPTER 4

3D MODELING OF DISCONTINUITY SURFACES WITH CLOSE-RANGE DIGITAL PHOTOGRAMMETRY

The shear tests on real rock discontinuities, for investigating the co-dependency of various factors requires producing replicas of discontinuity surfaces. For this purpose, the 3D digital models of the rock discontinuity surfaces are used for producing accurate replicas using close-range digital photogrammetry. In this chapter, first, a review of studies using photogrammetry in discontinuity surface modeling is given. Then the proposed methodology to obtain test samples to conduct the direct shear experiments is explained in detail.

4.1. Overview of Photogrammetry of Discontinuity Surface Modeling

Photogrammetry is a remote sensing technique that allows the determination of shape and dimensions of an object from photogrammetric images (Linder, 2003). Photogrammetry has been used in various fields of engineering, for mapping and 3D modeling. In geotechnical engineering fieldwork, mapping of rock discontinuities is a fundamental but also time-consuming and dangerous task. In addition, parts of discontinuities that can easily be mapped are limited and the considerable sections of discontinuities are out-of-reach by foot (Haneberg, 2008). Digital photogrammetric methods offers a time-saving and easy-to-implement procedure for rock discontinuity mapping while preventing field personnel from dangerous situations such as rock falls and slides. Moreover, owing to the advances in DSLR camera technologies and modern photogrammetry softwares, detection of even small features of any shape is

now possible with close range digital photogrammetry. Therefore, this method can also be employed to identify roughness degree of rock discontinuities.

Ohnishi et al. (2006) proposed a new approach for slope monitoring using digital photogrammetry. The application consists of processing digital camera images and comparing the distances between each model produced at different times. They also verified the precision and accuracy of the proposed approach.

Haneberg (2007) explained the procedure to extract roughness profiles from digital photogrammetric or laser scanner point clouds of discontinuity surfaces. Estimation of asperity angles and JRC values of discontinuity profiles extracted from the point clouds is explained with an example study.

Haneberg (2008) described the application of close range terrestrial digital photogrammetry for rock slope modeling and discontinuity mapping. He explained the process with five case studies. Advantages of the digital photogrammetry over the 3D scanning for discontinuity mapping are listed as; cost-effectiveness, equipment convenience and detection of features such as veins or joint traces that would not be possible with a 3D scanner.

Firpo et al. (2011) utilized digital terrestrial photogrammetry to model a discontinuous rock slope and used the 3D model of the rock mass for stability investigation by distinct element numerical method. The study showed that data coming from photogrammetric techniques is sufficient and accurate enough to make a numerical analysis.

Ünal et al. (2012) assessed the use of the photogrammetry in the measurement of surface roughness and compared it with other existing methods. The topographic features of a rock discontinuity are determined by photogrammetry, comparator, profilometer and drag measurement system. They concluded that photogrammetry offers many advantages compared to other methods. For example, photogrammetry makes it possible to perform measurements with sufficient precision, to obtain very large amounts of data in a short time, to control the results and to repeat them if necessary, since the obtained data is permanent. Another advantage is that photogrammetry is less costly than laser scanning which gives the highest sensitivity in such studies.

4.2. Photogrammetric Analysis of Rock Discontinuity Samples

In order to create 3D surface models, two discontinuity samples are selected. Samples are named A and B (Figure 4.1). The sample A is from a discontinuity in a volcanic rock and the sample B is from a discontinuity in limestone.

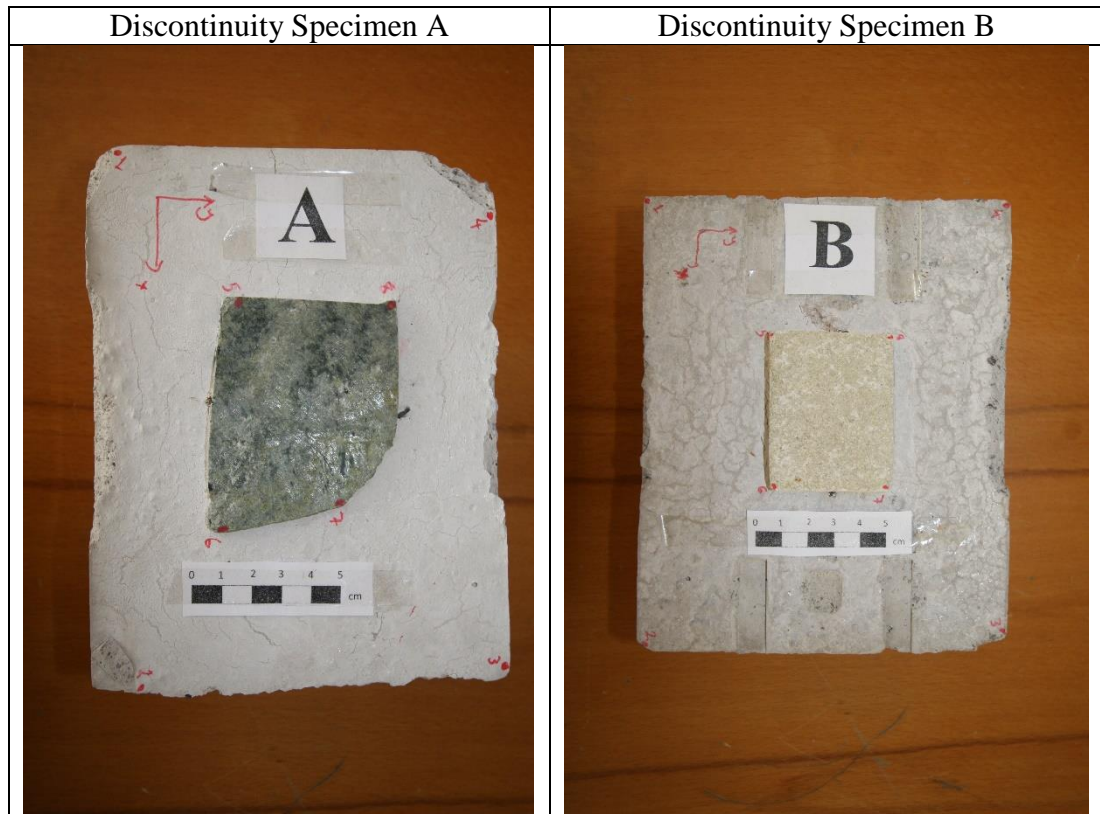


Figure 4.1. Rock discontinuity specimens A and B

Canon EOS 30D Digital SLR camera is utilized to take photographs of the specimens. 18 mm lens is used on the camera. Eight fixed points are determined on the specimens to be used as markers in the photogrammetric analysis (Figure 4.2). Purpose of the markers is to introduce dimension and to align photos accurately. 21 photographs are taken for both specimens from various angles.

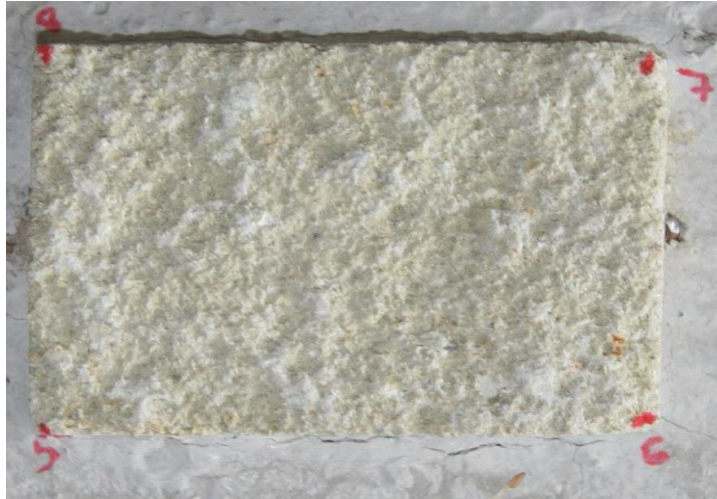


Figure 4.2. Fixed points marked on specimen B

Agisoft Photoscan software is used to perform photogrammetric processing. Agisoft Photoscan is an advanced 3D modelling solution, which aims creating 3D models from images. Workflow of photogrammetric processing is given in Figure 4.3.

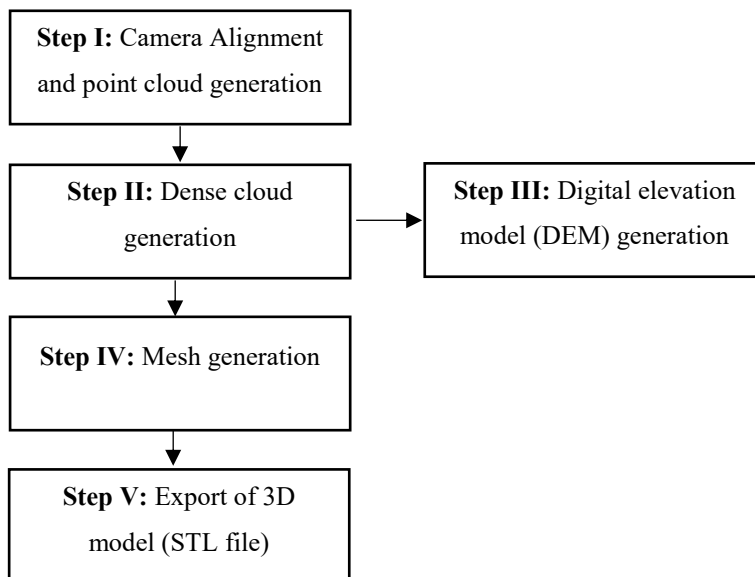


Figure 4.3. Photogrammetric processing workflow

Step I: Camera Alignment and Point Cloud Generation

The images are loaded on the Agisoft Photoscan software. The fixed points marked on the specimens are flagged on each image (Figure 4.4). Markers are used for setting a coordinate system, camera alignment optimization and measuring distances on the model. Parts of the photographs other than the rock discontinuity sample surface, are masked out from the processing, so that a less noisy point cloud can be obtained. Masked areas are excluded during sparse point cloud generation.

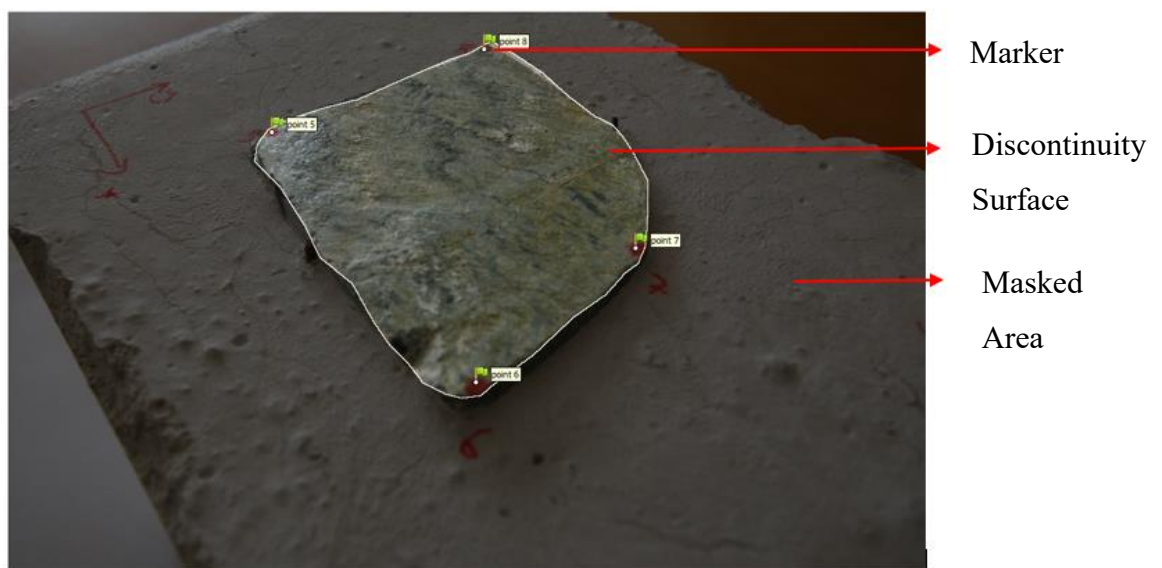


Figure 4.4. The masked areas and the markers

The software estimates the position of the camera in each image and refines camera calibration parameters by matching the common points between images and using markers as fixed positions on each image. Eventually, a sparse point cloud and a set of camera positions are obtained. The sparse point cloud just represents the results of image alignment and it can not be used in 3D model construction (Agisoft LLC, 2016).

The sparse point clouds of Specimen A and Specimen B consists of 9388 and 9813 points, respectively (Figure 4.5).

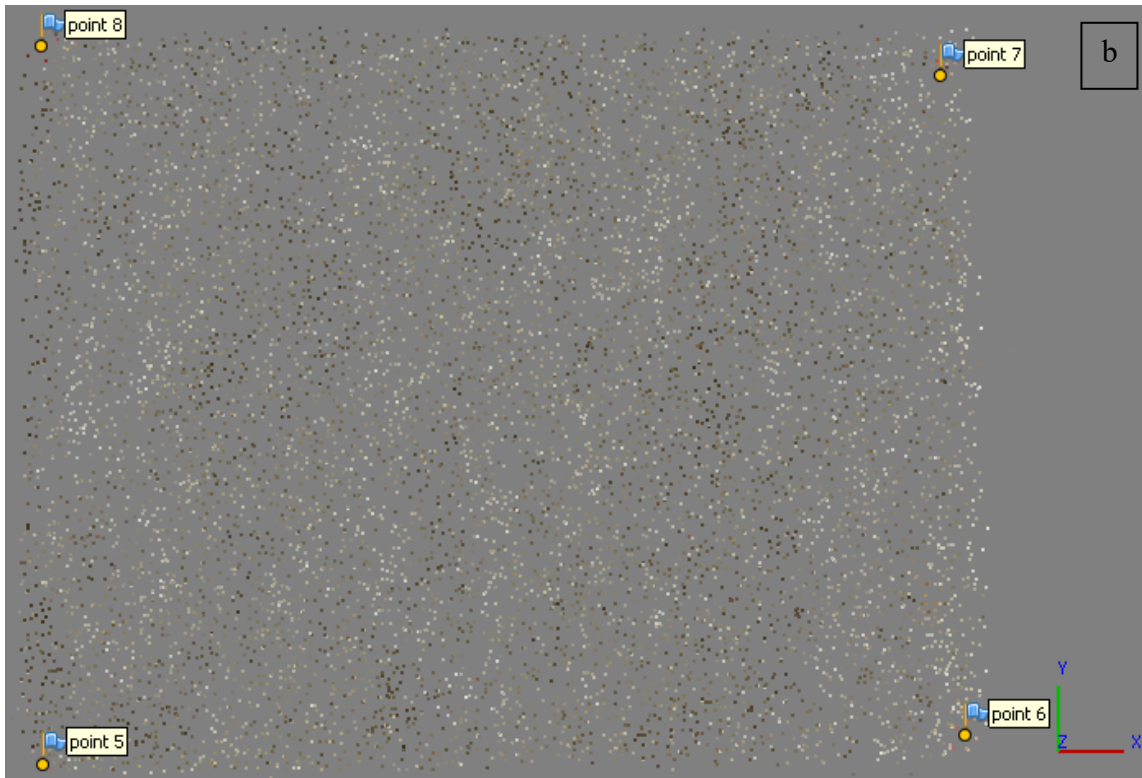
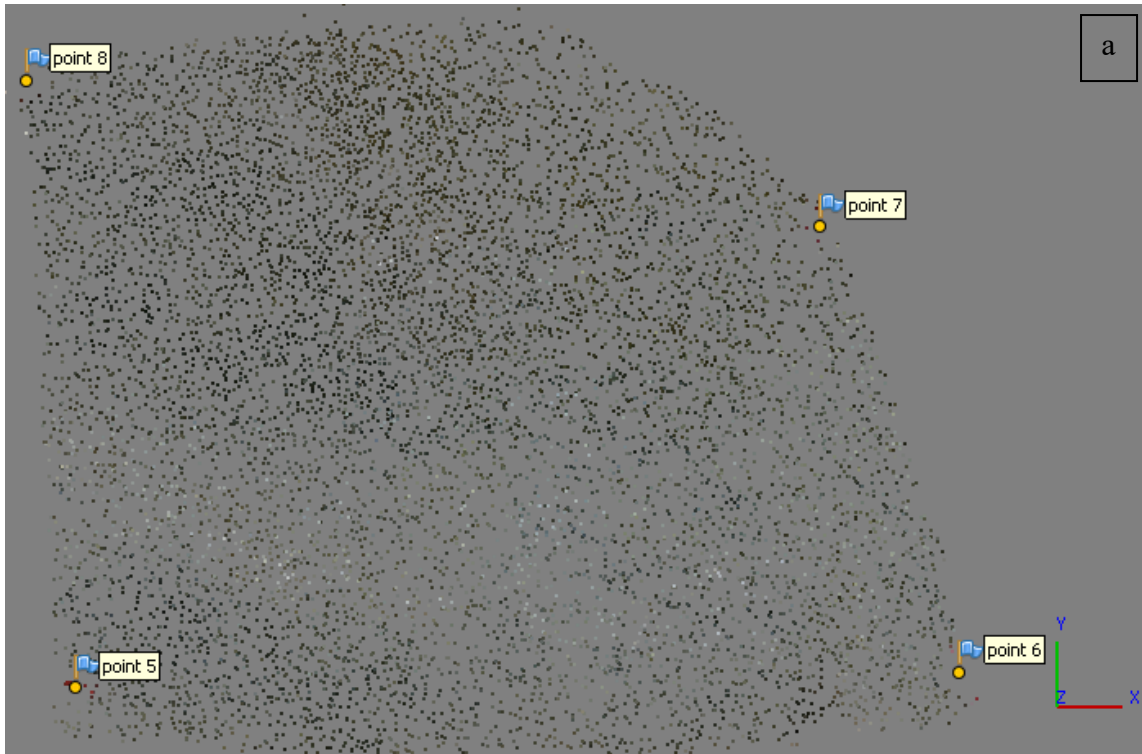


Figure 4.5. Sparse point clouds of specimens; (a) specimen A, (b) specimen B

Step II: Dense Cloud Generation

Based on the camera position, the software calculates the depth information for each image and combines them into a single dense point cloud. Aggressive depth filtering mode is selected in order to sort out outliers which are meaningless small details. Dense clouds obtained for Specimen A and Specimen B consists of 244,663 and 124,408 points, respectively (Figure 4.6).

Step III: Digital Elevation Model (DEM) Generation

The DEM of the selected discontinuity surfaces are constructed based on the dense clouds (Figure 4.7). The DEM represents the surface models as a regular height grid (Agisoft LLC, 2016). Resolution of the DEM's for Specimen A and Specimen B are, 0.081 mm/pixel and 0.178 mm/pixel, respectively. Reference level (0 mm) is the surface of the concrete frame around the discontinuity samples.

Step IV: Mesh Generation

The Agisoft Photoscan software constructs 3D Mesh representing object surface based on the dense cloud. The height field algorithmic method is selected for mesh generation, which is the recommended algorithm for planar type surfaces. The 3D model meshes of the both specimens are given in Figure 4.8.

Step V: Export of 3D Model

The software supports exporting of models in different file formats. 3D Meshes obtained in Step IV, exported as STL files. STL is the supported file format by 3D printer softwares. The 3D Models are imported to 3D Builder application of Windows for further editing (Figure 4.9).



Figure 4.6. Dense clouds of specimens; (a) specimen A, (b) specimen B

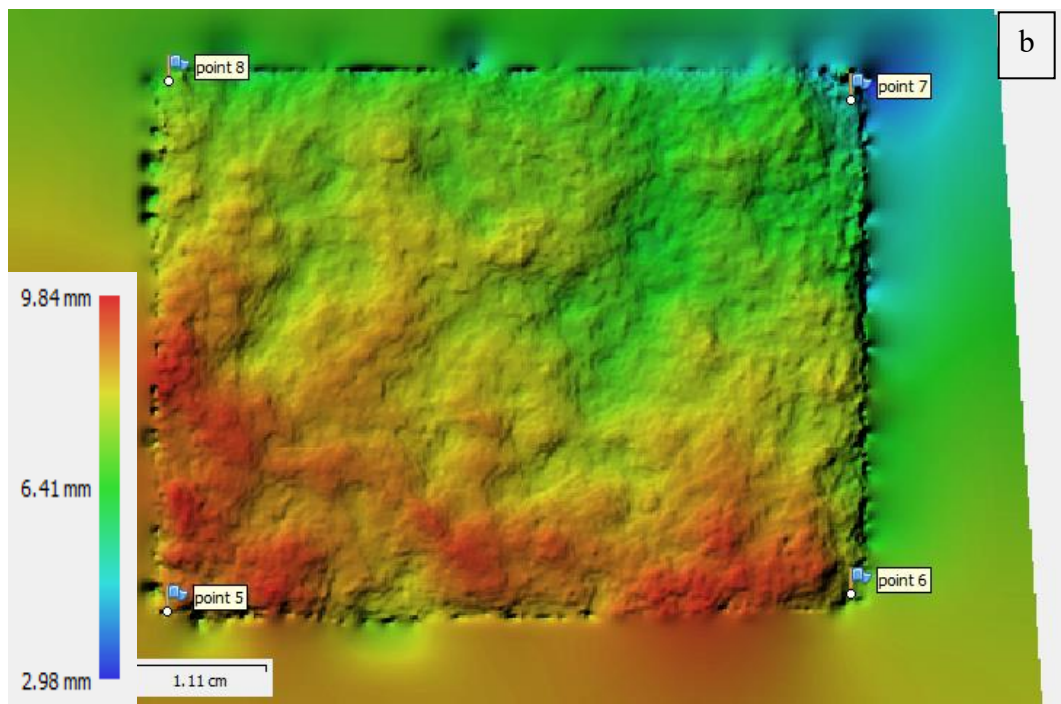
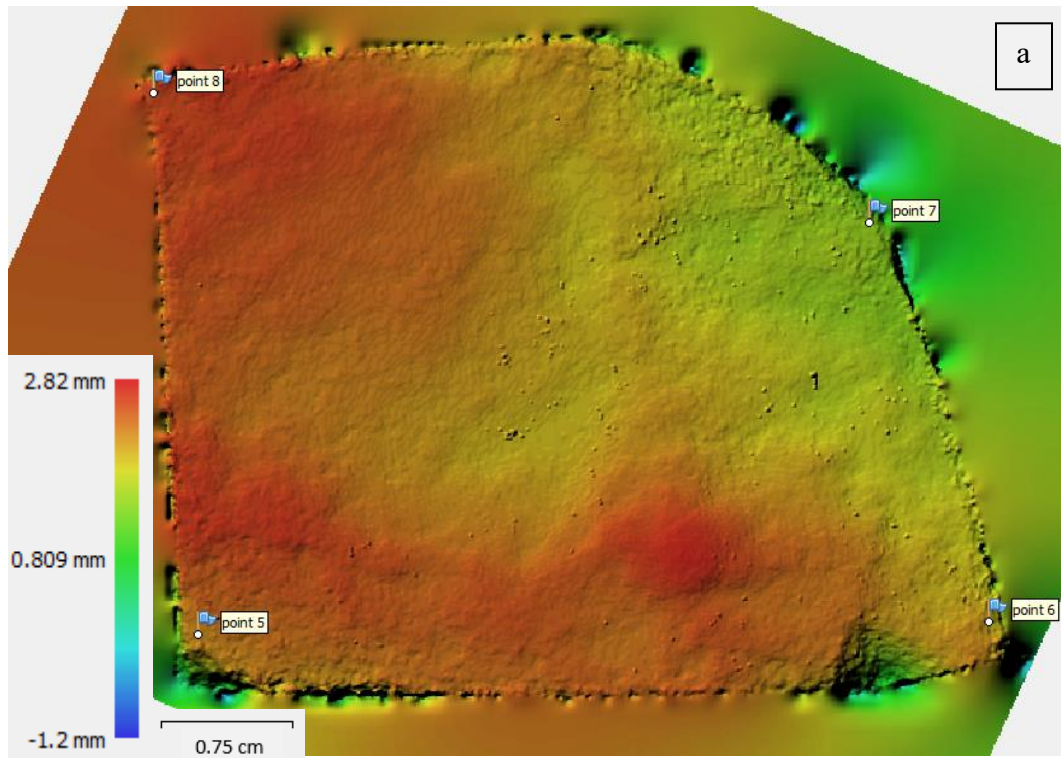


Figure 4.7. Digital elevation models of specimens; (a) specimen A, (b) specimen B

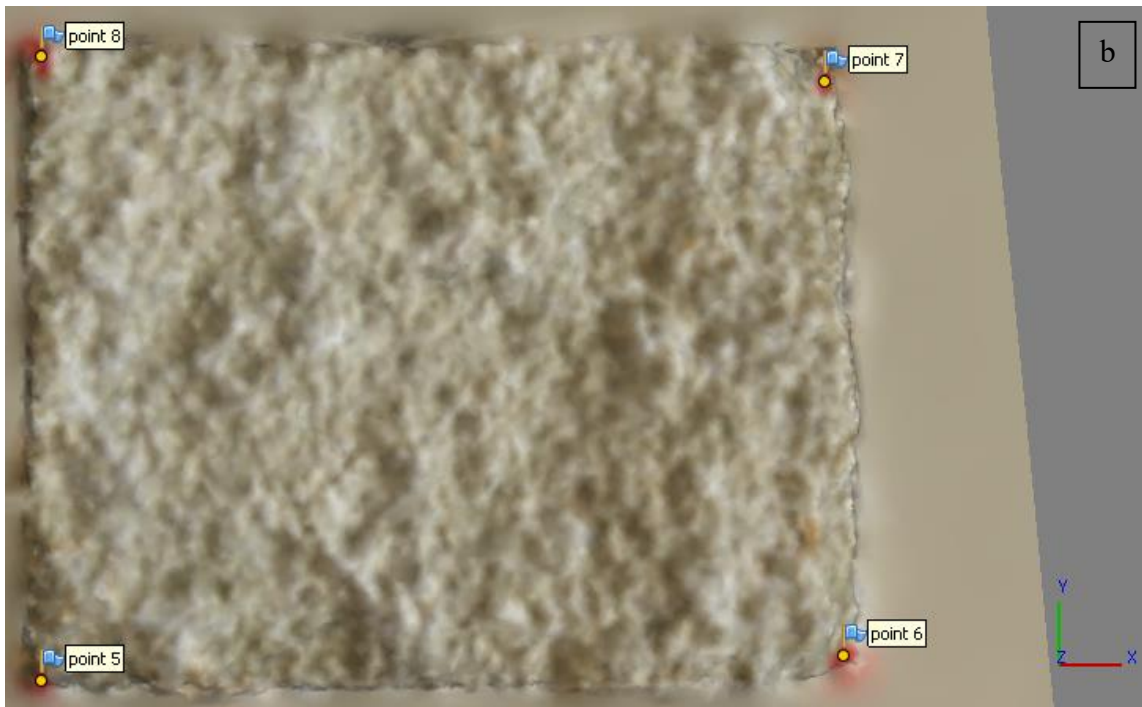
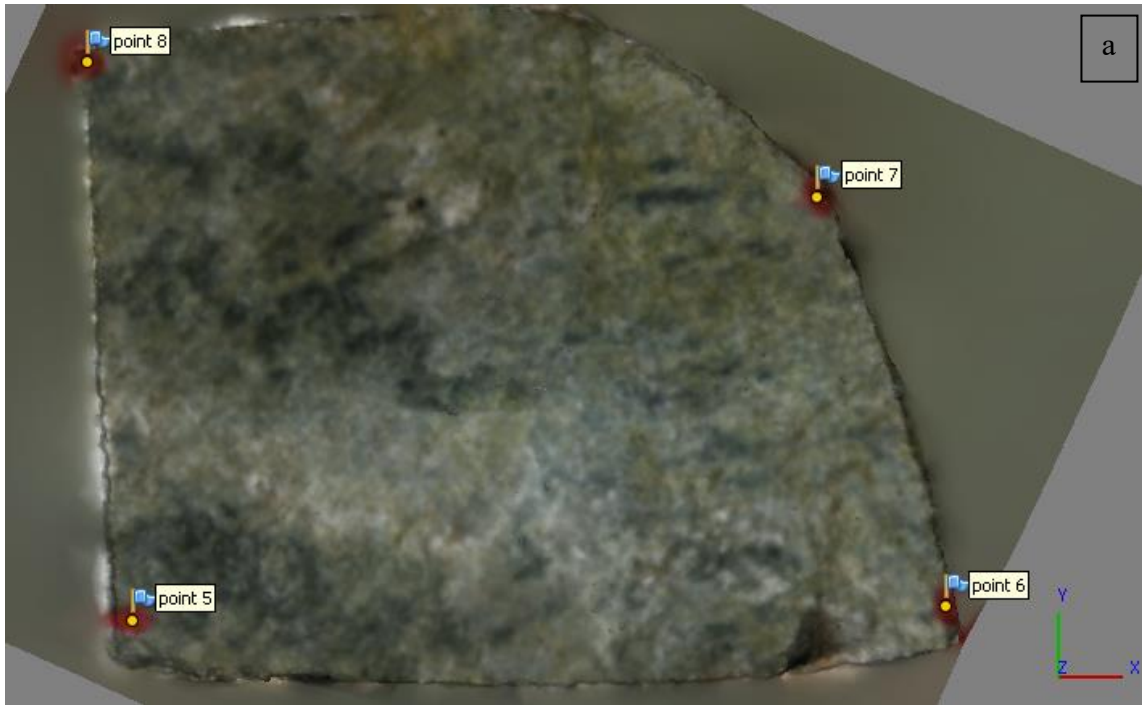


Figure 4.8. 3D models of specimens; (a) specimen A, (b) specimen B

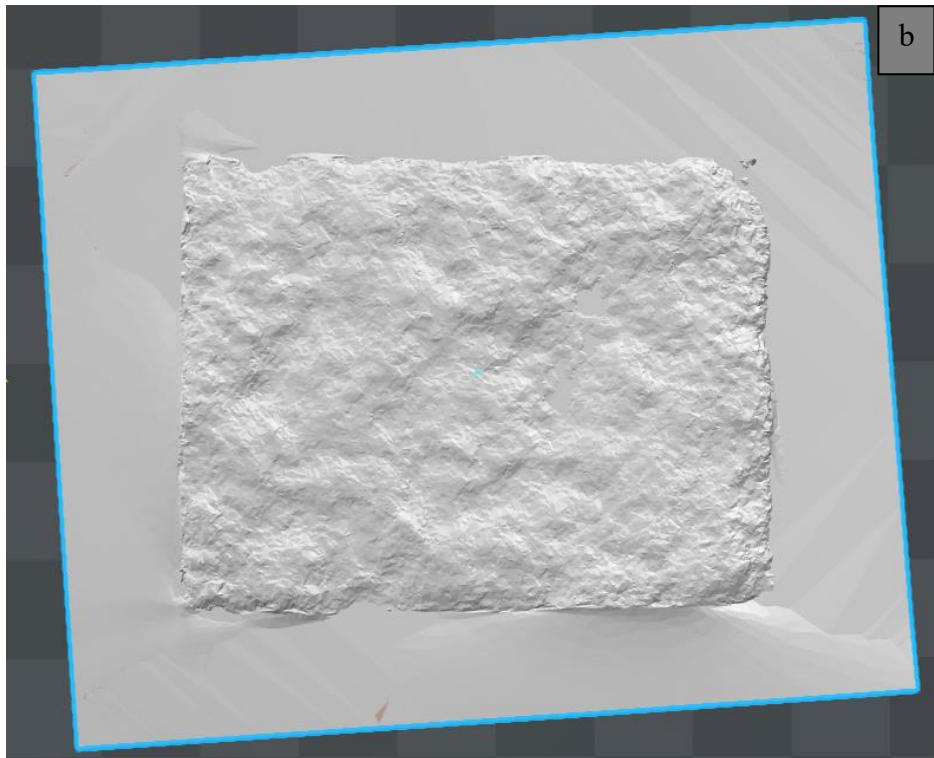
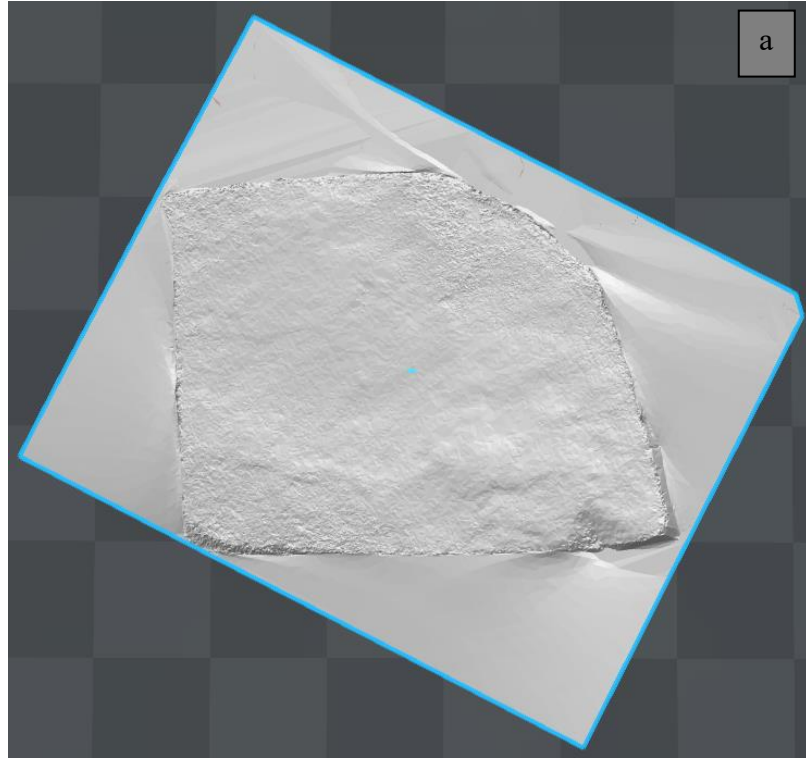


Figure 4.9 Exported 3D models (STL); (a) specimen A, (b) specimen B

4.3.Preparation of Rock Discontinuity Replicas

The photogrammetric analysis of the two rock discontinuity samples successfully resulted in 3D models of the surfaces of the discontinuities. These 3D models are used for producing two rock discontinuity replicas corresponding to two different roughness levels. For this purpose, only a specific part of the each discontinuity sample, shown in Figure 4.10, is used. Specified parts of the discontinuity samples on the 3D models are split, enlarged and distorted to become a rock discontinuity with the desired roughness levels and dimensions (20 cm x 20 cm) which is required by the 3D printing process.

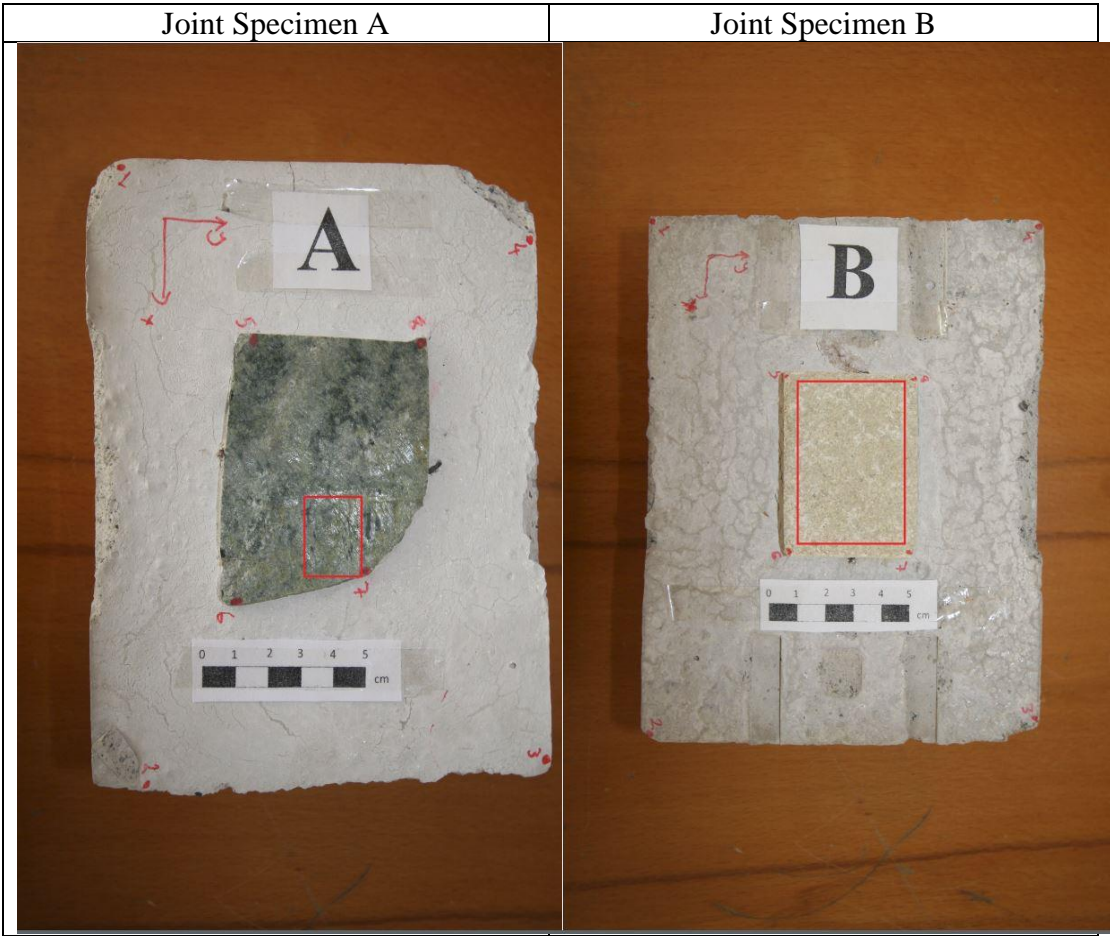


Figure 4.10. Modelled parts of the rock joint samples

The final 3D models to be used as rock discontinuity surface replicas in the next chapters are presented in Figure 4.11.

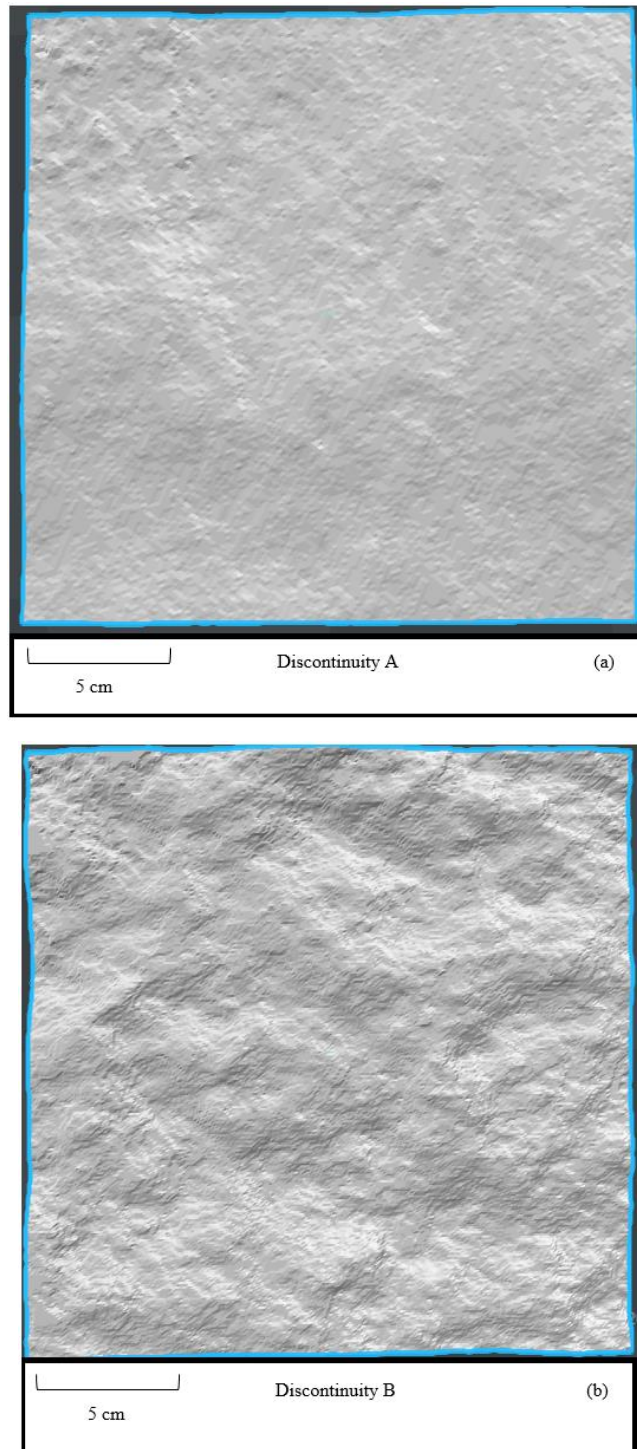


Figure 4.11. Replicated rock discontinuity surface models; (a) discontinuity A, (b) discontinuity B

CHAPTER 5

3D PRINTING AND ROUGHNESS MEASUREMENT OF ROCK DISCONTINUITY REPLICAS

In laboratory experiments conducted for the natural rock discontinuities, all test specimens are used only once and it is impossible to conduct experiments with the same surface morphology of the natural specimen. This phenomenon limits the experimental procedure dramatically, under conditions where it's necessary to investigate surface characteristics of the rock discontinuity with other varying conditions (normal stress, shear rate etc.). Therefore, replication of rock discontinuity specimens are needed. Various studies attempted to produce discontinuity replicates using silicon or aluminium moulds and concrete (e.g. Stimpson, 1970; Jafari et al., 2004; Roosta et al., 2006; Atapour and Moosavi, 2013; Jiang et al., 2016). In recent years, developments in 3D printing technology introduced a new way of producing rock discontinuity moulds with the same surface morphology at high precision levels. In this chapter, 3D printing of rock discontinuity models prepared with close-range digital photogrammetry is explained. Surface characteristics of the 3D models, moulds and cast concrete blocks are evaluated and compared in order to evaluate the accuracy of the method to reflect the original roughness degree.

5.1.Overview of 3D Printing Applications in Rock Mechanics

Applicability of 3D printers in rock mechanics is first analyzed by Jiang and Zhao (2014). Polylactic acid (PLA) is used as raw material. Uniaxial compressive strength and direct tensile strength tests were conducted on specimens printed by a 3D printer with fused deposition modelling technique, and the Young's modulus and Poisson's

ratio of the material were determined. The PLA samples exhibited elastic-plastic behavior in uniaxial compressive strength tests and elastic-brittle behavior in direct tensile strength tests. The mechanical properties of the printed test specimens have revealed that a more suitable printing material must be developed to better imitate rock behavior. However, Jiang and Zhao (2014) noted that future technological developments in 3D printing technology and raw materials can make this field more attractive for researchers in rock mechanics.

Fereshtenejad and Song (2016) investigated the effect of printing conditions such as printing direction, layer thickness and binding agent saturation level on 3D printed test samples. The samples obtained using a powder-based raw material exhibited low strength and flexible material behavior. They concentrated on methods that can make the samples behave like a rock by improving material properties. By testing the conditions mentioned above, they studied the uniaxial compressive strength and stress-strain behavior of the material. They obtained samples with low uniaxial compressive strength behaving like natural rock. Despite the success of these results, they emphasized the need for further developments in rock mechanics applications using the 3D printing technology.

Jiang et al. (2016) used molds produced with 3D printers to cast concrete test specimens. Thus, the natural discontinuity surface is formed in concrete samples in order to conduct direct shear test. With the 3D scanning method, the discontinuity surface was transferred to the computer environment and the point cloud was created. Later, 3D model of the surface was created from 3D point cloud with a CAD software. Polylactic acid (PLA) was used as raw material in 3D printer. Using PLA mould, concrete discontinuity blocks were cast. Direct shear tests were carried out on the concrete blocks. The normal stress and shear rates used in the experiment were 0.5 MPa and 0.01 mm / s, respectively. The deviation from the shear strength of the surface was determined as 4-6%. Deviations in the shear stresses of discontinuity surfaces simulated by other methods were between 8 and 20%. The study confirmed the success and promising future of 3D printer applications in rock mechanics.

5.2. 3D Printing of Rock Discontinuity Surface Replicas

The produced 3D models are printed out as solid objects with Ultimaker 2 Extended 3D printer. Polylactic acid (PLA) is used as raw material. The PLA is a biodegradable thermoplastic obtained from plant wastes such as corn starch and sugar cane. The PLA has several advantages over other plastics used in 3D printing. The PLA is a cheap, widely available environment-friendly material. In addition, the PLA is a more rigid material than Acrylonitrile Butadiene Styrene (ABS) which is another commonly used petroleum based 3D printing raw material.

Fused deposition modelling (FDM) technique is employed for printing. In FDM, raw material is melted at high temperature and extruded from a nozzle to form a section of 3D model as the material cools down and solidifies. This process is repeated layer by layer from bottom to top of the model (Ahn et al., 2009). Graphical explanation of working mechanism of FDM is presented in Figure 5.1.

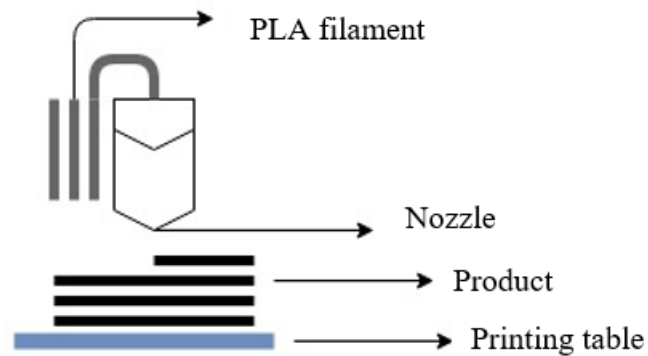


Figure 5.1. Fused deposition modelling (FDM) method in 3D printing

The 3D printed rock discontinuities are shown in Figure 5.2. These are later used as moulds to produce concrete discontinuity specimens in the next stages of the study.

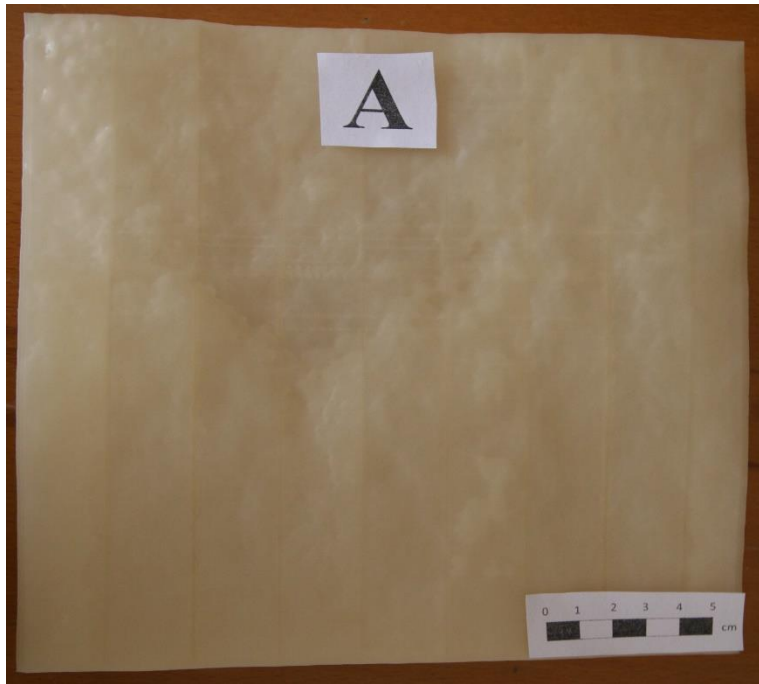


Figure 5.2. 3D printed rock discontinuity surface replicas

5.3. Dilation Angle of Rock Discontinuity Replicas

The surface topography of rock discontinuities consists of asperities which has significant influence on shear resistance of rock masses (Patton, 1966). When a shear stress applied on a rock joint, sliding along the surface occurs by climbing the asperities. Therefore, inclination angle of the asperities is a major factor controlling the shear behavior of the rock joints. Inclination angle, also referred as dilation angle, is denoted as i (Figure 5.3).

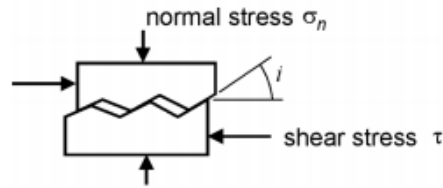


Figure 5.3. Dilation angle (i), retrieved from www.rocscience.com/documents/hoek/corner/05_Shear_strength_of_discontinuities.pdf

In this study, dilation angle is measured along the profiles taken at different angles throughout the surfaces. 18 cross-sections are taken on the constructed 3D models of artificial discontinuities, ranging from 0° to 180° . Cross-section lines are given in Figure 5.4. Cross-sections are taken at all directions, in order to estimate the overall roughness of the surface. Thus, roughness difference between two models can be observed.

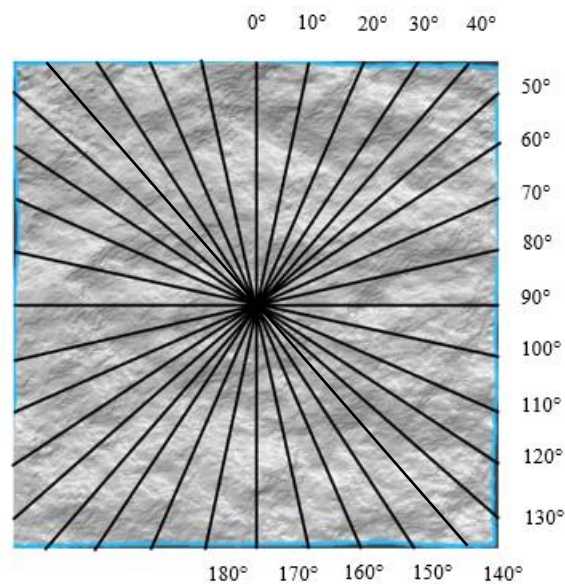


Figure 5.4. Position of crosssections along the discontinuity replicas (plan view)

The 3D models of the profiles of the both discontinuity replicas (Sample A and B) are imported to SketchUp Make 2017 software. Using the protractor tool of SketchUp, dilation angles are measured. Figure 5.5 presents the process of angle measurement on the discontinuity A's profile at 0°.

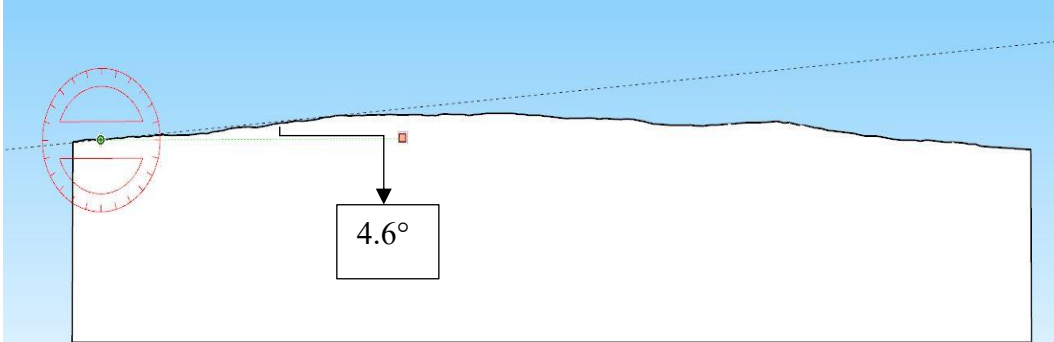


Figure 5.5. Angle measurement at SketchUp using protractor tool

Angle measurement results and descriptive statistics of the dilation angle for both discontinuities are given in Tables 5.1 and 5.2. The difference between the average dilation angles between two models confirms the preliminary assumption for the models to have two different roughness degrees before going into detailed roughness characterization study.

Table 5.1. Descriptive statistics of dilation angles for Discontinuity A

Profile Angle	i (1st)	i (2nd)	i (3rd)	Min.	Max.	Mean	Standard Deviation
A-0°	4.6			4.6	4.6	4.6	0.00
A-10°	2.5			2,5	2.5	2.5	0.0
A-20°	5.2	1.8		1.8	5.2	3.5	1.70
A-30°	3.2	2.5		2.5	3.2	2.9	0.35
A-40°	4.7	3		3	4.7	3.9	0.85
A-50°	3.8	4		3.8	4	3.9	0.10
A-60°	2.7	1.4	3.2	1.4	3.2	2.4	0.76
A-70°	3.1	3.9	6.2	3.1	6.2	4.4	1.31
A-80°	5,2	6.8	7.8	5.2	7.8	6.6	1.07
A-90°	5,3	5.3	4.5	4.5	5.3	5.0	0.38
A-100°	4.6	4.9	4.1	4.1	4.9	4.5	0.33
A-110°	6.3	3.8		3.8	6.3	5.1	1.25
A-120°	5	2.7		2.7	5	3.9	1.15
A-130°	7	2.2		2.2	7	4.6	2.40
A-140°	5.2	2.3		2.3	5.2	3.8	1.45
A-150°	5.3			5.3	5.3	5.3	0.00
A-160°	5.6			5.6	5.6	5.6	0.00
A-170°	5.2			5.2	5.2	5.2	0.00
AVERAGE						4.3	
St. Dev.						1.1	

The mean dilation angle for Discontinuity A is 4.3° and standard deviation is 1.1°. Therefore, it can be stated that the Discontinuity A represents a low roughness degree.

Table 5.2. Descriptive statistics of dilation angle for Discontinuity B

Profile Angle	i (1st)	i (2nd)	i (3rd)	i (4th)	i (5th)	Min.	Max.	Mean	Standard Deviation
B-0°	9.8	8.2	18.3	9.7	10.9	8.2	18.3	11.4	3.57
B-10°	17	17.4	20.6	9.5	12	9.5	20.6	15.3	4.00
B-20°	15	10	21.1	11.7	11.4	10	21.1	13.8	3.98
B-30°	10	12.6	8.3			8.3	12.6	10.3	1.77
B-40°	8	6.8	7.3	11	13	6.8	13	9.2	2.39
B-50°	15	15	13.1	15.8		13.1	15.8	14.7	0.99
B-60°	5.3	2	4	5.4	8.1	2	8.1	5.0	1.99
B-70°	11.8	9.1	3.5	8.8		3.5	11.8	8.3	3.01
B-80°	8.1	3.7	19.6	10.1		3.7	19.6	10.4	5.81
B-90°	15	16.5	6.6	15.8		6.6	16.5	13.5	4.00
B-100°	20.3	8.8	10.9	12.7	12.2	8.8	20.3	13.0	3.90
B-110°	13.4	15	10.7	10.9		10.7	15	12.5	1.79
B-120°	23.4	8.7	9.1	12.4	7.8	7.8	23.4	12.3	5.77
B-130°	15	5.6	9	10.3	10.6	5.6	15	10.1	3.03
B-140°	11.8	15	12.1	8.2		8.2	15	11.8	2.41
B-150°	9.3	13.1	8.7	10.6	10.2	8.7	13.1	10.4	1.51
B-160°	15	5.7	9.5	16.2		5.7	16.2	11.6	4.24
B-170°	7.7	9.1	8.7	8.4	13.8	7.7	13.8	9.5	2.18
AVERAGE								11.3	
St. Dev.								2.4	

The mean dilation angle of discontinuity B is 11.3° and the standard deviation is 2.4°. In addition, for discontinuity B, number of individual asperities is higher than discontinuity A, because of the rougher surface of the discontinuity B.

Therefore, it can be stated that Discontinuity B represents a high roughness degree. The difference between the dilation angle of the two discontinuities verifies the roughness differences of the two samples.

5.4. Roughness Characterization of the 3D Models of Discontinuity Surfaces

The shear behavior of rock discontinuities has been known to be influenced by several factors, among which roughness of the discontinuity surface has major significance. Quantifying the surface roughness of a rock joint widely accomplished by the ten standard rock joint profiles presented by Barton and Choubey (1977), each corresponding to a Joint Roughness Coefficient (JRC) value defined in the empirical shear strength criterion described by Barton (1973). Since JRC determination by standard profiles depends heavily on the subjective visual observation, many attempts

have been made to statistically determine JRC value. Tse and Cruden (1979) offered an empirical relationship (Eqn.1) between the Z_2 (root mean square of the first derivative of the profile), and JRC. In their study, JRC values of the two discontinuity surfaces are determined by Equation 8.

$$\text{JRC} = 32.2 + 32.47 \log Z_2 \quad (\text{Eqn. 8})$$

The 3D models of discontinuities are used for obtaining the amplitude values of several profiles taken along the direction of sliding. In order to have an accurate transition from Z_2 to JRC, number of profiles should be large enough to represent whole of the discontinuity surface. Workflow of determining Z_2 values are given in Figure 5.6.

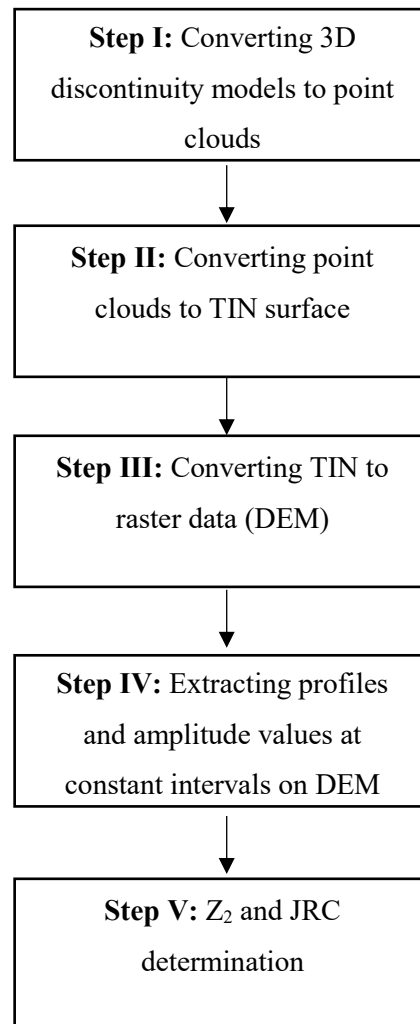


Figure 5.6. Workflow of Z_2 and JRC determination

Step I: 3D models of discontinuities (STL Files) are converted to point clouds using MeshLab software which assigns each point X and Y local coordinates and an elevation value corresponding to Z coordinate. The point cloud of the Discontinuity A consists of 19000 points, whereas the Discontinuity B's has 84000 points since Discontinuity B has a more irregular surface with large elevation differences.

Step II: The point clouds are imported to ArcGIS software. Triangular irregular networks (TIN) data are created using Create TIN tool of ArcGIS (Figures 5.8-5.10). The tool connects points to construct a network of triangles to represent surface morphology (ESRI, 2015). The highest elevation in the TIN and the 3D models are 40 mm, and the size of them are 20 cm x 20 cm (Figure 5.7).

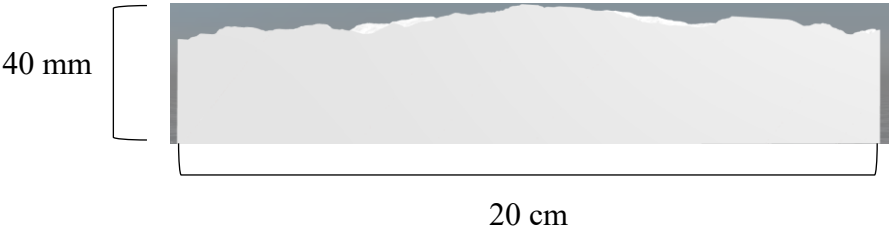


Figure 5.7. Reference level and size of the TIN and the 3D models

In order to investigate the size effect the large size samples (20 cm x 20 cm) are cut into four to obtain 10 cm x 10 cm four small size samples. These samples are named as B10-1, B10-2, B10-3 and B10-4 for Discontinuity B.

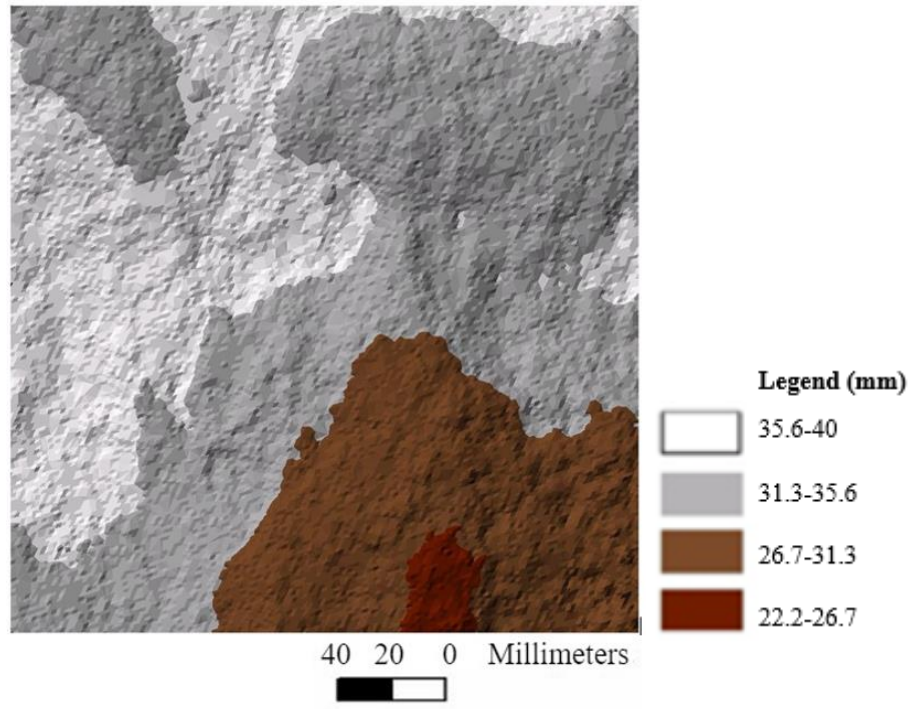


Figure 5.8. TIN of Discontinuity A

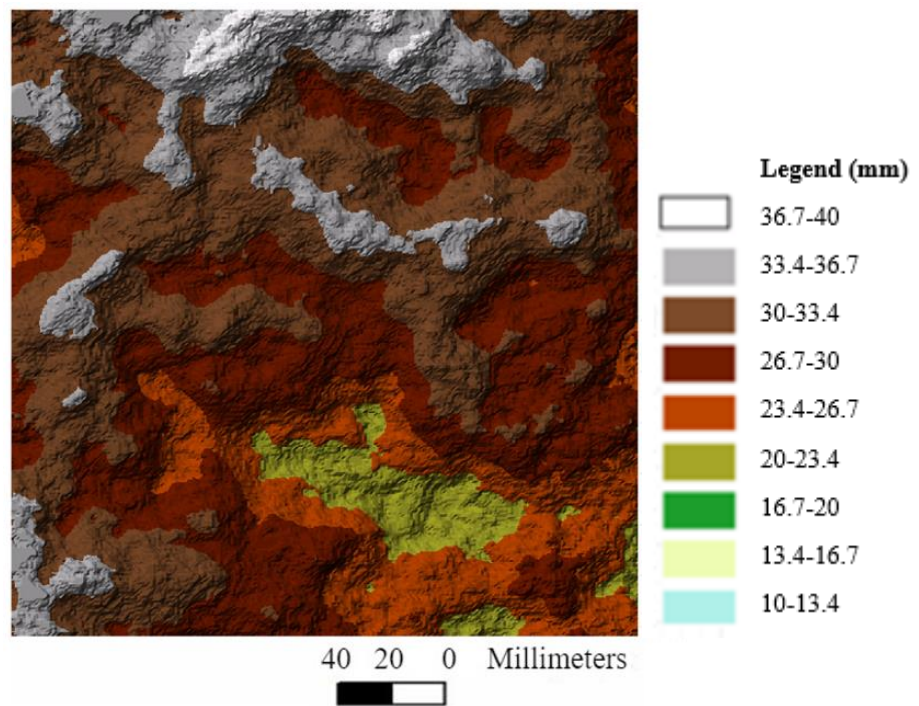


Figure 5.9. TIN of Discontinuity B

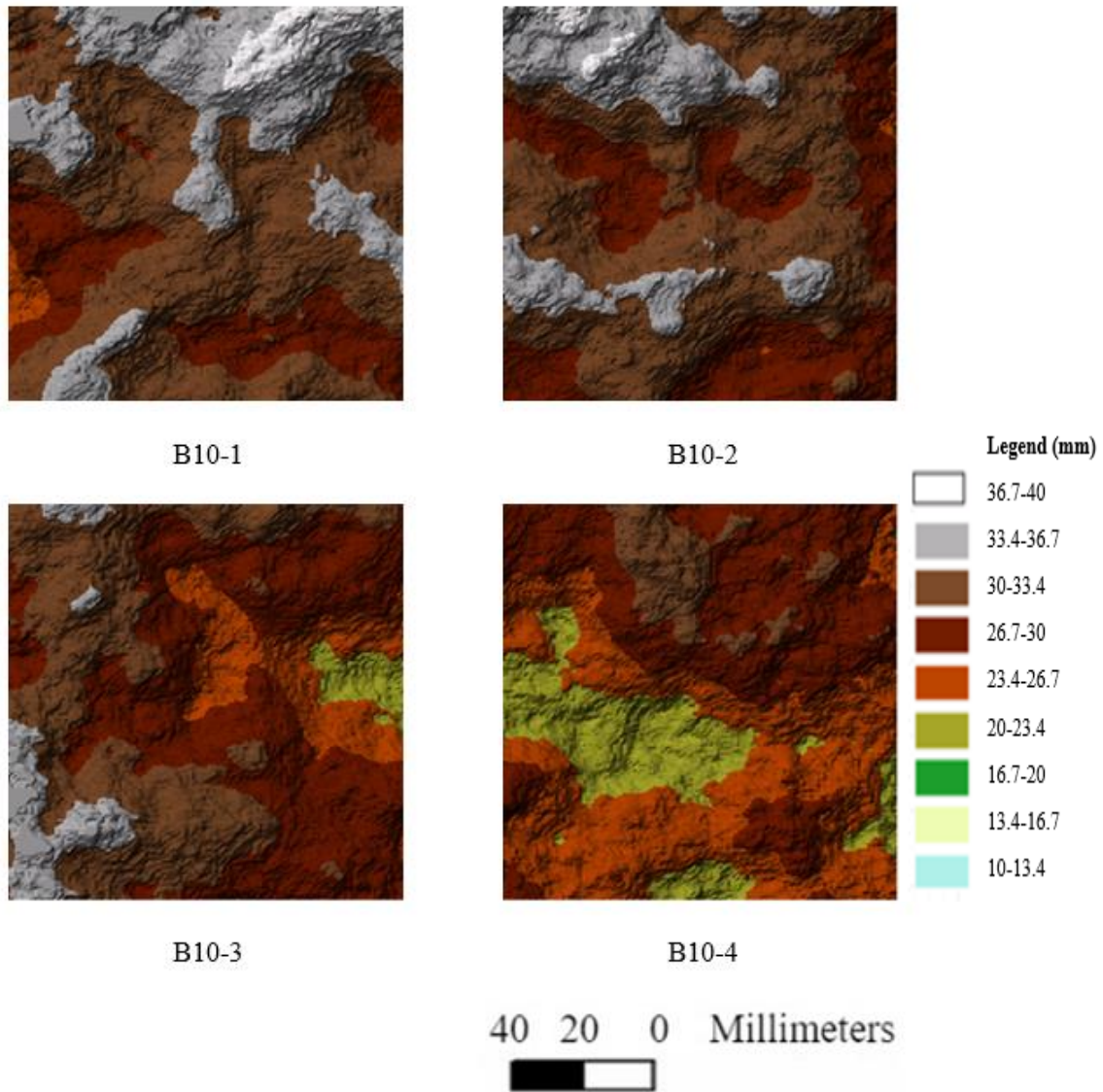


Figure 5.10. TIN of small size samples of Discontinuity B

Step III: The TIN data obtained in Step II are transformed to raster data using TIN to Raster tool of ArcGIS. A linear interpolation method is used to assign elevation values for cells in raster data. Resulting rasters are used as digital elevation models (DEM) for identifying amplitude values. Digital elevation models of discontinuities are shown in Figures 5.11-5.13.

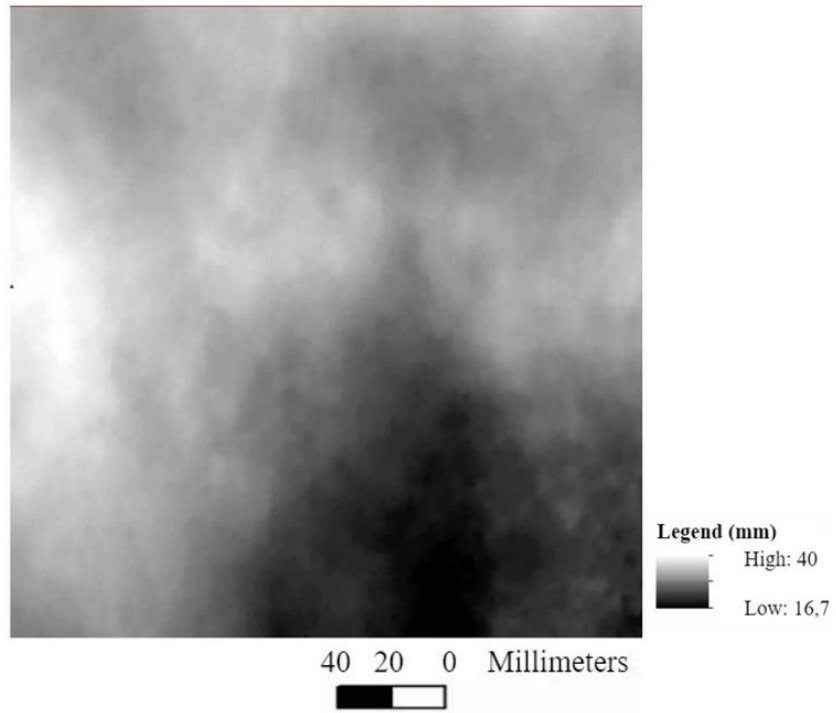


Figure 5.11. Digital Elevation Model of Discontinuity A

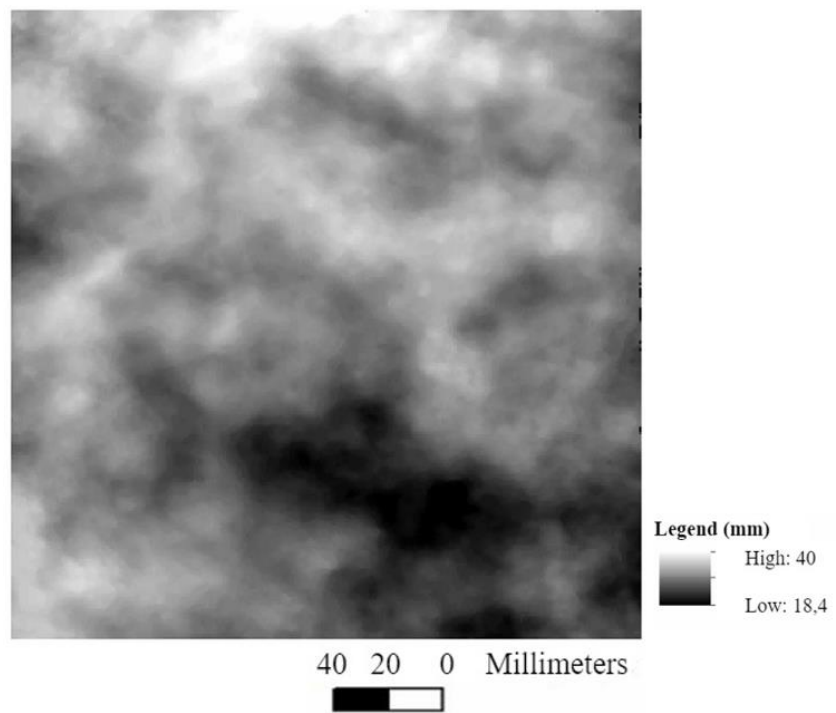


Figure 5.12. Digital Elevation Model of Discontinuity B

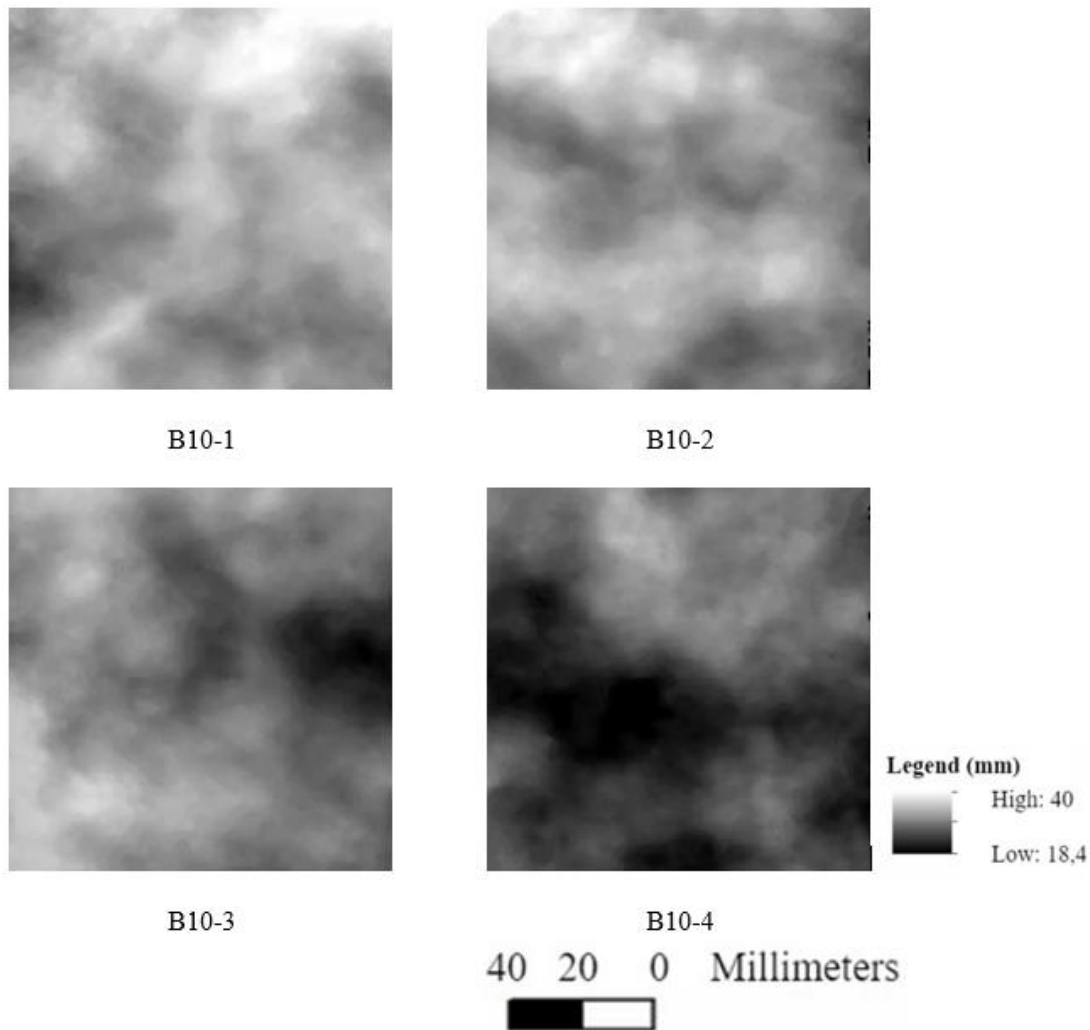


Figure 5.13. DEM of small size samples of Discontinuity B

Step IV: 11 profiles are extracted along the sliding direction using Stack Profile tool of ArcGIS. Figure 5.14 shows the lines used for specifying the profile paths. The lines start from lower end of the models (0 mm) with 20 mm intervals to the upper end of the models (200 mm). The stack profile tool provides a table or a graph denoting the profile of a line over a raster dataset (ESRI, 2015).

Amplitude values along the profiles are obtained at 1.27 mm intervals as proposed by Tse and Cruden (1979). Since the Stack Profile tool provide amplitude values at 0.8 mm intervals, linear interpolation is made to obtain amplitude values at required distances using Matlab.

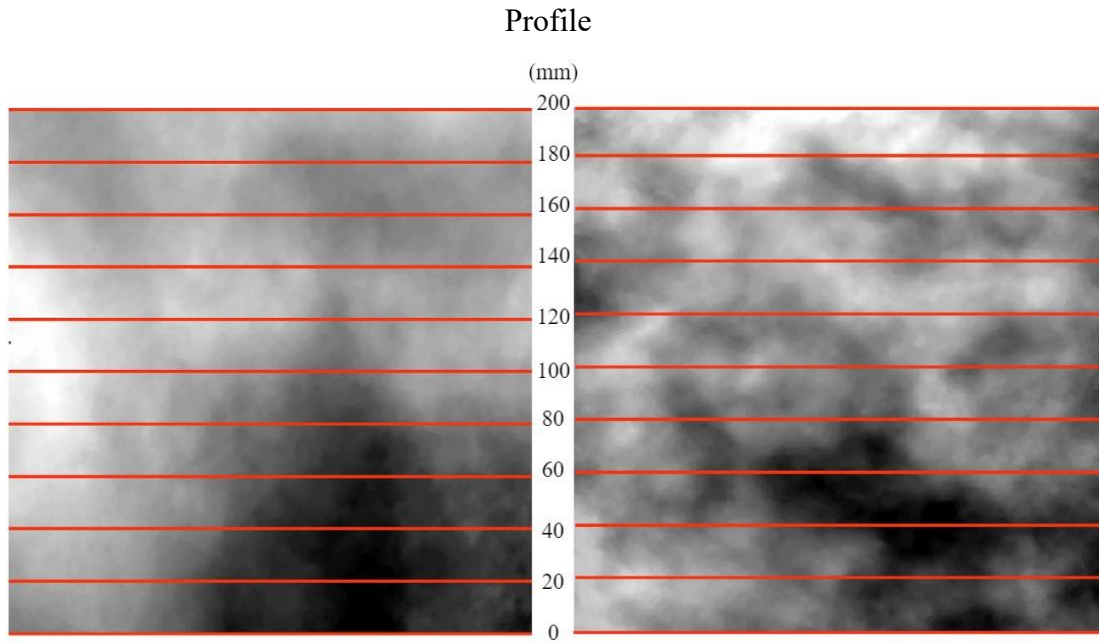


Figure 5.14. Profile Locations on Digital Elevation Models

Step V: Z_2 values are calculated using the amplitude values obtained in step IV. The methodology described by Tse and Cruden (1979) is employed. Z_2 equation in discrete form, which is used in this analysis, is given in Equation 9.

$$Z_2 = \left[\frac{1}{M(Dx)^2} \sum_{i=1}^M (y_{i+1} - y_i)^2 \right]^{1/2} \quad (\text{Eqn. 9})$$

Where M = Number of intervals

Dx = Constant distance between two adjacent amplitude readings

y = Amplitude of the roughness about the centreline

After calculating Z_2 , transition to JRC is completed using Equation 1. Results of the analysis are given in Table 5.3 and Table 5.4.

Table 5.3. Z_2 and JRC values of Discontinuity A and B

Profile	Discontinuity A		Discontinuity B	
	Z_2	JRC	Z_2	JRC
0	0.077	0.0	0.204	9.80
20	0.089	0.0	0.234	11.72
40	0.105	0.0	0.215	10.55
60	0.105	0.4	0.218	10.73
80	0.111	1.2	0.244	12.33
100	0.299	15.2	0.444	20.00
120	0.129	3.3	0.212	10.30
140	0.118	2.0	0.209	10.16
160	0.132	3.7	0.423	20.00
180	0.117	1.9	0.266	13.53
200	0.146	5.0	0.266	13.50
Mean	0.127	3.0	0.267	12.97
Standard Deviation	0.058	4.2	0.081	3.53

Table 5.4. Z_2 and JRC values of small size samples of Discontinuity B

Profile	B10-1		B10-2	
	Z_2	JRC	Z_2	JRC
100	0.370	18.28	0.532	20.00
120	0.447	20.00	0.257	13.12
140	0.347	17.39	0.481	20.00
160	0.448	20.00	0.454	20.00
180	0.454	20.00	0.622	20.00
200	0.424	20.00	0.694	20.00
Mean	0.415	19.47	0.507	18.85
Standard Deviation	0.041	1.23	0.138	2.57

Profile	B10-3		B10-4	
	Z_2	JRC	Z_2	JRC
0	0.386	18.87	0.544	20.00
20	0.374	18.43	0.466	20.00
40	0.461	20.00	0.342	17.15
60	0.518	20.00	0.335	16.89
80	0.480	20.00	0.506	20.00
100	0.370	18.28	0.532	20.00
Mean	0.431	19.26	0.454	19.01
Standard Deviation	0.058	0.76	0.085	1.14

The mean JRC values for small size samples of Discontinuity B are 19.47, 18.85, 19.26 and 19.01, respectively. Degree of roughness increases significantly as the sample size decreases.

5.5. Roughness Characterization of the PLA Moulds and the Concrete Samples

The 3D models are used for obtaining the PLA moulds and using the PLA moulds, concrete test samples are produced. Therefore, the 3D models, the PLA moulds and the concrete test samples are expected to have similar Z_2 values. In order to validate the applicability of the methodology for replicating test samples, Z_2 values of the PLA moulds and the concrete test samples are computed and compared with the Z_2 of the 3D models. For this purpose, the 3D models of the PLA moulds and the concrete test samples are produced with close range digital photogrammetry using the same methodology described in Chapter 4.

The dense point clouds obtained as the result of photogrammetric analysis are given in Figure 5.15.

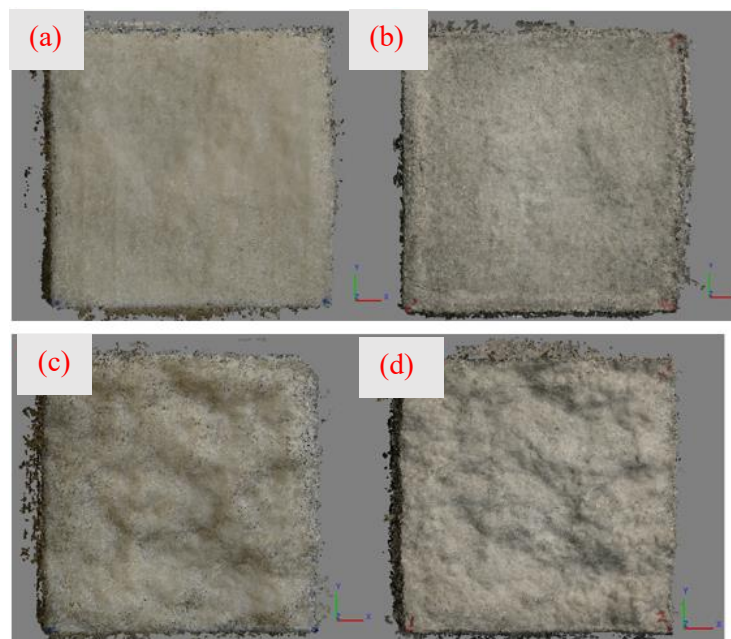


Figure 5.15. The dense clouds, (a): The PLA of Discontinuity A, (b): The concrete sample of Discontinuity A, (c): The PLA of Discontinuity B, (d): The concrete sample of Discontinuity B

The dense clouds are converted to the 3D models (STL files). Then, the STL files are converted to point clouds in MeshLab and the point clouds are imported to ArcGIS software where digital elevation models are created and amplitude values for the selected profiles are exported. The DEM's for the PLA moulds and the concrete test samples for the Discontinuities A and B are given in Figure 5.16 and 5.17, respectively.

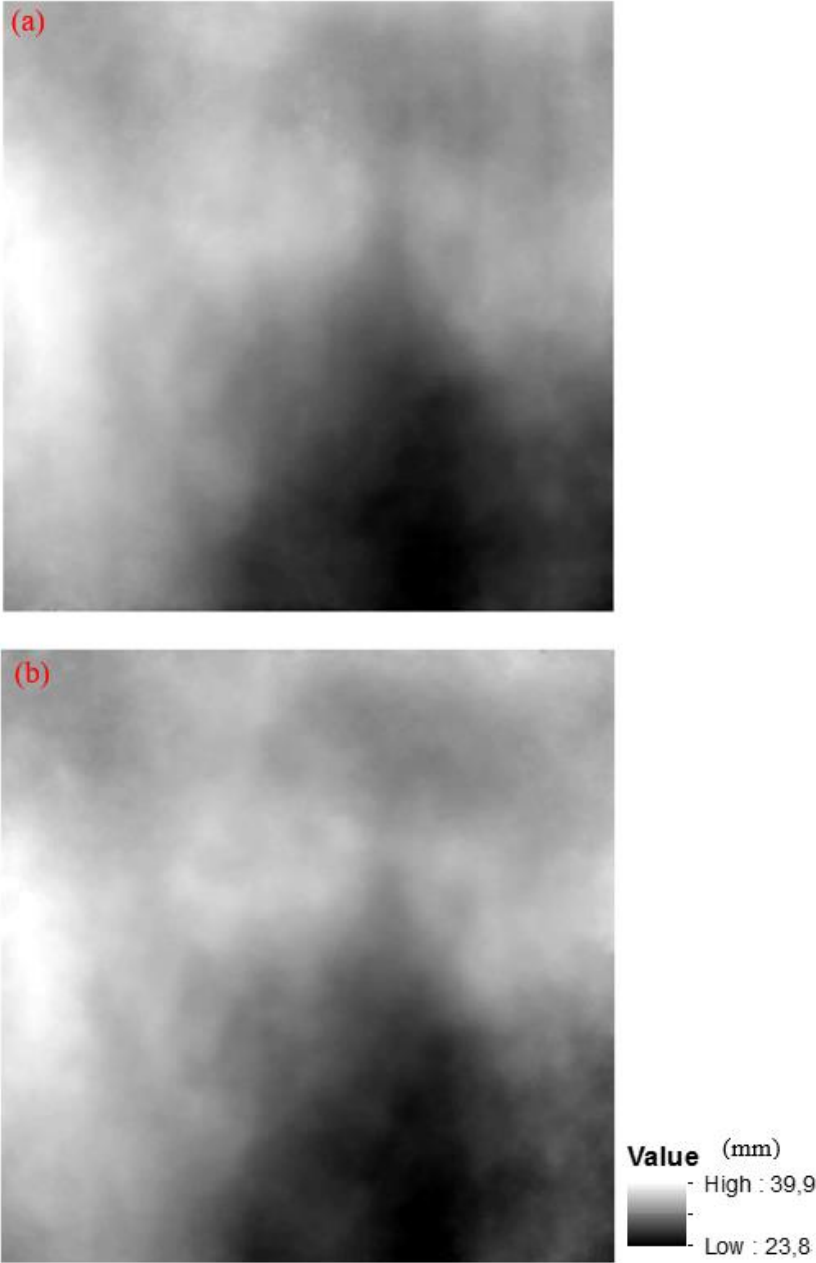


Figure 5.16. The DEM of the Discontinuity A, (a): PLA mould, (b): Concrete test sample

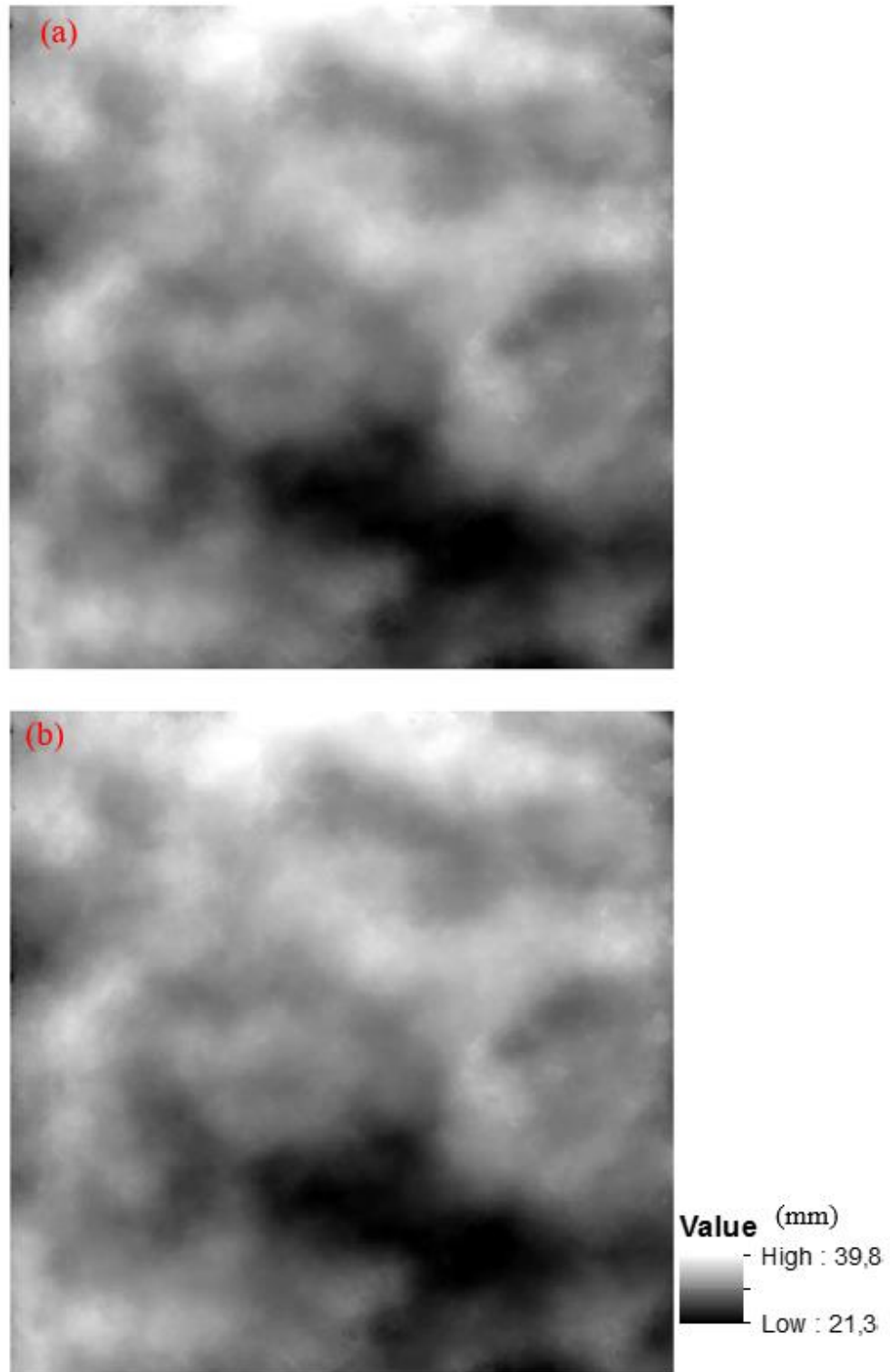


Figure 5.17. The DEM of the Discontinuity B, (a): PLA mould, (b) Concrete test sample

The DEM's of small size samples for the Discontinuity B are also obtained for the PLA moulds and the concrete test samples as given in Figure 5.18 and 5.19.

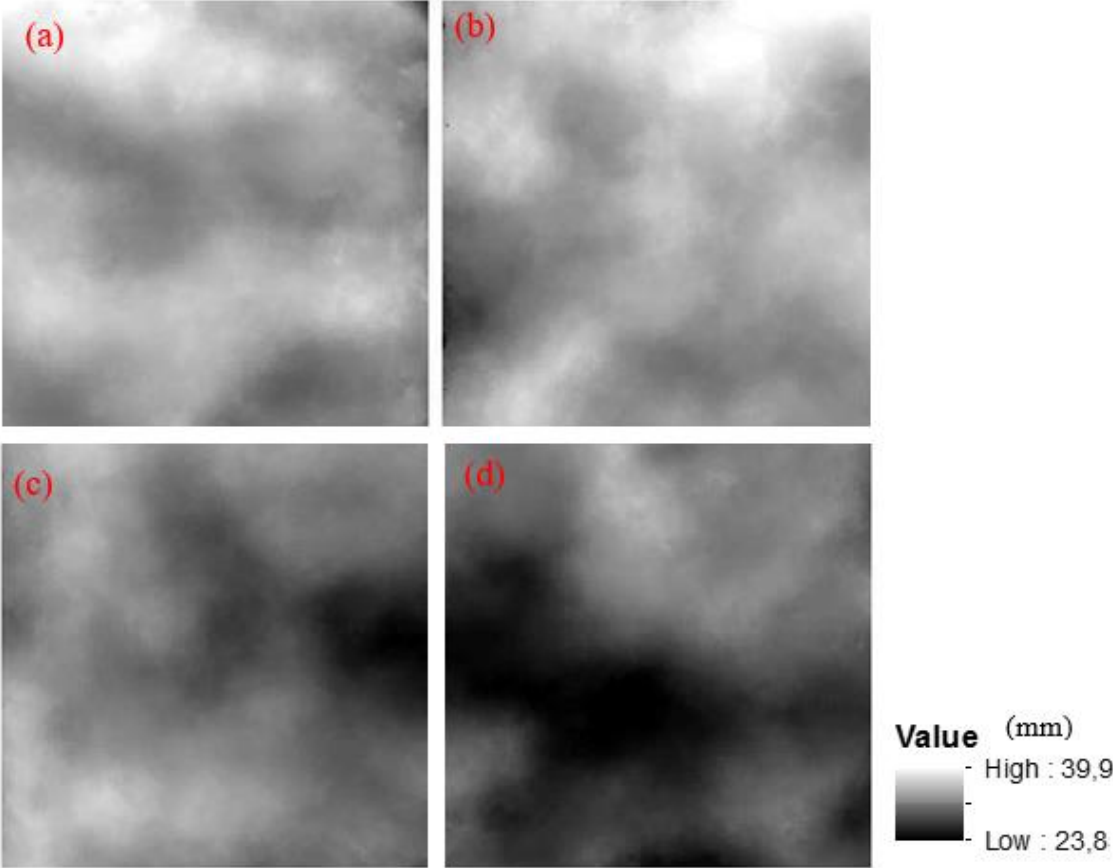


Figure 5.18. The DEM's for the PLA moulds, (a): B10-1, (b): B10-2, (c): B10-3, (d): B10-4

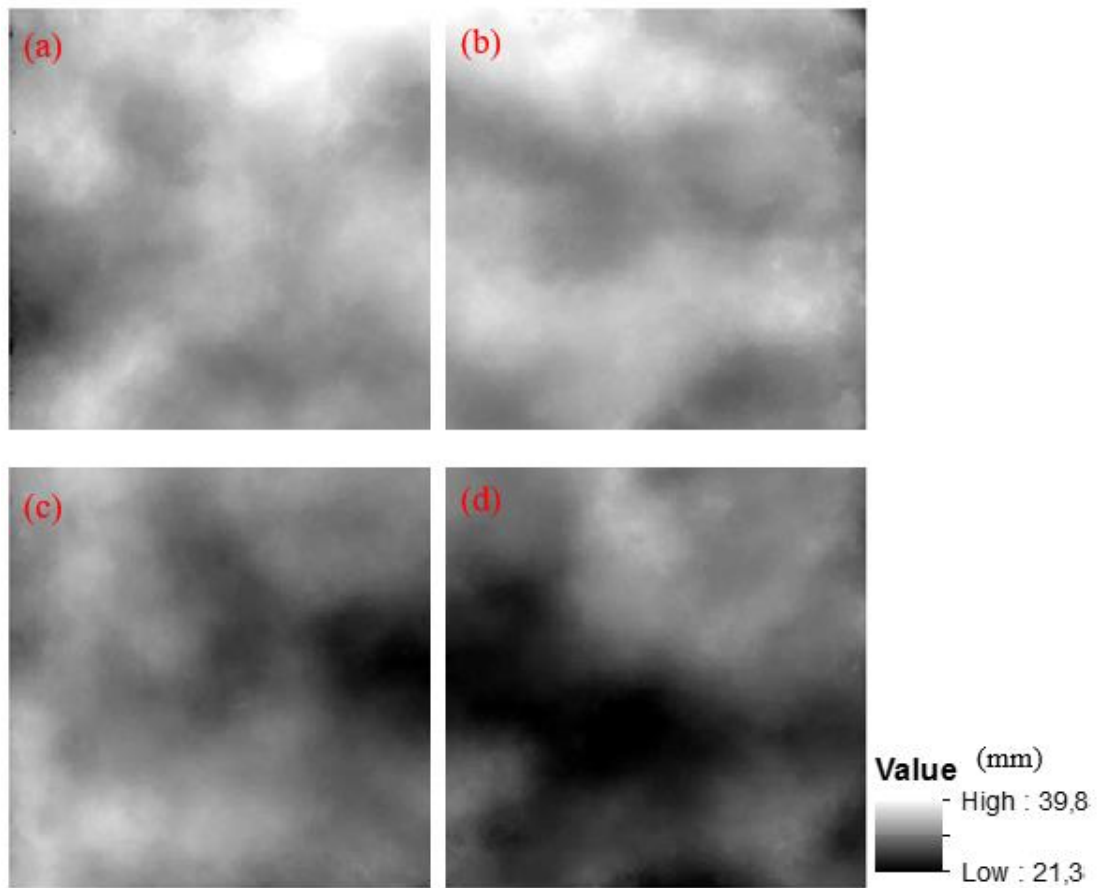


Figure 5.19. The DEM's for the concrete test samples, (a): B10-1, (b): B10-2, (c): B10-3, (d): B10-4

The Z_2 and JRC values for all the PLA moulds and the concrete test samples are given in Tables 5.5-5.8.

Table 5.5. Z_2 and JRC values of PLA moulds of Discontinuities A and B

Profile	PLA Mould Discontinuity A		PLA Mould Discontinuity B	
	Z_2	JRC	Z_2	JRC
0	0.077	0.0	0.199	9.47
20	0.081	0.0	0.197	9.27
40	0.089	0.0	0.158	6.16
60	0.091	0.0	0.193	9.01
80	0.097	0.0	0.208	10.10
100	0.110	1.03	0.197	9.30
120	0.110	1.07	0.311	15.72
140	0.103	0.17	0.170	7.25
160	0.106	0.56	0.161	6.45
180	0.102	0.0	0.209	10.11
200	0.133	3.78	0.286	14.56
Mean	0.100	0.60	0.208	9.77
Standard Deviation	0.015	0.06	0.046	2.86

The JRC values of the PLA moulds for the Discontinuities A and B are, 0.60 and 9.77, respectively. The JRC values are lower than that of 3D models for both discontinuity samples.

Table 5.6. Z_2 and JRC values of concrete samples of Discontinuities A and B

Profile	Concrete Sample Discontinuity A		Concrete Sample Discontinuity B	
	Z_2	JRC	Z_2	JRC
0	0.113	1.45	0.199	9.47
20	0.084	0.0	0.196	9.28
40	0.098	0.0	0.158	6.16
60	0.102	0.0	0.193	9.00
80	0.111	1.20	0.208	10.10
100	0.120	2.35	0.197	9.30
120	0.135	3.99	0.356	17.66
140	0.123	2.69	0.170	7.25
160	0.117	1.97	0.161	6.45
180	0.115	1.69	0.208	10.11
200	0.151	5.52	0.286	14.56
Mean	0.115	1.90	0.212	11.71
Standard Deviation	0.017	1.65	0.056	3.25

The JRC values of the concrete samples for the Discontinuities A and B are, 1.90 and 11.71, respectively. JRC values are higher than that of the PLA moulds and lower than that of the 3D models.

Table 5.7. Z_2 and JRC values of PLA moulds of Discontinuities B10-1, B10-2, B10-3, B10-4

Profile	PLA Mould Discontinuity B10-1		PLA Mould Discontinuity B10-2	
	Z_2	JRC	Z_2	JRC
100	0.309	15.76	0.479	20.00
120	0.456	20.00	0.227	11.37
140	0.228	11.42	0.401	19.42
160	0.375	18.48	0.204	9.88
180	0.512	20.00	0.386	18.87
200	0.571	20.00	0.652	20.00
Mean	0.408	17.61	0.391	16.59
Standard Deviation	0.118	3.15	0.152	4.26

Profile	PLA Mould Discontinuity B10-3		PLA Mould Discontinuity B10-4	
	Z_2	JRC	Z_2	JRC
0	0.267	13.68	0.582	20.00
20	0.284	14.53	0.515	20.00
40	0.363	18.01	0.175	7.73
60	0.542	20.00	0.279	14.32
80	0.441	20.00	0.472	20.00
100	0.309	15.76	0.479	20.00
Mean	0.368	17.00	0.417	17.01
Standard Deviation	0.097	2.51	0.142	4.64

The JRC values for the PLA moulds of B10-1, B10-2, B10-3, B10-4 are 17.61, 16.59, 17.00 and 17.01, respectively. The JRC values are lower than that of 3D models for all discontinuity samples.

Table 5.8. Z_2 and JRC values of concrete samples of Discontinuities B10-1, B10-2, B10-3, B10-4

Profile	Concrete Sample Discontinuity B10-1		Concrete Sample Discontinuity B10-2	
	Z_2	JRC	Z_2	JRC
100	0.309	15.76	0.382	18.66
120	0.443	20.00	0.386	18.66
140	0.228	11.42	0.341	17.09
160	0.375	18.48	0.290	14.86
180	0.512	20.00	0.385	18.87
200	0.482	20.00	0.395	19.02
Mean	0.391	17.61	0.361	17.09
Standard Deviation	0.099	3.15	0.036	1.49

Profile	Concrete Sample Discontinuity B10-3		Concrete Sample Discontinuity B10-4	
	Z_2	JRC	Z_2	JRC
0	0.267	13.68	0.582	20.00
20	0.284	14.53	0.515	20.00
40	0.363	18.01	0.175	7.73
60	0.542	20.00	0.279	14.32
80	0.441	20.00	0.472	20.00
100	0.309	15.76	0.479	20.00
Mean	0.368	17.00	0.416	17.01
Standard Deviation	0.097	2.51	0.142	4.64

The JRC values for the concrete samples of B10-1, B10-2, B10-3, B10-4 are 17.61, 17.09, 17.00 and 17.01, respectively. The JRC values for the concrete samples are higher than that of the PLA moulds and lower than that of the 3D models for all discontinuity samples.

The Z_2 and the JRC values of the 3D models and the concrete samples are significantly close to each other. For Discontinuity A, Z_2 value of the concrete sample is 90% of the 3D model and for Discontinuity B, Z_2 value of the concrete sample is 80% of the 3D model. Therefore, it's concluded that methodology is successful enough to be applied in this study, although there is a small amount of loss of the roughness degree in terms of Z_2 and JRC in the concrete samples from that of the original discontinuity surfaces.

CHAPTER 6

THE EXPERIMENTAL SETUP

In order to obtain estimates of shear strength of the rock discontinuities, direct shear tests are conducted. Generally, direct shear tests are conducted with a constant normal load boundary condition, which is applicable for a broad range of engineering cases. However, this boundary condition may not be suitable for every problem like around an underground excavation in which normal stress changes as the sliding continues. In this case, normal stiffness boundary condition becomes more appropriate. In constant normal loading conditions, several experiments should be carried out with different normal stress magnitudes on samples from the same discontinuity to determine the shear strength (Muralha et al., 2014).

The direct shear test equipments generally include a stiff testing system which allows shear displacement with a constant rate without distortion, a specimen holder such as a shear box in which lower and upper blocks are placed, loading devices which apply normal and shear loads at an appropriate rate, and devices to measure stresses and displacements (Figure 6.1) (Muralha et al., 2014).

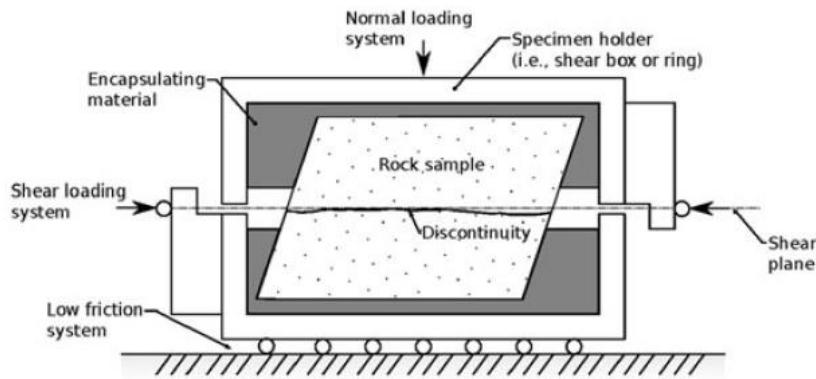


Figure 6.1. Arrangement of a direct shear test equipment (Retrieved from Muralha et al., 2014)

Accurate estimates of the shear strength requires experiments to be conducted on large numbers of discontinuity samples. However, obtaining discontinuity samples in the field is a challenging and costly task. Also, no two samples have the same surface characteristic even if they are from the same discontinuity. Therefore, replicating discontinuity samples that possess the same surface morphology has been seen as an important goal by many researchers in rock mechanics. Replicating discontinuity samples would make it possible to conduct roughness level controlled direct shear tests under different normal loads or other variables. Consequently, the impact of the roughness on the shear strength can be better investigated. Recent technological developments in 3D printing technology has opened paths for developing efficient methodologies to replicate discontinuity samples.

In this study, concrete discontinuity samples are produced using the 3D printed model of discontinuities as mould. Then, direct shear tests are conducted on these samples in the Rock Mechanics Laboratory of Mining Engineering Department at METU.

6.1. The Sample Preparation

The discontinuity test samples are prepared as concrete blocks which represent the surfaces of two discontinuity models prepared previously. First of all, the PLA moulds are used for casting concrete moulds. Because of the fact that surfaces of the PLA moulds could be damaged with daily concrete casting procedure, they are replaced with concrete moulds. Since only lower parts of the discontinuities are 3D printed,

firstly PLA mould are used for casting upper mould. Then upper mould is used for casting the lower mould which has the same surface with the PLA mould. These moulds are re-casted if the surfaces of the old ones wear, so that roughness levels of test samples are not affected. The concrete mould casting procedure involves five steps (Figure 6.2). Steps; (1): Placing the PLA moulds in iron boxes and pouring the cement mix, (2): Taking out upper concrete mould, (3): Placing the upper concrete mould in the iron box and pouring the cement mix, (4) Taking out lower concrete mould, (5) Obtaining the upper and the lower concrete moulds.

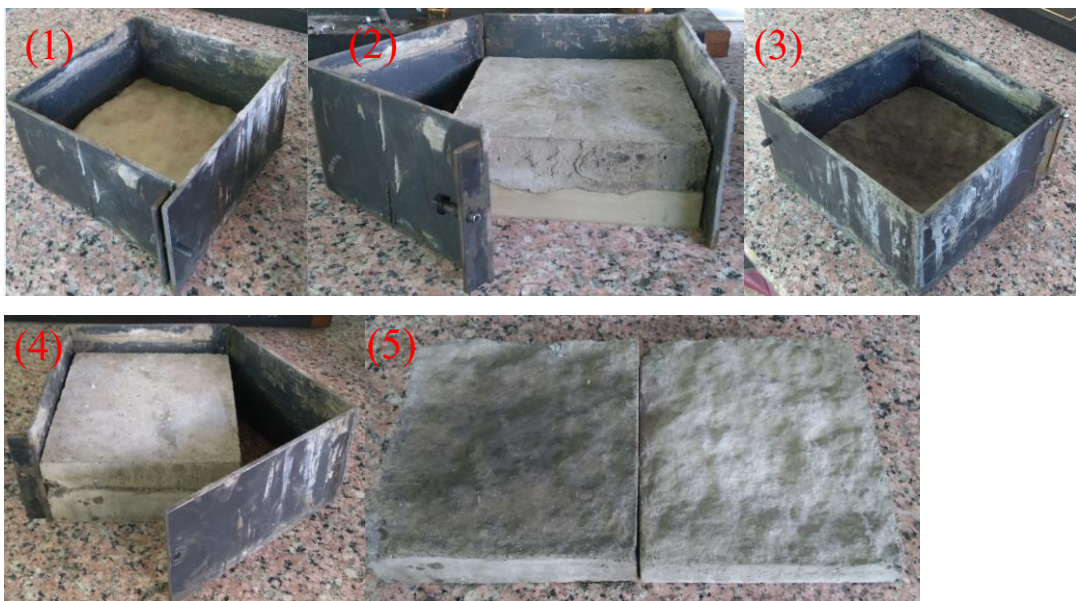


Figure 6.2. Concrete mould casting procedure

In order to cast concrete test samples, cement mix is prepared with the cement:sand:water ratio of 1:1:0.5 by weight. Particle size of the sand is < 3.0 mm. Moulds are placed in iron boxes, then the cement is poured. After one day, the test sample is taken out of the box. In order to prepare 10 cm x 10 cm samples, concrete blocks are cut into four parts. Then, upper and lower parts of a test sample is tied together with wire. Since the dimensions of the test samples (20 cm x 20 cm and 10 cm x 10 cm) are different from the size of the shear box (30 cm x 30 cm), they are placed in another iron box (30 cm x 30 cm) to cast an outer frame for the test samples.

Outer frame for the lower part is casted first and that of the upper part is casted the following day (Figure 6.3). After that, test specimens are left for setting. Total setting time for test specimens is seven days. The test samples are also produced with a cement mix prepared with -1.0 mm sand. However, direct shear tests conducted with these samples showed residual behavior. In other words, since the material was so weak, its peak and residual shear strength values were the same, which generally not observed for a rock-type material. Therefore, testing samples are prepared with the -3.0 mm sand. Particle size distribution of the sand is not considered, which may be another important factor to affect the behavior of the material. The sample preparation steps are; (1):Placing the concrete moulds in the iron boxes, (2)Pouring the cement mix in the iron boxes, (3)Taking out the test specimens from the iron boxes, (4) Detaching the test samples from the moulds, (5) Attaching the upper and the lower blocks of a sample together with wire, (6) Preparing 30 cm x 30 cm iron boxes for casting frame, (7) Pouring the cement mix for the lower frame, (8) Pouring the cement mix for the upper frame.

Preparation of 10 cm x 10 cm test samples starts with casting a 20 cm x 20 cm specimen as explained previously. Then, it's cut into four equal parts, each had dimensions of 10 cm x 10 cm. Further steps includes the casting of concrete frame with 30 cm x 30 cm iron boxes (Figure 6.4). Photographs of samples before the experiments are given in Figures 6.5-6.10. The 10 cm x 10 cm sample preparation steps are; (1) Placing concrete moulds in iron boxes, (2) Pouring the cement mix in the iron boxes, (3) Taking out the test specimens and marking, (4) Cutting specimens in four equal parts, (5) Attaching upper and lower parts of each specimen with wire, (6) Preparing 30 cm x 30 cm iron boxes for casting concrete frame, (7) Pouring the cement mix for the lower frame, (8) Pouring cement mix for the upper frame.

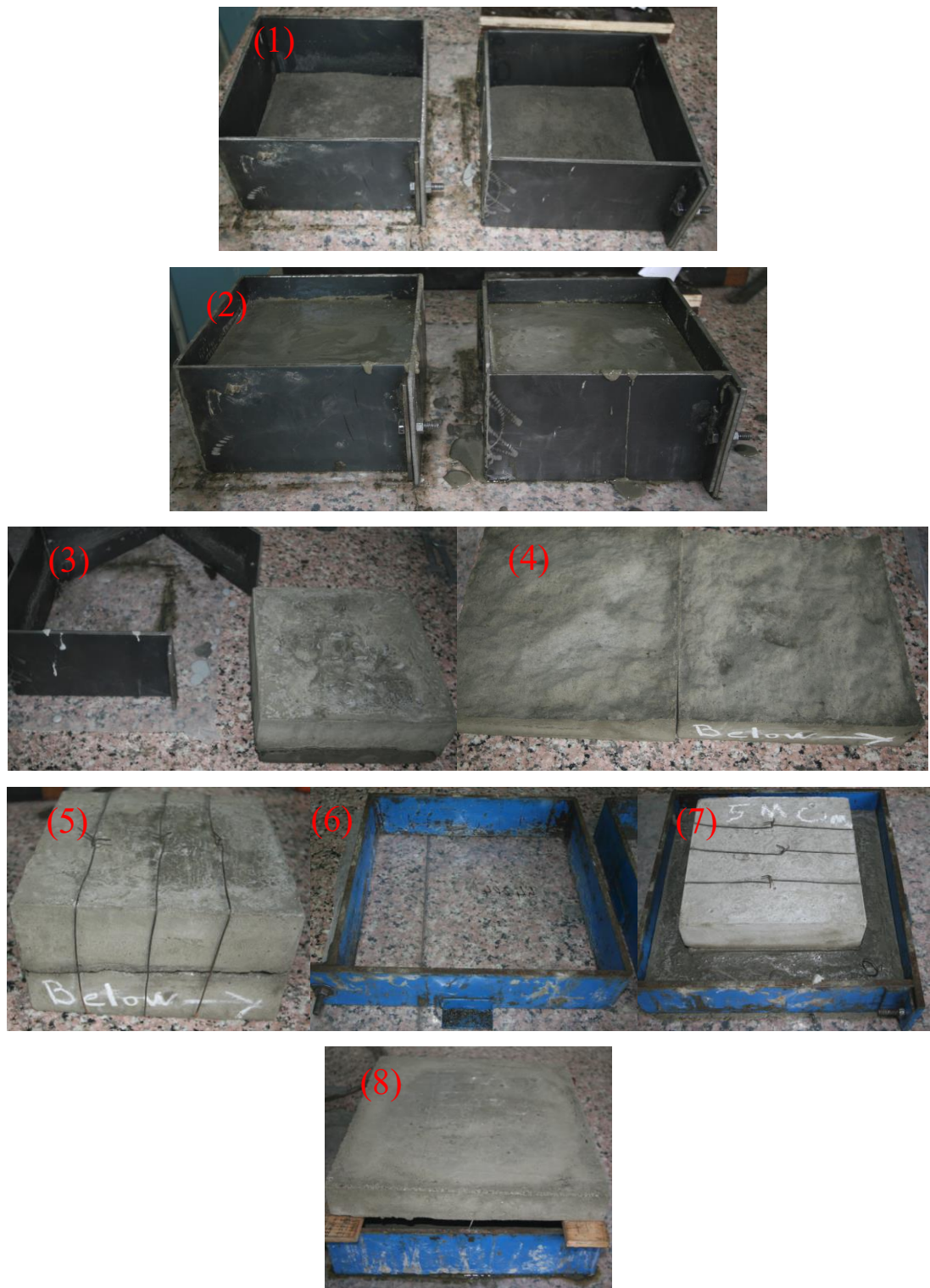


Figure 6.3. Concrete sample casting procedure



Figure 6.4. Casting 10 cm x 10 cm size specimens



Figure 6.5. A20 sample (Before the experiment)



Figure 6.6. B20 sample (Before the experiment)



Figure 6.7. B10-1 sample (Before the experiment)



Figure 6.8. B10-2 sample (Before the experiment)



Figure 6.9. B10-3 sample (Before the experiment)



Figure 6.10. B10-4 sample (Before the experiment)

6.2. Direct Shear Test of the Specimens

The direct shear tests are conducted in the Rock Mechanics Laboratory in Mining Engineering Department at METU. Testing equipment has a 30 cm x 30 cm shear box. Constant normal load boundary condition is used in all experiments. Shear and normal displacement values acquired with horizontal and vertical linear variable displacement transducers (LVDT). Figure 6.11 shows the components of the direct shear test equipment.



Figure 6.11. Direct Shear Test Equipment

The direct shear tests are conducted under three constant normal load condition and at three different shear rates (0.00100 mm/sec, 0.00075 mm/sec, 0.00050 mm/sec) with two discontinuity replicas having two different roughness levels ($JRC_A = 1.90$, $JRC_B = 11.71$).

Moreover, in order to study effect of specimen size, Discontinuity B is divided into four equal parts (B10-1, B10-2, B10-3, B10-4) and the experiments are repeated for the small size specimens. Size effect is studied only for the Discontinuity B, since the size effect is expected to be more prevalent in rougher surfaces. The large size specimens are called A20 and B20, while the small size specimens are named as B10-1, B10-2, B10-3, B10-4, according to length of the specimens. Photographs of all

specimens after the experiments are given in Appendix A. Table 6.1 presents the list of the experiments used for testing.

Experiments are conducted with constant normal load condition, since the constant normal stress condition can not be achieved due to the limitations of the test equipment. Normal load levels for testing of 20 cm x 20 cm samples are 60 kN, 48 kN and 32 kN. Normal loads are decreases when testing 10 cm x 10 cm samples, in order to preserve the constant normal stress range. Normal loads used for testing 10 cm x 10 cm samples are 15 kN, 12 kN and 8 kN. Normal stresses at the beginning of the experiments are 1.5 MPa, 1.2 MPa and 0.8 MPa, respectively. Normal stress levels on the sample surfaces increase with continuing shear displacement since the surface area decreases. However, range of the normal stress is small. Therefore, constant normal stress assumption can be made. Normal stress levels used in this study are in the range of the normal stresses generally used in previous studies investigating the similar effects.

Table 6.1: Experiment list

Discontinuity	Normal Stress (MPa)	Shear Rate (mm/sec)	JRC	Specimen Name
A20	1.5	0.00100	1.90	A20-N1.5-V0.001
A20	1.5	0.00075	1.90	A20-N1.5-V0.00075
A20	1.5	0.00050	1.90	A20-N1.5-V0.0005
A20	1.2	0.00100	1.90	A20-N1.2-V0.001
A20	1.2	0.00075	1.90	A20-N1.2-V0.00075
A20	1.2	0.00050	1.90	A20-N1.2-V0.0005
A20	0.8	0.00100	1.90	A20-N0.8-V0.001
A20	0.8	0.00075	1.90	A20-N0.8-V0.00075
A20	0.8	0.00050	1.90	A20-N0.8-V0.0005
B20	1.5	0.00100	11.71	B20-N1.5-V0.001
B20	1.5	0.00075	11.71	B20-N1.5-V0.00075
B20	1.5	0.00050	11.71	B20-N1.5-V0.0005
B20	1.2	0.00100	11.71	B20-N1.2-V0.001
B20	1.2	0.00075	11.71	B20-N1.2-V0.00075
B20	1.2	0.00050	11.71	B20-N1.2-V0.0005
B20	0.8	0.00100	11.71	B20-N0.8-V0.001
B20	0.8	0.00075	11.71	B20-N0.8-V0.00075
B20	0.8	0.00050	11.71	B20-N0.8-V0.0005
B10-1	1.5	0.00100	17.61	B10-1-N1.5-V0.001
B10-1	1.5	0.00075	17.61	B10-1-N1.5-V0.00075
B10-1	1.5	0.00050	17.61	B10-1-N1.5-V0.0005

Discontinuity	Normal Stress (MPa)	Shear Rate (mm/sec)	JRC	Specimen Name
B10-1	1.2	0.00100	17.61	B10-1-N1.2-V0.001
B10-1	1.2	0.00075	17.61	B10-1-N1.2-V0.00075
B10-1	1.2	0.00050	17.61	B10-1-N1.2-V0.0005
B10-1	0.8	0.00100	17.61	B10-1-N0.8-V0.001
B10-1	0.8	0.00075	17.61	B10-1-N0.8-V0.00075
B10-1	0.8	0.00050	17.61	B10-1-N0.8-V0.0005
B10-2	1.5	0.00100	17.09	B10-2-N1.5-V0.001
B10-2	1.5	0.00075	17.09	B10-2-N1.5-V0.00075
B10-2	1.5	0.00050	17.09	B10-2-N1.5-V0.0005
B10-2	1.2	0.00100	17.09	B10-2-N1.2-V0.001
B10-2	1.2	0.00075	17.09	B10-2-N1.2-V0.00075
B10-2	1.2	0.00050	17.09	B10-2-N1.2-V0.0005
B10-2	0.8	0.00100	17.09	B10-2-N0.8-V0.001
B10-2	0.8	0.00075	17.09	B10-2-N0.8-V0.00075
B10-2	0.8	0.00050	17.09	B10-2-N0.8-V0.0005
B10-3	1.5	0.00100	17.00	B10-3-N1.5-V0.001
B10-3	1.5	0.00075	17.00	B10-3-N1.5-V0.00075
B10-3	1.5	0.00050	17.00	B10-3-N1.5-V0.0005
B10-3	1.2	0.00100	17.00	B10-3-N1.2-V0.001
B10-3	1.2	0.00075	17.00	B10-3-N1.2-V0.00075
B10-3	1.2	0.00050	17.00	B10-3-N1.2-V0.0005
B10-3	0.8	0.00100	17.00	B10-3-N0.8-V0.001
B10-3	0.8	0.00075	17.00	B10-3-N0.8-V0.00075
B10-3	0.8	0.00050	17.00	B10-3-N0.8-V0.0005
B10-4	1.5	0.00100	17.01	B10-4-N1.5-V0.001
B10-4	1.5	0.00075	17.01	B10-4-N1.5-V0.00075
B10-4	1.5	0.00050	17.01	B10-4-N1.5-V0.0005
B10-4	1.2	0.00100	17.01	B10-4-N1.2-V0.001
B10-4	1.2	0.00075	17.01	B10-4-N1.2-V0.00075
B10-4	1.2	0.00050	17.01	B10-4-N1.2-V0.0005
B10-4	0.8	0.00100	17.01	B10-4-N0.8-V0.001
B10-4	0.8	0.00075	17.01	B10-4-N0.8-V0.00075
B10-4	0.8	0.00050	17.01	B10-4-N0.8-V0.0005

Total number of the experiments is 54. 18 of the experiments are conducted on 20 cm x 20 cm samples and 36 of the experiments are conducted on 10 cm x 10 cm samples.

Co-dependency of roughness and shear rate effects is investigated by evaluating the test results of A20 and B20 discontinuity samples. Co-dependency of sample size and shear rate effects is investigated by evaluating the test results of B20, B10-1, B10-2, B10-3, B10-4 discontinuity samples.

6.3. Investigation of Material Properties for the Replicas

In order to determine the material properties of the testing material, such as uniaxial compressive strength, tensile strength, Young's modulus (elastic modulus) and poisson's ratio, uniaxial compressive strength test and brazilian test (indirect tensile strength test) are conducted. To prepare testing material, the cement mix is poured in a bucket and left to setting for seven days. Then, test sample cores are drilled with the core-drilling machine in the Rock Mechanics Laboratory in Mining Engineering Department at METU (Figure 6.12).

The drilled cores are sawed to obtain required sizes for testing. Figure 6.13 shows the test samples for uniaxial compressive strength and Brazilian test. Properties of the test samples are presented in Table 6.2.



Figure 6.12: Coring

Table 6.2: Properties of UCS and Brazilian Test Samples

Uniaxial Compressive Strength Test Samples					
Sample Number	Length (mm)	Diameter (mm)	Weight (g)	Volume (cm³)	Density (g/cm³)
1	131.91	55.01	611.5	313.35	1.95
2	128.47	55.04	593.6	305.51	1.94
3	129.41	55.03	599.6	307.64	1.95
4	131.78	54.94	611.1	312.25	1.96
5	131.29	53.46	568.8	294.55	1.93

Brazilian Test Samples					
Sample Number	Length (mm)	Diameter (mm)	Weight (g)	Volume (cm³)	Density (g/cm³)
1	36.73	55.05	165.7	87.38	1.90
2	36.92	55.01	166.4	87.70	1.90
3	33.14	54.98	148.7	78.64	1.89
4	35.24	54.98	156.5	83.62	1.87
5	35.24	54.89	161.2	84.06	1.92

Average density of the material is 1.92 g/cm³. This value corresponds to a very low density for a rock material. However, some sedimentary rocks such as shale and sandstone are known to exhibit densities in a range as low as 1.60 – 2.00 g/cm³ (Sharma, 1997).

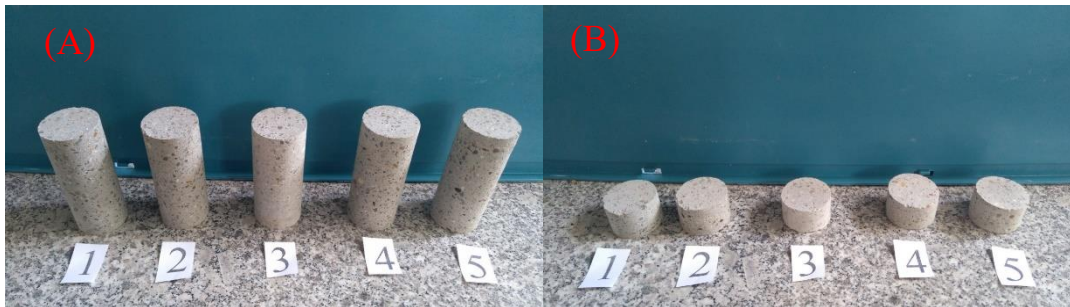


Figure 6.13. Test samples; (A) Uniaxial compressive strength test, (B) Brazilian test

6.3.1. Uniaxial Compressive Strength Tests

The uniaxial compressive strength (UCS) tests are conducted using MTS stiff testing device (Figure 6.14). The samples after testing are shown in Figure 6.15.



Figure 6.14. Uniaxial compressive strength test



Figure 6.15. Specimens after the UCS test

The test results are presented as axial stress – axial strain curves in Figures 6.16.

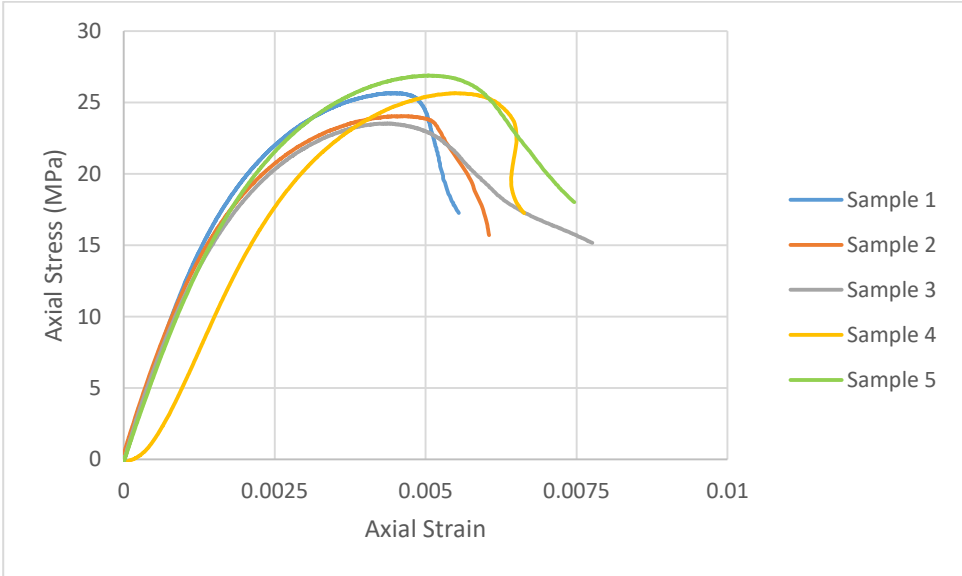


Figure 6.16. Axial stress-axial strain curves

The uniaxial compressive strengths, elastic modulus values and poisson’s ratios determined from UCS tests and the averages of these values are given in Table 6.3.

Table 6.3. UCS test results

Sample Number	UCS (MPa)	E (GPa)	ν
1	25.7	12.5	0.3
2	24.1	12.7	0.29
3	23.5	11.98	0.44
4	25.7	6.6	0.24
5	26.9	11.25	0.35
Average	25.18	11.0	0.32

The average UCS of the material is 25.18 MPa which corresponds to a low strength soft rock such as sandstone or claystone (Kanji, 2014). The elastic modulus of the

material is 11.0 GPa which is a value that generally observed in sedimentary rocks such as sandstone and siltstone. The poisson's ratio of the material is 0.32 which is a high value for rock materials and the value may be observed in some soft rocks such as sandstone and shale. (Gercek, 2007)

6.3.2. Indirect Tensile Strength Tests (Brazilian Tests)

The brazilian tests are conducted to determine tensile strength of the material (Figure 6.17). The specimens after testing are shown in Figure 6.18. Brazilian test results are given in Table 6.4.



Figure 6.17. Brazilian test



Figure 6.18. Specimens after the Brazilian test

Table 6.4: Brazilian Test Results

Sample Number	Tensile Strength (MPa)
1	2.92
2	3.17
3	3.05
4	3.08
5	3.27
Average	3.10

The tensile strength of the material is 3.10 MPa which is a value that usually measured in soft sedimentary rocks such as sandstone, claystone and shale (Perras and Diederichs, 2014).

6.3.3. The Joint Wall Compressive Strength (JCS)

The compressive strength of the discontinuity surfaces is an important parameter, especially if the surfaces directly contacts each other with no filling material. Use of Schmidt Hammer for determining JCS is explained by ISRM (1977). Schmidt Hammer is applied perpendicularly to discontinuity surface (Figure 6.19). JCS values of all samples are determined.



Figure 6.19. Application of Schmidt Hammer

Average rebound number is used in the correlation chart (Figure 6.20). The chart is the representation of the Equation 10 proposed by Miller (1965). ISRM (1977) suggested to discard five lowest reading of total ten readings since low readings are generally caused by loose rock grains or crushing.

$$\log_{(10)}(\sigma_c) = 0.00088\gamma R + 1.01 \quad (\text{Eqn. 10})$$

where σ_c = Unconfined compressive strength of the surface (MPa)

γ = Dry density of rock (kPa)

R = Rebound number

The schmidt hammer readings and the respective JCS values obtained from the Equation 10 are given in Table 6.5. The lowest half of the readings are discarded from the calculation and only the readings used in the calculations are given.

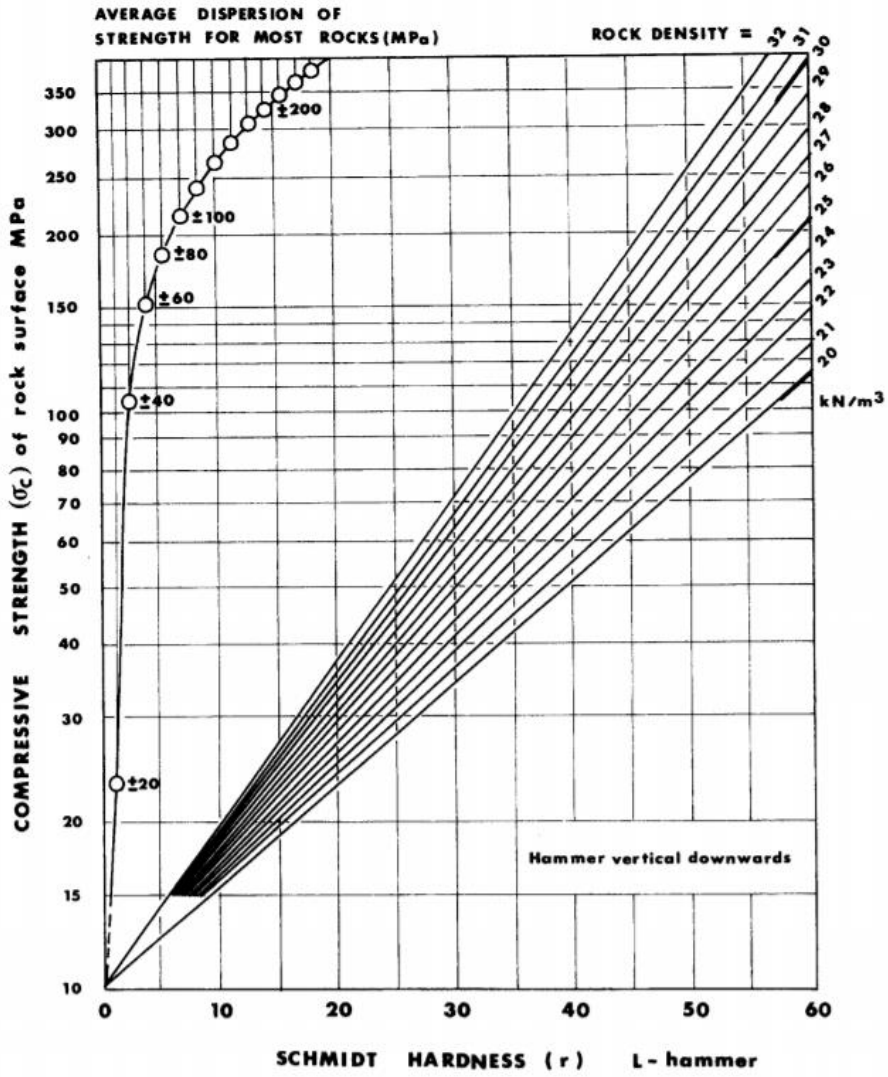


Figure 6.20. Correlation chart for schmidt hammer (Retrieved from ISRM, Suggested Methods for the Quantitative Description of Discontinuities, 1977)

Table 6.5. Joint wall compressive strengths (JCS)

Discontinuity	Schmidt Hammer Readings (R)					
	A20	B20	B10-1	B10-2	B10-3	B10-4
	23	30	22	21	21	20
	20	22	20	22	20	18
	22	26	21	21	19	16
	18	20	20	21	19	16
	18	20	20	21	18	15
	16	21	19	19	16	15
	16	20	18	20	15	15
	16	20	18	20	15	12
	14	20	17	18	15	12
	14	19				
	14	18				
	13	16				
	13	16				
R (mean)	16,7	20,6	19,4	20,3	17,6	15,4
Density (kN/m ³)	18.8	18.8	18.8	18.8	18.8	18.8
JCS (Mpa)	19.3	22.4	21.5	22.1	20.0	18.4

The JCS values for A20 and B20 are 19.3 and 22.4 MPa, respectively. This shows that, JCS is effected by the roughness degree even though the materials of the surfaces are the same. The JCS values for B10-1, B10-2, B10-3 and B10-4 are 21.5, 22.1, 20.0 and 18.4 MPa, respectively. Comparing these values to that of B20 reveals that there is a small sample size effect on JCS. As the sample size decreases, JCS also decreases.

CHAPTER 7

RESULTS AND DISCUSSIONS

In this part, firstly, results of the rock discontinuity sample replication methodology are analyzed by comparing the Z_2 values of the 3D model, the PLA moulds and the concrete test samples. Secondly, results of the direct shear experiments which are conducted to investigate the effects of roughness characteristics, shear rate and size on the shear strength of rock discontinuities and the co-dependency of these effects.

7.1. Results of Rock Discontinuity Replica Production Methodology

In this study, rock discontinuity replicas are produced using close-range digital photogrammetry and 3D printing technologies. Firstly, 3D models of rock discontinuities are obtained with photogrammetric analysis. The 3D models are printed-out with a 3D printer, using PLA as the raw material. Then, concrete test samples are produced using the 3D printer outputs as moulds. Z_2 parameters of the 3D models, the PLA moulds and the concrete test samples are calculated.

Z_2 parameters are compared to each other, in order to validate the success of replicating surfaces of the discontinuities. Z_2 parameters of all the models are given in Table 7.1. Percent success (%) column represents what percentage of roughness of the 3D models are replicated in the concrete samples. Figure 7.1 shows the evolution Z_2 values through the sample reproduction process.

Table 7.1. Z_2 parameters of the models

Discontinuity	3D Model	PLA Mould	Concrete Sample	Percent Success (%)
A20	0.127	0.0999	0.115	90.6
B20	0.267	0.208	0.212	79.4
B10-1	0.415	0.408	0.391	94.2
B10-2	0.507	0.391	0.361	71.2
B10-3	0.431	0.368	0.368	85.4
B10-4	0.454	0.417	0.416	91.6

According to the comparison of Z_2 values of the models, sample reproduction methodology is the most efficient for planar surfaces and small size samples. For A20, 90% of the 3D model's roughness is replicated in the test samples, whereas for B20, nearly 80% of the 3D model's roughness is replicated in the test samples. For small size samples of the discontinuity B (B10 samples), success rates show significant variance because of the high roughness levels of these models .

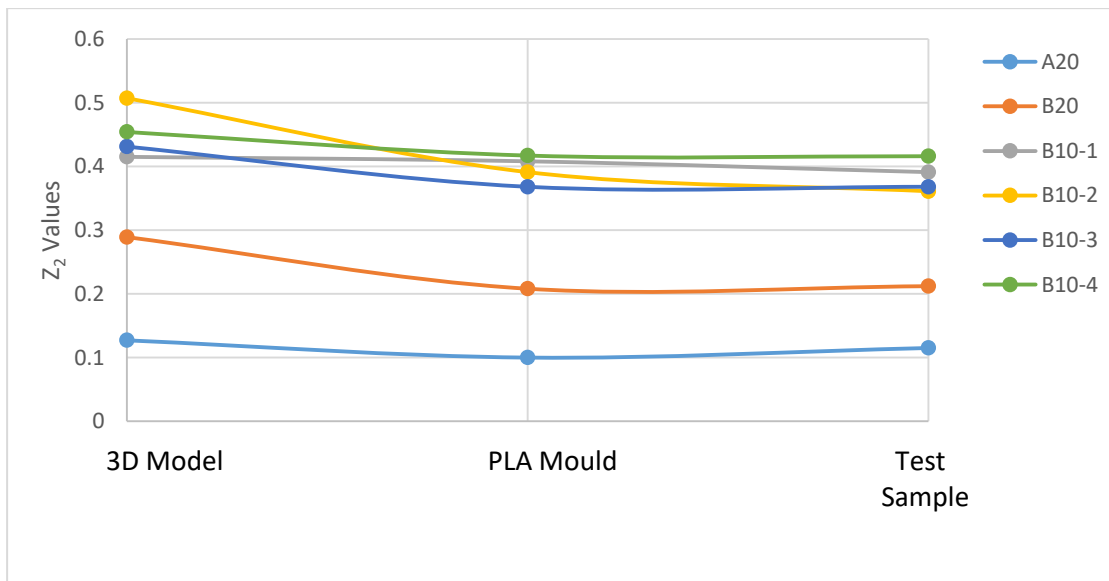


Figure 7.1. Evolution of Z_2 values

Results showed that Z_2 values are the lowest for the PLA Moulds, but transition to the concrete test samples causes an increase in the Z_2 , thus the roughness degree

approaches to the original value. The success of the methodology is more apparent in less rough surfaces (A20) with 90.6% success rate. However, as the roughness degree increases, success of surface replication lose some amount of precision as observed with B20 discontinuity (79% success rate). Moreover, small size samples of Discontinuity B showed significant success in surface replication, despite their high roughness degrees. This shows that, the developed methodology is fairly successful in replicating the small scale asperities, but it may cause deviations in Z_2 parameter while replicating large scale undulations. In planar surfaces, the methodology yields significantly good results.

7.2.Direct Shear Test Results

Direct shear tests are conducted on rock discontinuity replicas with varying conditions such as normal stress, shear rate, specimen size and roughness characteristics. Total number of experiments is 54. Experimental results are presented in Figures 7.2-7.19 for the same shear rates. Figures 7.20-7.37 shows the results for the same shear rates.

Moving averages of the experimental data are used to plot the graphs, in order to provide a better representation of shearing trends. Original plots are given in Appendix B.

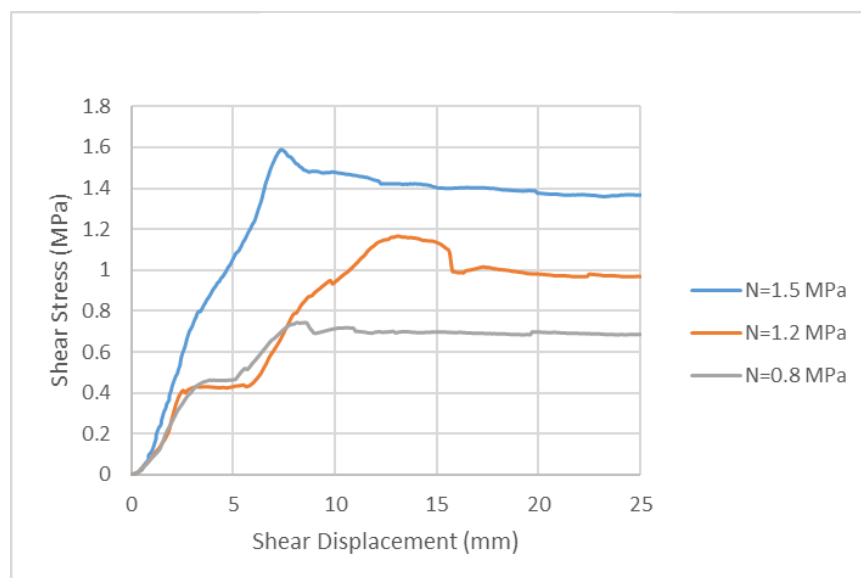


Figure 7.2. Test results (A20, $V=10 \times 10^{-4}$ mm/sec)

For A20, at 10×10^{-4} mm/sec shear rate, shear strength increases with increasing normal load.

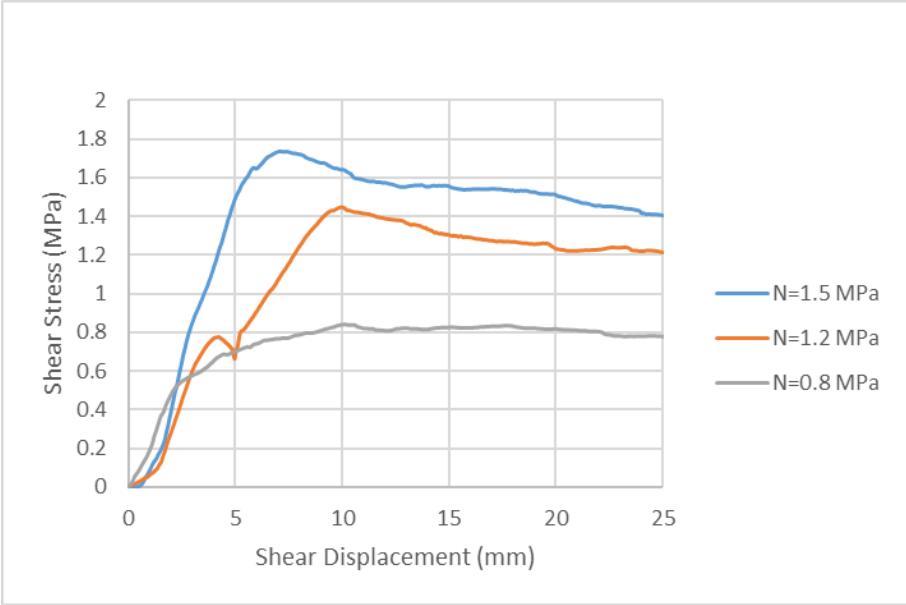


Figure 7.3. Test results (B20, $V=10 \times 10^{-4}$ mm/sec)

For B20, at 10×10^{-4} mm/sec shear rate, shear strength increases with increasing normal load.

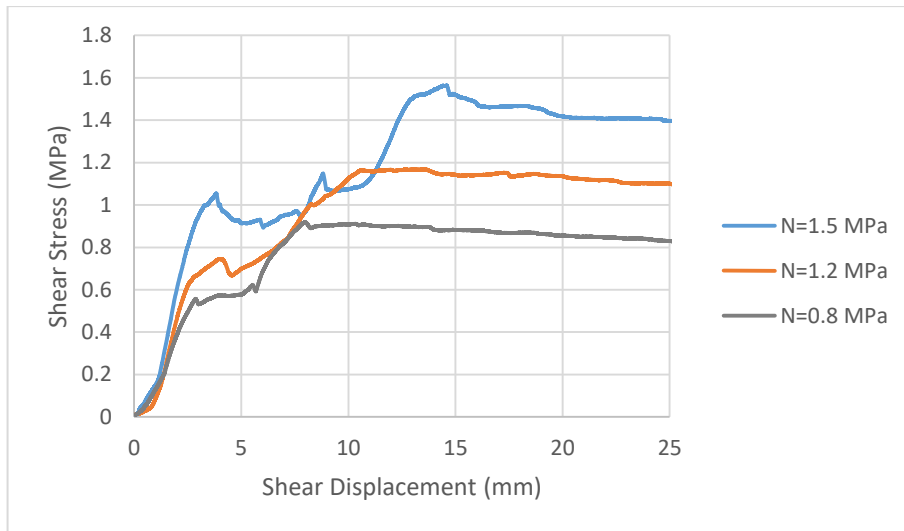


Figure 7.4. Test results (A20, $V=7.5 \times 10^{-4}$ mm/sec)

For A20, at 7.5×10^{-4} mm/sec shear rate, shear strength increases with increasing normal load.

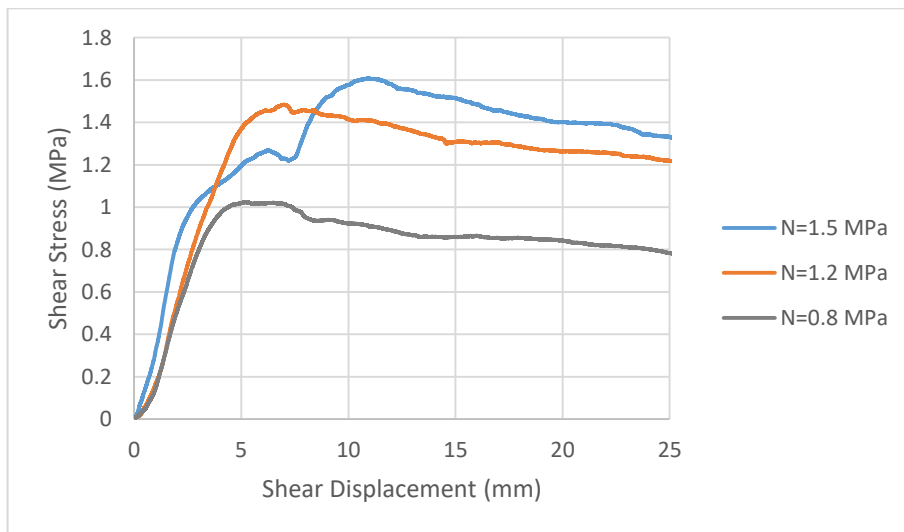


Figure 7.5. Test results (B20, $V=7.5 \times 10^{-4}$ mm/sec)

For B20, at 7.5×10^{-4} mm/sec shear rate, shear strength increases with increasing normal load.

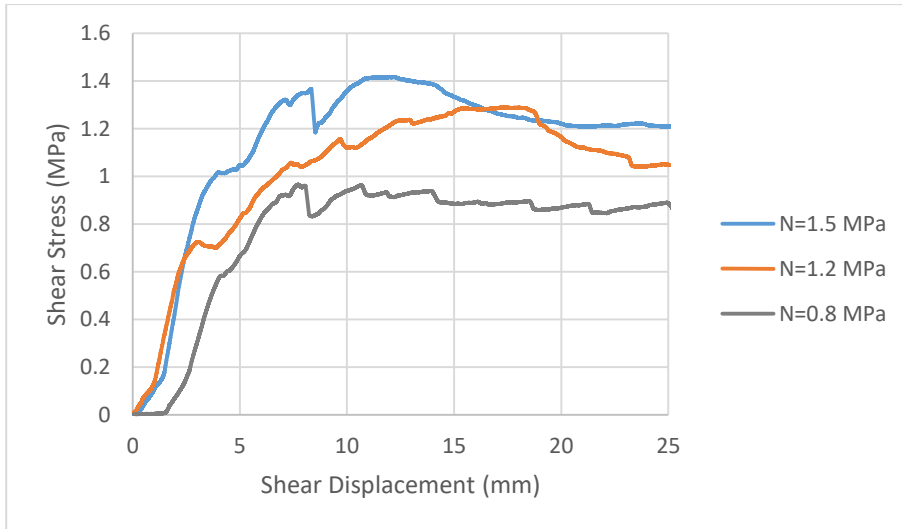


Figure 7.6. Test results (A20, $V=5 \times 10^{-4}$ mm/sec)

For A20, at 5×10^{-4} mm/sec shear rate, shear strength increases with increasing normal load.

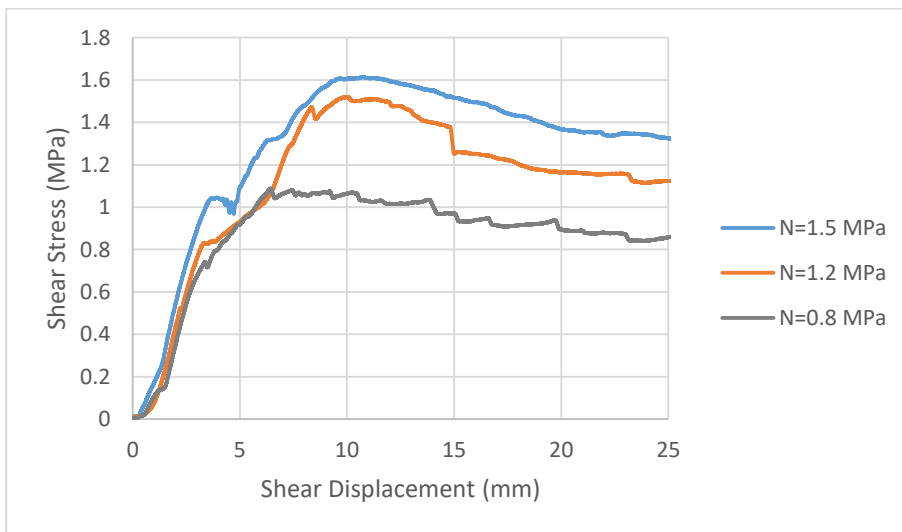


Figure 7.7. Test results (B20, $V=5 \times 10^{-4}$ mm/sec)

For B20, at 5×10^{-4} mm/sec shear rate, shear strength increases with increasing normal load.

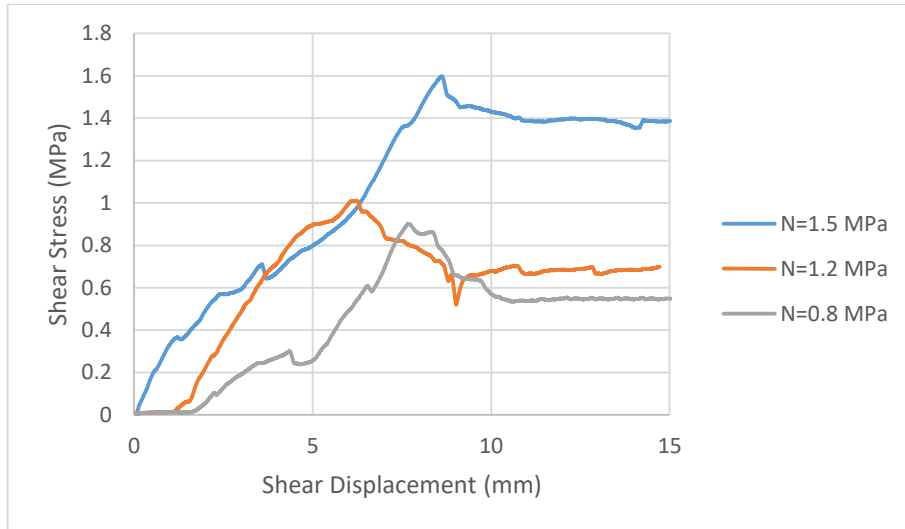


Figure 7.8. Test results (B10-1, $V=10 \times 10^{-4}$ mm/sec)

For B10-1, at 10×10^{-4} mm/sec shear rate, shear strength increases with increasing normal load.

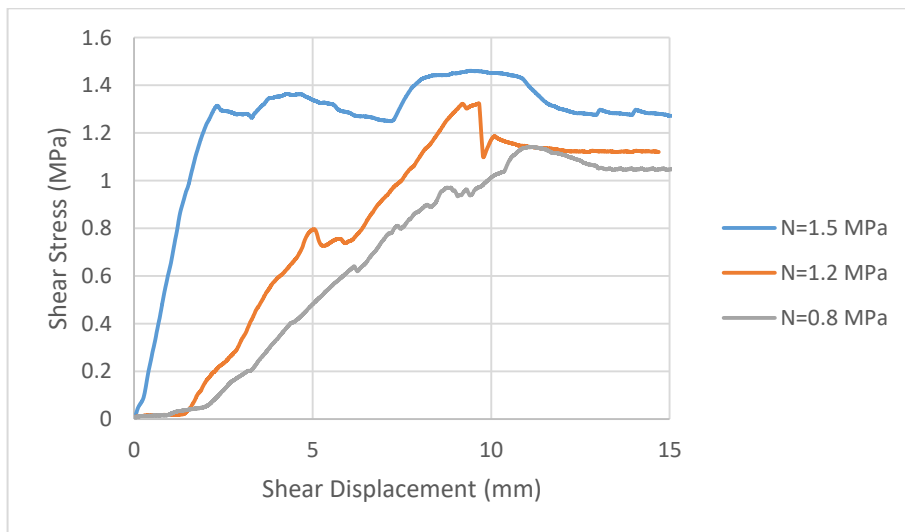


Figure 7.9. Test results (B10-2, $V=10 \times 10^{-4}$ mm/sec)

For B10-2, at 10×10^{-4} mm/sec shear rate, shear strength increases with increasing normal load.

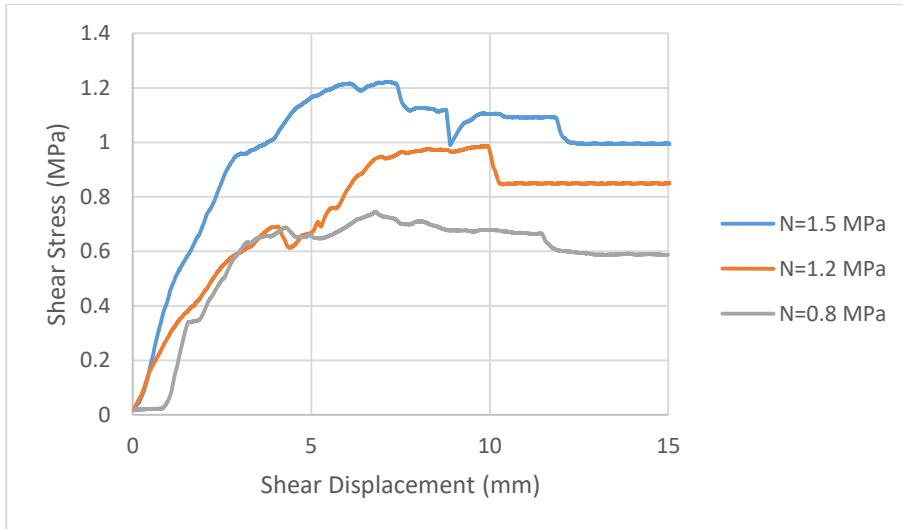


Figure 7.10. Test results (B10-3, $V=10 \times 10^{-4}$ mm/sec)

For B10-3, at 10×10^{-4} mm/sec shear rate, shear strength increases with increasing normal load.

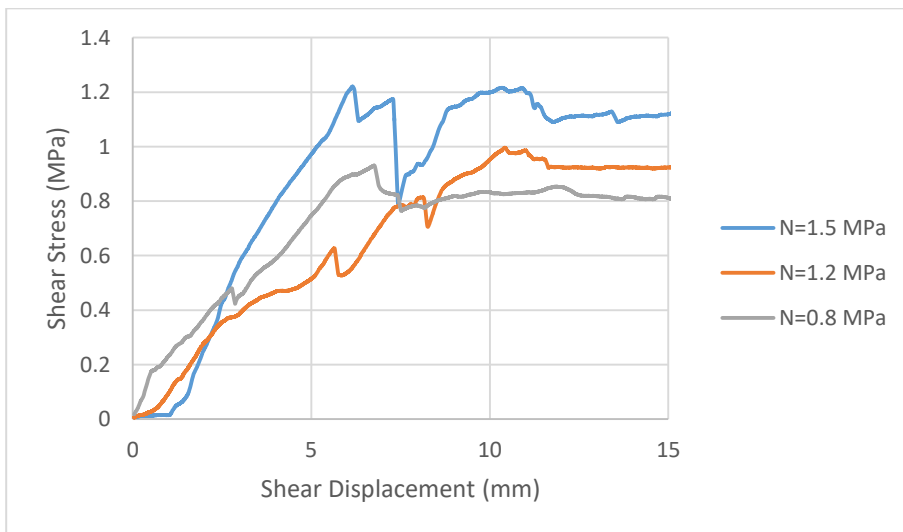


Figure 7.11. Test results (B10-4, $V=10 \times 10^{-4}$ mm/sec)

For B10-4, at 10×10^{-4} mm/sec shear rate, shear strength increases with increasing normal load

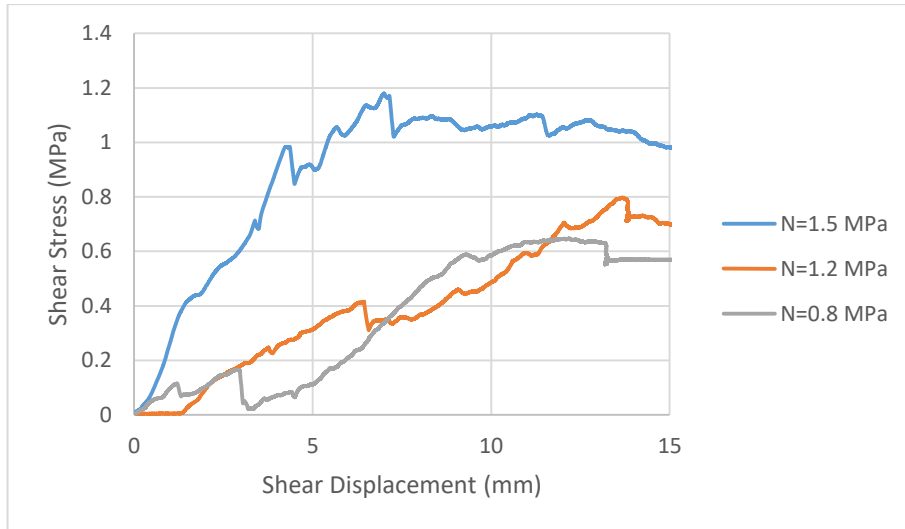


Figure 7.12. Test results (B10-1, $V=7.5 \times 10^{-4}$ mm/sec)

For B10-1, at 7.5×10^{-4} mm/sec shear rate, shear strength increases with increasing normal load.

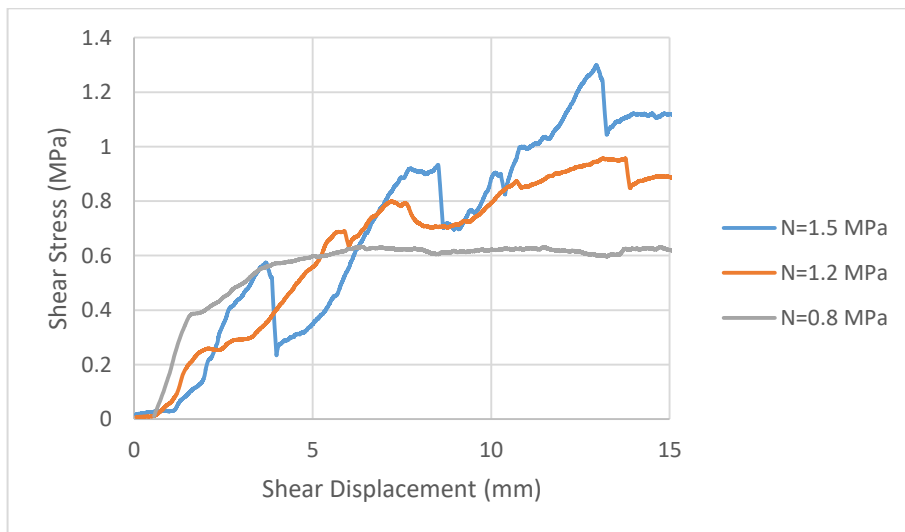


Figure 7.13. Test results (B10-2, $V=7.5 \times 10^{-4}$ mm/sec)

For B10-2, at 7.5×10^{-4} mm/sec shear rate, shear strength increases with increasing normal load.

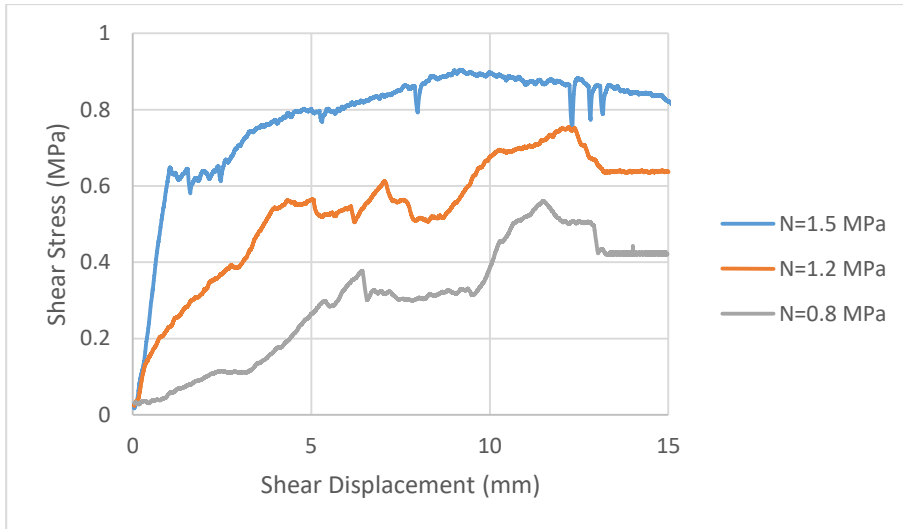


Figure 7.14. Test results (B10-3, $V=7.5 \times 10^{-4}$ mm/sec)

For B10-3, at 7.5×10^{-4} mm/sec shear rate, shear strength increases with increasing normal load.

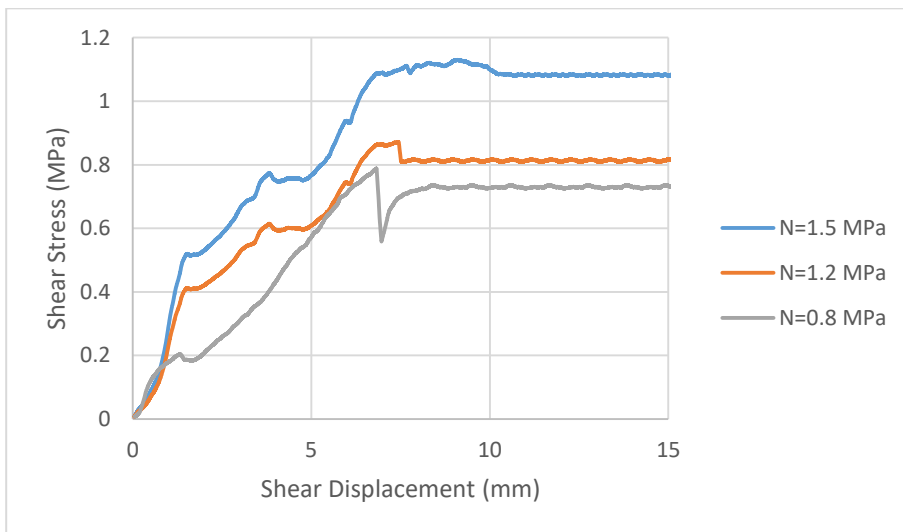


Figure 7.15. Test results (B10-4, $V=7.5 \times 10^{-4}$ mm/sec)

For B10-4, at 7.5×10^{-4} mm/sec shear rate, shear strength increases with increasing normal load.

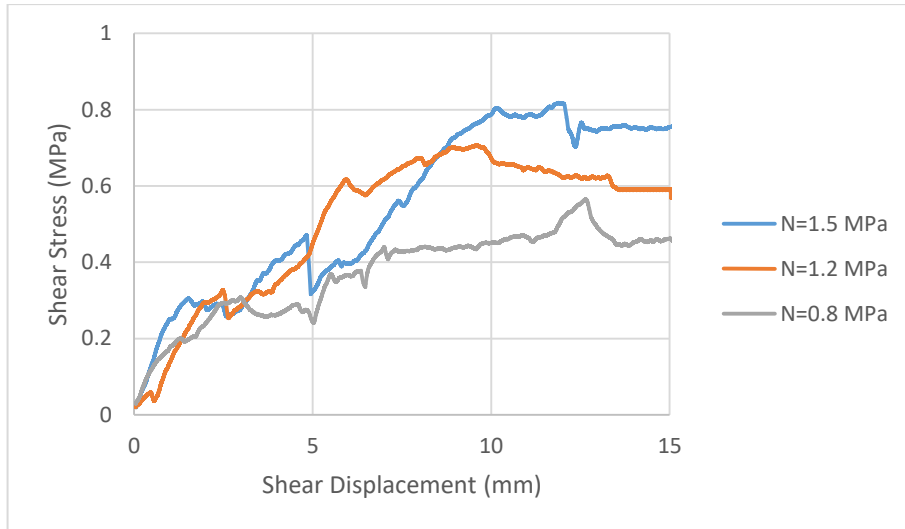


Figure 7.16. Test results (B10-1, $V=5 \times 10^{-4}$ mm/sec)

For B10-1, at 5×10^{-4} mm/sec shear rate, shear strength increases with increasing normal load.

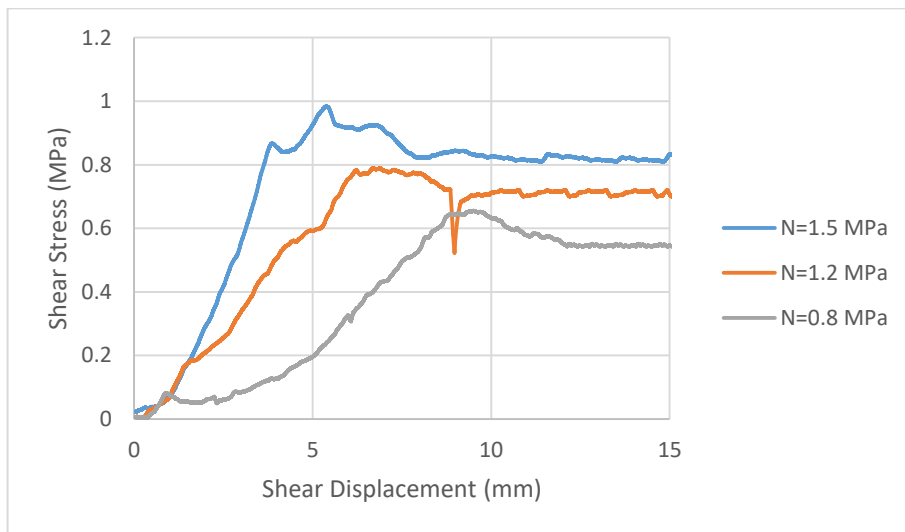


Figure 7.17. Test results (B10-2, $V=5 \times 10^{-4}$ mm/sec)

For B10-2, at 5×10^{-4} mm/sec shear rate, shear strength increases with increasing normal load.

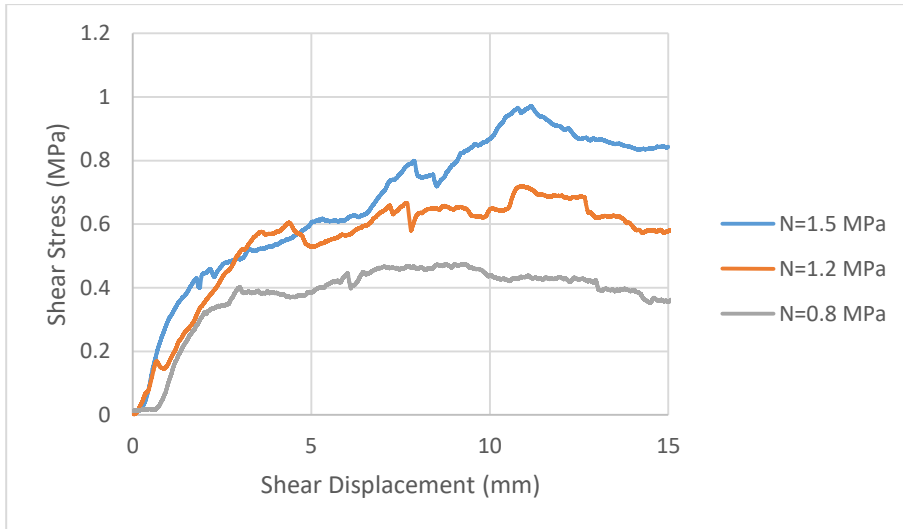


Figure 7.18. Test results (B10-3, $V=5 \times 10^{-4}$ mm/sec)

For B10-3, at 5×10^{-4} mm/sec shear rate, shear strength increases with increasing normal load.

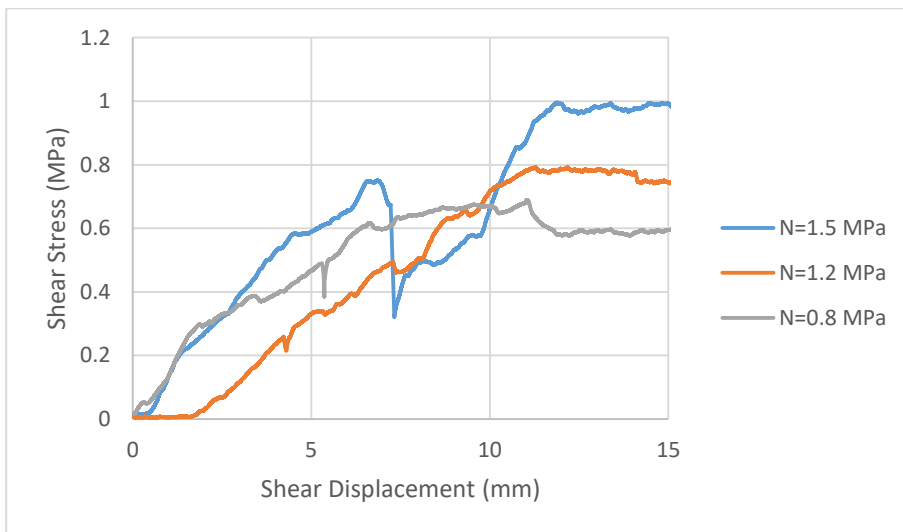


Figure 7.19. Test results (B10-4, $V=5 \times 10^{-4}$ mm/sec)

For B10-4, at 5×10^{-4} mm/sec shear rate, shear strength increases with increasing normal load.

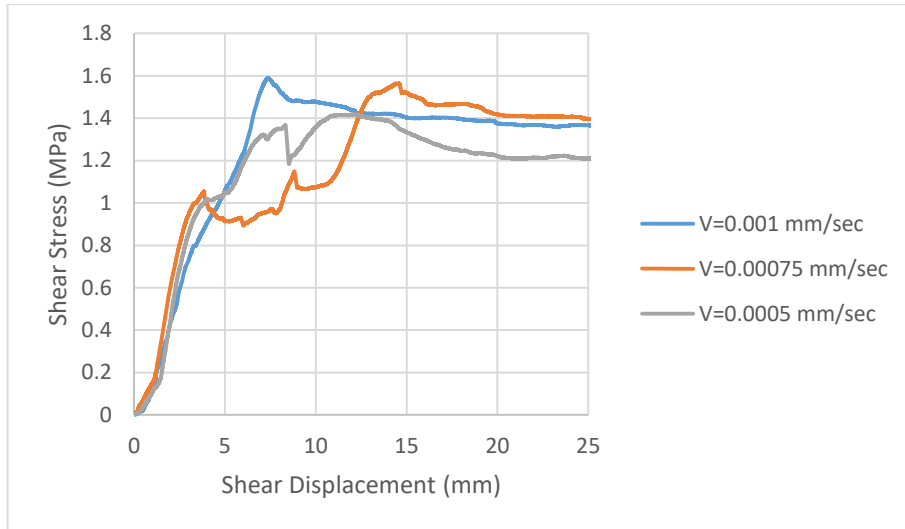


Figure 7.20. Test results (A20, N=1.5 MPa)

For A20, under 1.5 MPa normal stress, peak shear strength increases with increasing shear rate.

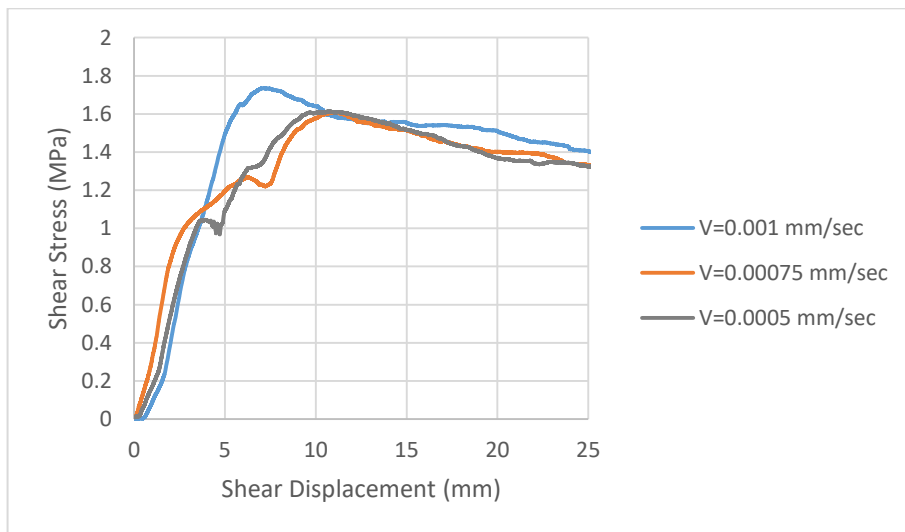


Figure 7.21. Test results (B20, N=1.5 MPa)

For B20, under 1.5 MPa normal stress, shear strength values increase with increasing shear rate.

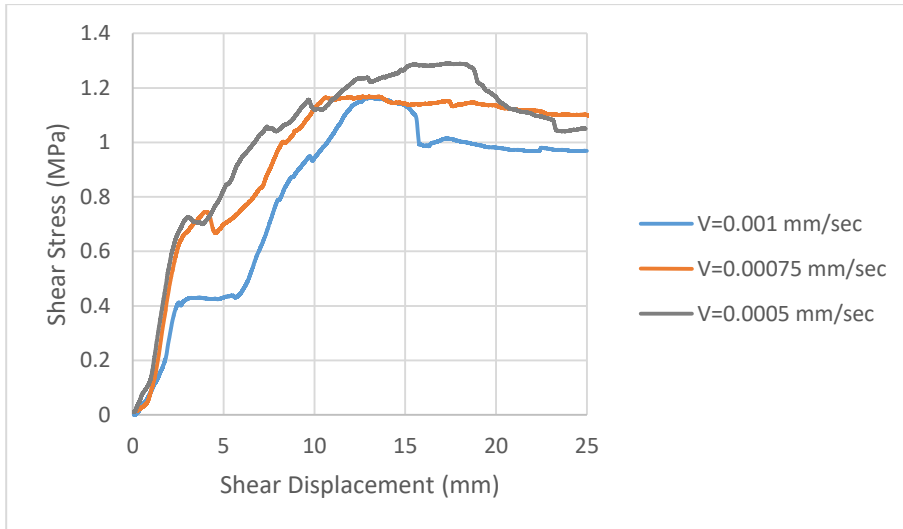


Figure 7.22. Test results (A20, N=1.2 MPa)

For A20, under 1.2 MPa normal stress, shear strength values decrease with increasing shear rate.

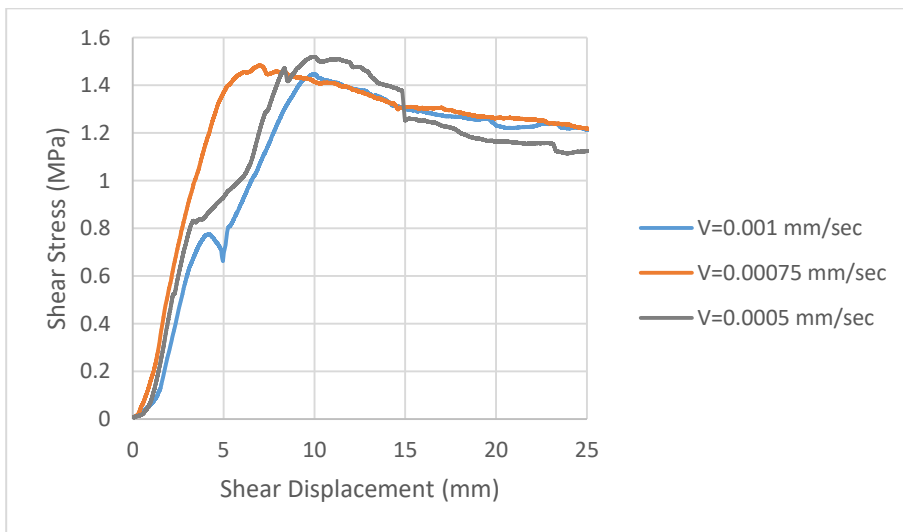


Figure 7.23. Test results (B20, N=1.2 MPa)

For B20, under 1.2 MPa normal stress, shear strength values decrease with increasing shear rate.

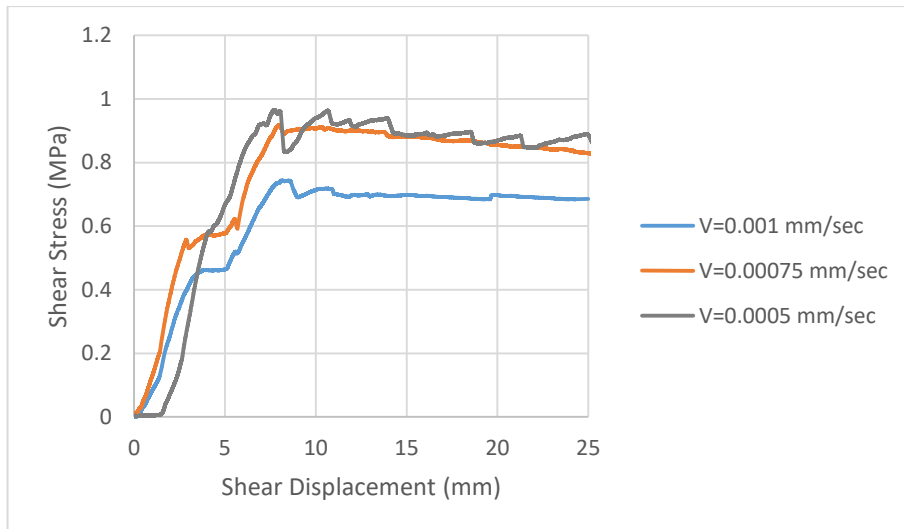


Figure 7.24. Test results (A20, N=0.8 MPa)

For A20, under 0.8 MPa normal stress, shear strength values decrease with increasing shear rate.

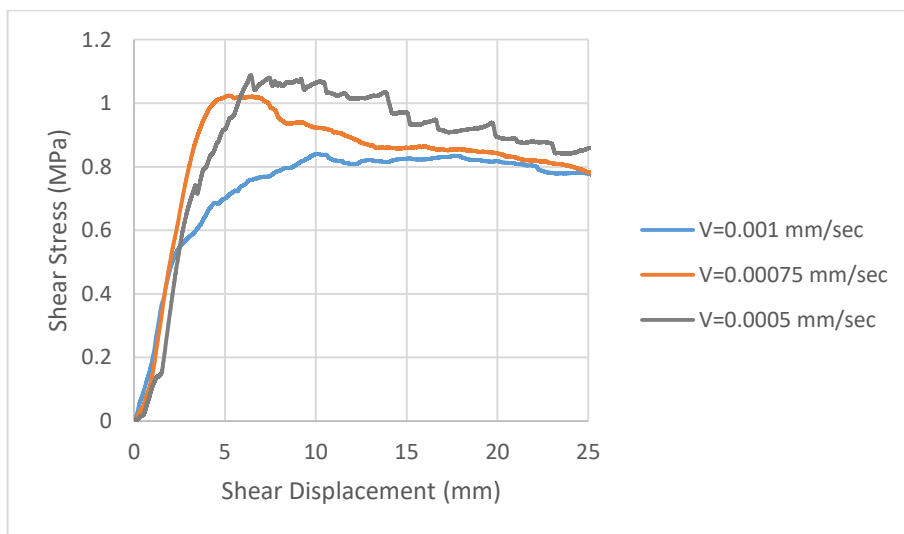


Figure 7.25. Test results (B20, N=0.8 MPa)

For B20, under 0.8 MPa normal stress, shear strength values decrease with increasing shear rate.

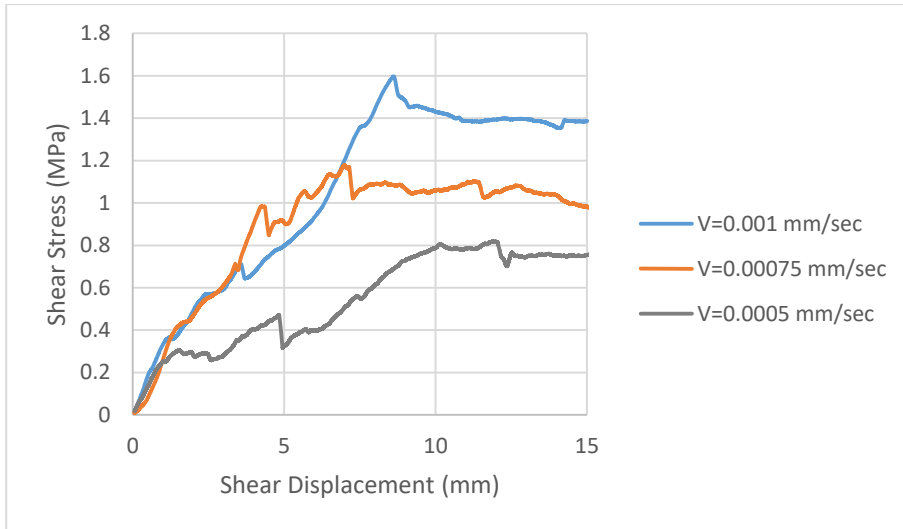


Figure 7.26. Test results (B10-1, N=1.5 MPa)

For B10-1, under 1.5 MPa normal stress, shear strength values increase with increasing shear rate.

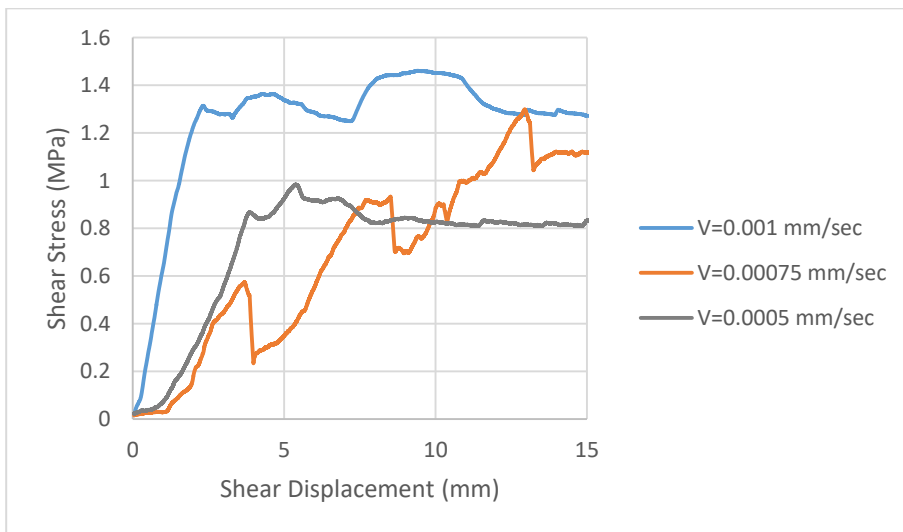


Figure 7.27. Test results (B10-2, N=1.5 MPa)

For B10-2, under 1.5 MPa normal stress, shear strength values increase with increasing shear rate.

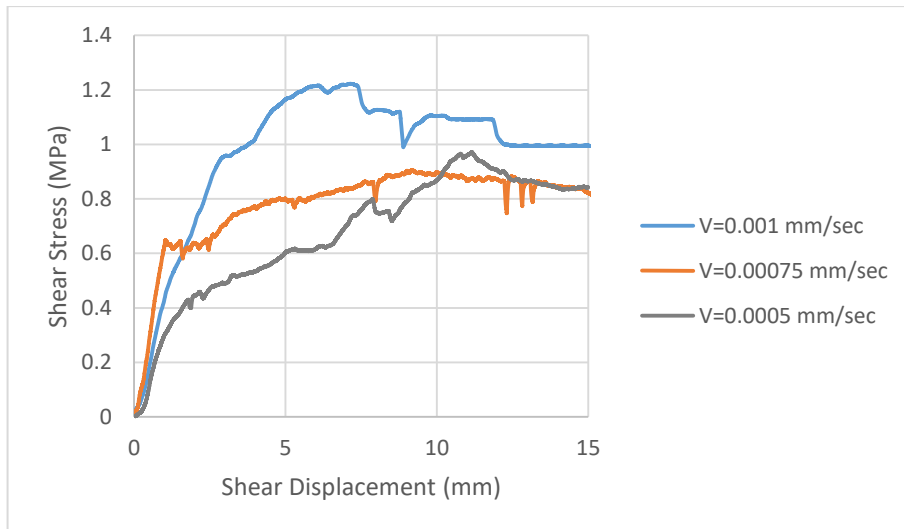


Figure 7.28. Test results (B10-3, N=1.5 MPa)

For B10-3, under 1.5 MPa normal stress, shear strength values increase with increasing shear rate.

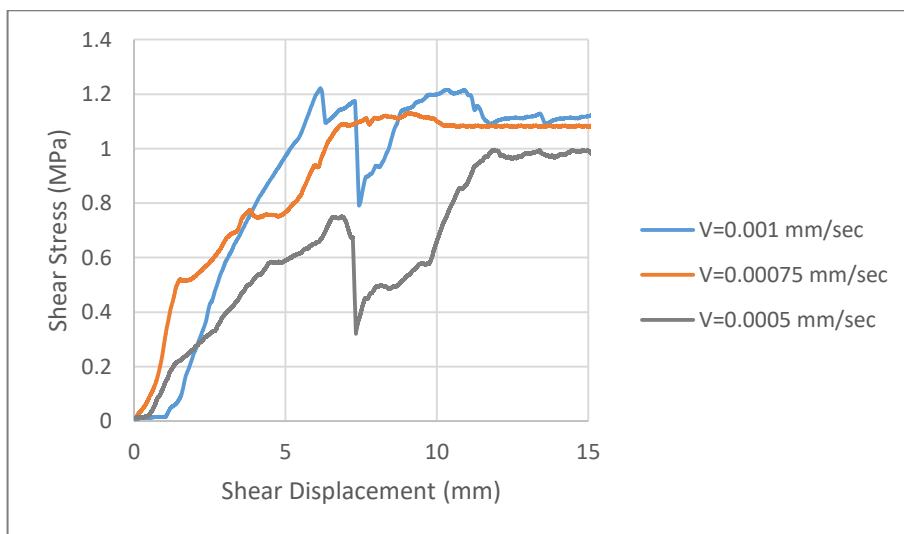


Figure 7.29. Test results (B10-4, N=1.5 MPa)

For B10-4, under 1.5 MPa normal stress, shear strength values increase with increasing shear rate.

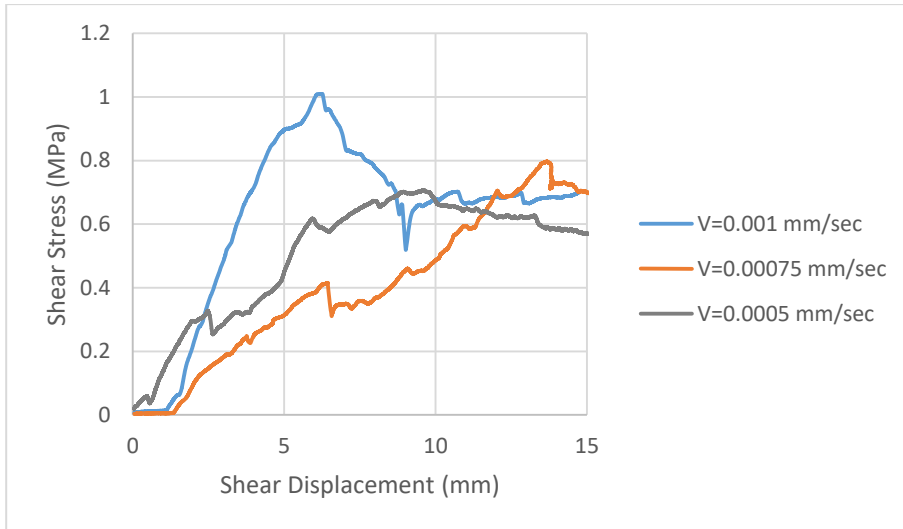


Figure 7.30. Test results (B10-1, N=1.2 MPa)

For B10-1, under 1.2 MPa normal stress, shear strength values increase with increasing shear rate.

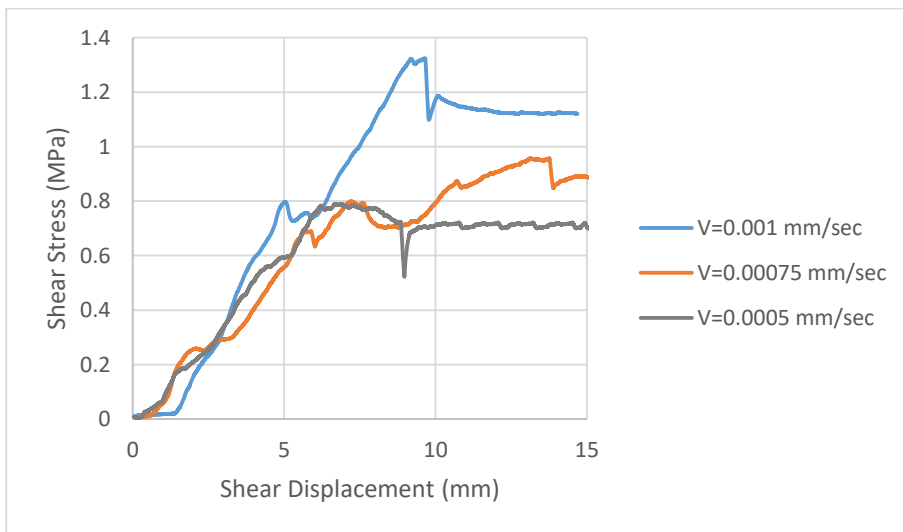


Figure 7.31. Test results (B10-2, N=1.2 MPa)

For B10-2, under 1.2 MPa normal stress, shear strength values increase with increasing shear rate.

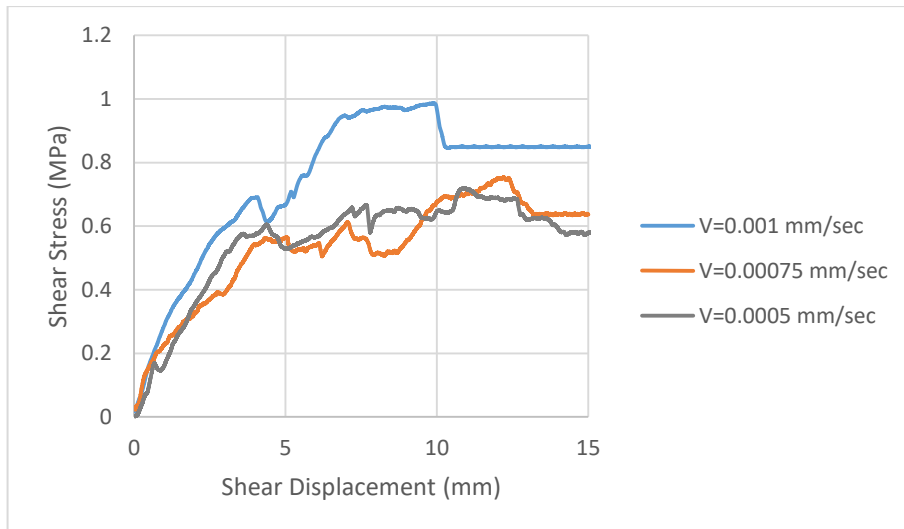


Figure 7.32 Test results (B10-3, N=1.2 MPa)

For B10-2, under 1.2 MPa normal stress, shear strength values increase with increasing shear rate.

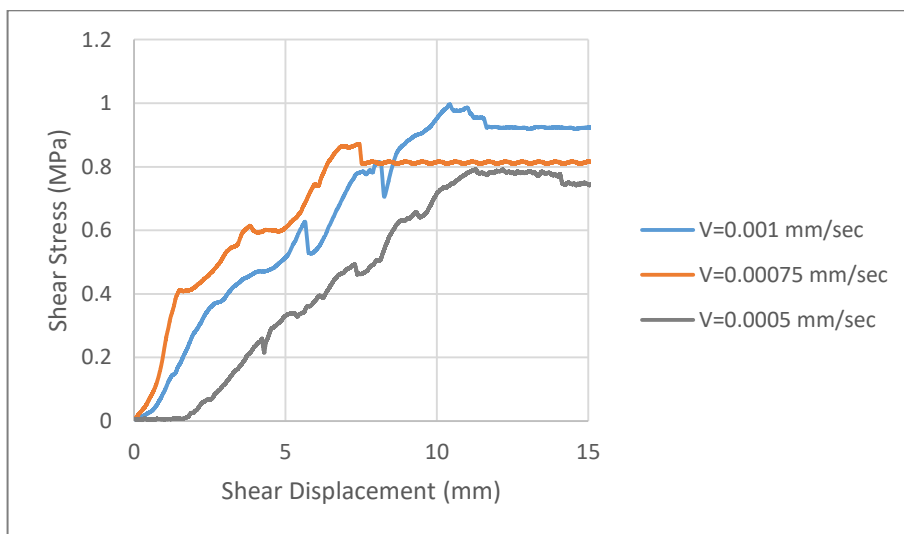


Figure 7.33. Test results (B10-4, N=1.2 MPa)

For B10-4, under 1.2 MPa normal stress, shear strength values increase with increasing shear rate.

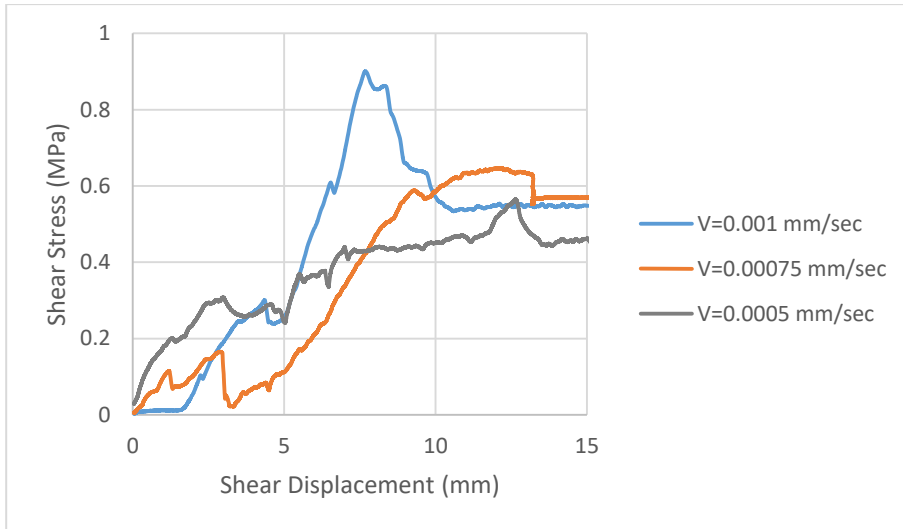


Figure 7.34. Test results (B10-1, N=0.8 MPa)

For B10-1, under 0.8 MPa normal stress, shear strength values increase with increasing shear rate.

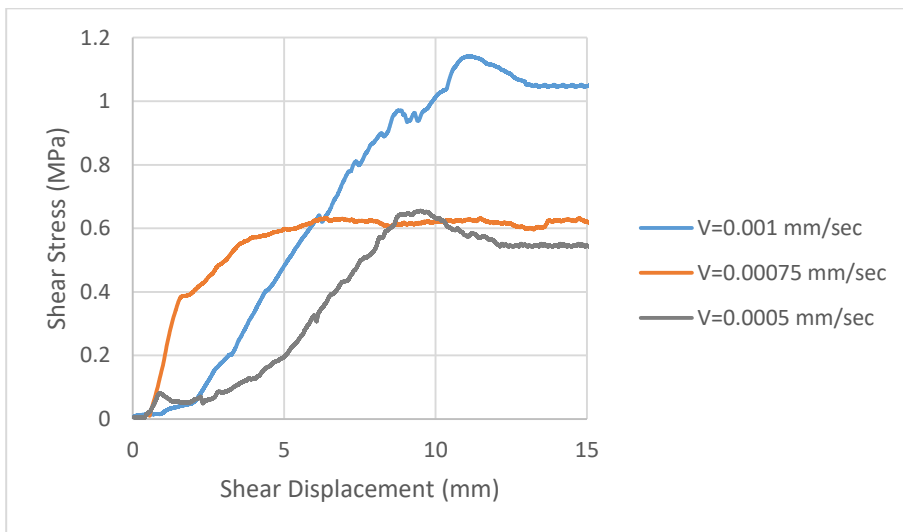


Figure 7.35. Test results (B10-2, N=0.8 MPa)

For B10-2, under 0.8 MPa normal stress, shear strength values increase with increasing shear rate.

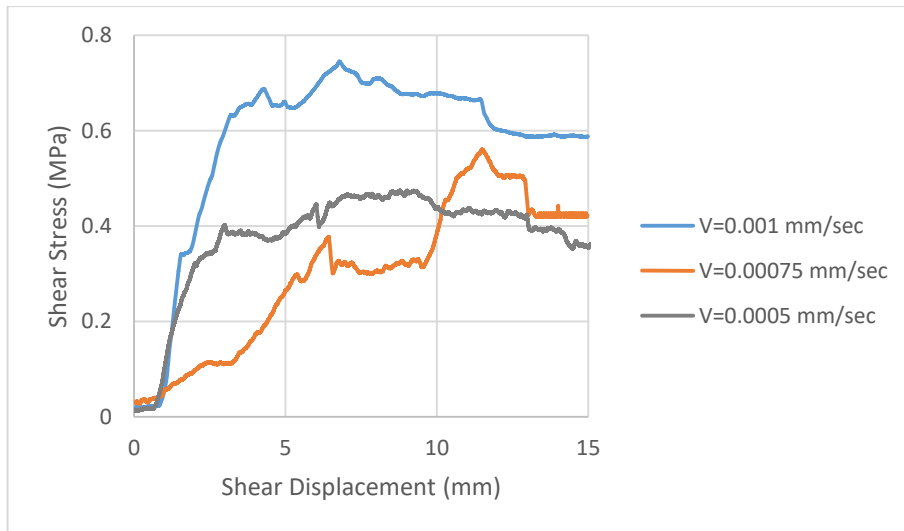


Figure 7.36. Test results (B10-3, N=0.8 MPa)

For B10-3, under 0.8 MPa normal stress, shear strength values increase with increasing shear rate.

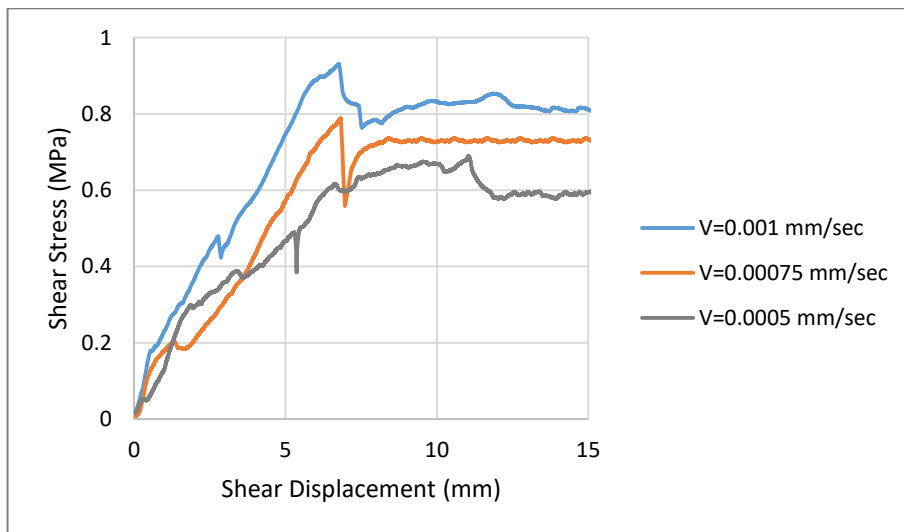


Figure 7.37. Test results (B10-4, N=0.8 MPa)

For B10-4, under 0.8 MPa normal stress, shear strength values increase with increasing shear rate.

Results of the experiments are tabulated in terms of peak and residual shear strength values in Table 7.2.

Table 7.2. Experimental results

Specimen	Normal Stress (MPa)	Shear Rate ($\times 10^{-4}$ mm/sec)	Peak Shear Strength (MPa)	Residual Shear Strength (MPa)
A20	1.5	10	1.59	1.38
		7.5	1.56	1.39
		5	1.42	1.21
	1.2	10	1.17	0.98
		7.5	1.17	1.1
		5	1.29	1.07
	0.8	10	0.74	0.7
		7.5	0.92	0.85
		5	0.97	0.89
B20	1.5	10	1.74	1.4
		7.5	1.61	1.33
		5	1.61	1.32
	1.2	10	1.45	1.21
		7.5	1.48	1.2
		5	1.52	1.12
	0.8	10	0.84	0.79
		7.5	1.02	0.82
		5	1.09	0.85
B10-1	1.5	10	1.60	1.30
		7.5	1.18	0.98
		5	0.82	0.73
	1.2	10	1.01	0.77
		7.5	0.80	0.73
		5	0.71	0.55
	0.8	10	0.9	0.62
		7.5	0.64	0.57
		5	0.57	0.48
B10-2	1.5	10	1.46	1.28
		7.5	1.30	1.1
		5	0.98	0.81
	1.2	10	1.32	1.12
		7.5	0.96	0.9
		5	0.79	0.7
	0.8	10	1.14	1.04
		7.5	0.63	0.62
		5	0.66	0.52
B10-3	1.5	10	1.22	0.99
		7.5	0.90	0.63
		5	0.97	0.85

Specimen	Normal Stress (MPa)	Shear Rate ($\times 10^{-4}$ mm/sec)	Peak Shear Strength (MPa)	Residual Shear Strength (MPa)
B10-4	1.2	10	0.99	0.85
		7.5	0.75	0.63
		5	0.72	0.59
	0.8	10	0.75	0.59
		7.5	0.56	0.46
		5	0.47	0.39
	1.5	10	1.22	1.09
		7.5	1.13	1.06
		5	1.00	0.92
	1.2	10	1.00	0.92
		7.5	0.87	0.8
		5	0.78	0.71
	0.8	10	0.93	0.83
		7.5	0.79	0.75
		5	0.69	0.62

Results of the experiments showed that as the roughness increases, the peak and the residual shear strength values increase. Also, under 1.5 MPa normal stress, the peak and the residual shear strength values increase as the shear rate increases and under 0.8 MPa normal stress, the peak and the residual shear strength values decrease as the shear rate increases. Results under 1.2 MPa normal stress showed a few contradictory results. Therefore, in order to make a comment for 1.2 MPa normal stress level, more experiments with different shear rates should be conducted. Lastly, as the samples size decreases, the peak and the residual shear strength values decrease.

Peak and residual values of friction angle cohesion of specimens are calculated from shear stress-normal stress graphs. Shear stress-normal stress graphs are presented in Figures 7.38-7.55.

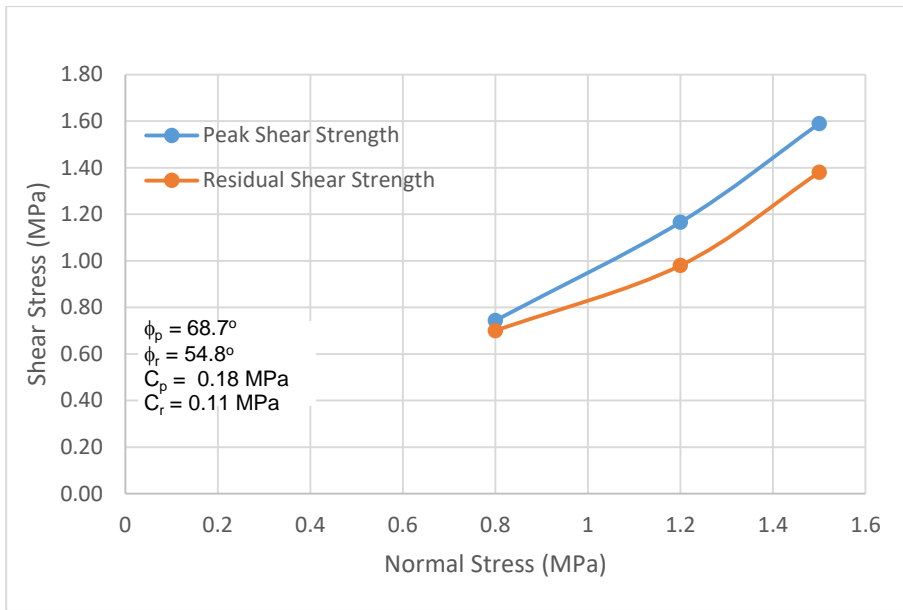


Figure 7.38. Shear stress-normal stress graph (A20, $V=10 \times 10^{-4}$ mm/sec)

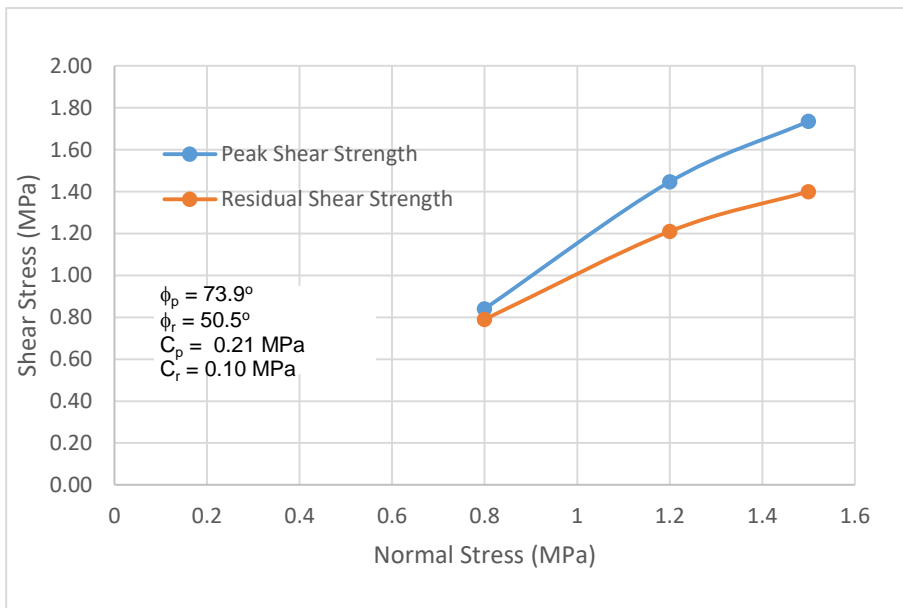


Figure 7.39. Shear stress-normal stress graph (B20, $V=10 \times 10^{-4}$ mm/sec)

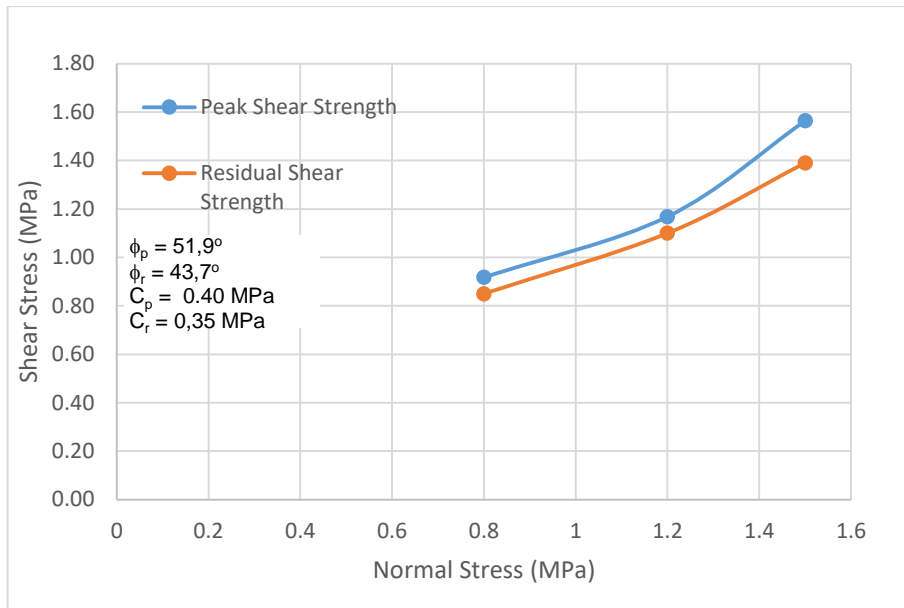


Figure 7.40. Shear stress-normal stress graph (A20, $V=7.5 \times 10^{-4}$ mm/sec)

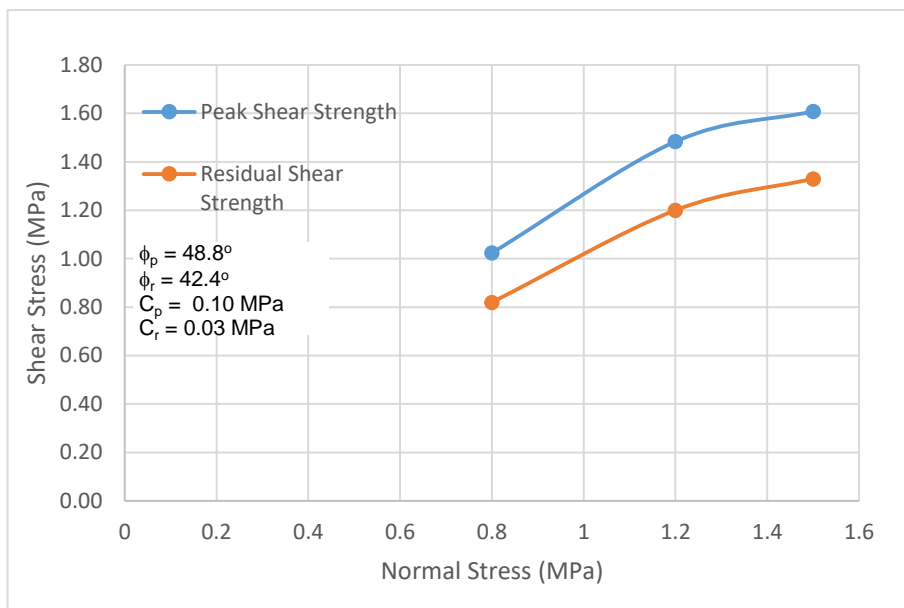


Figure 7.41. Shear stress-normal stress graph (B20, $V=7.5 \times 10^{-4}$ mm/sec)

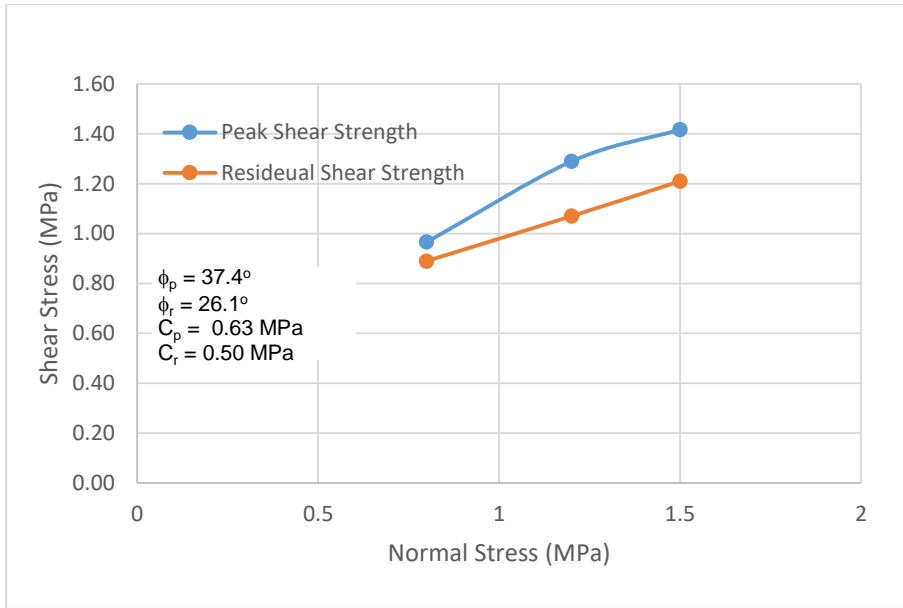


Figure 7.42. Shear stress-normal stress graph (A20, V=5x10⁻⁴ mm/sec)

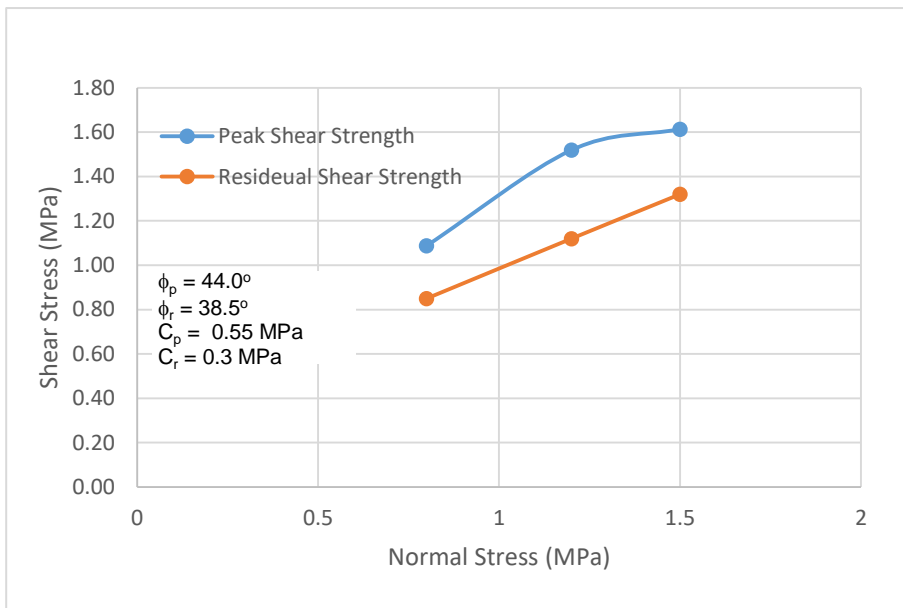


Figure 7.43. Shear stress-normal stress graph (B20, V=5x10⁻⁴ mm/sec)

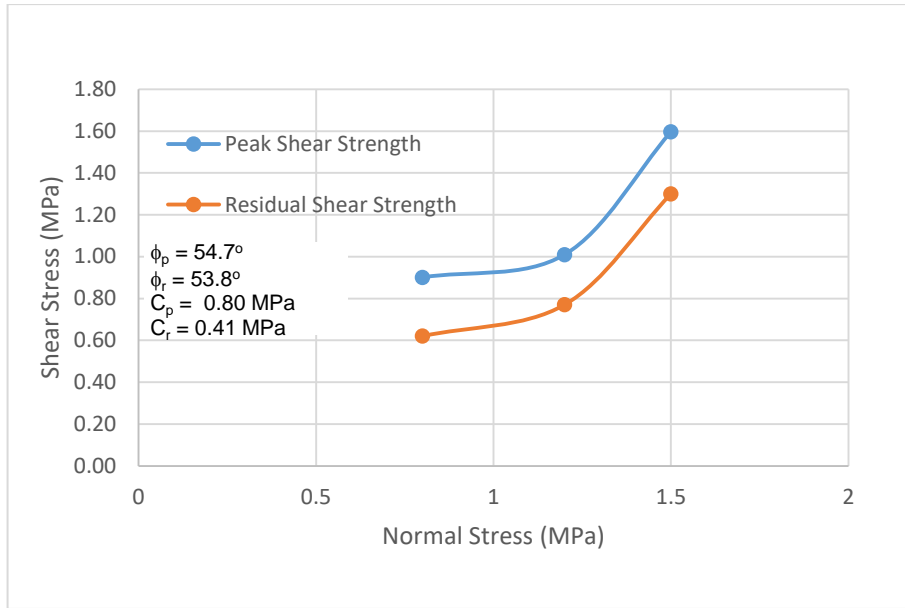


Figure 7.44. Shear stress-normal stress graph (B10-1, $V=10 \times 10^{-4}$ mm/sec)

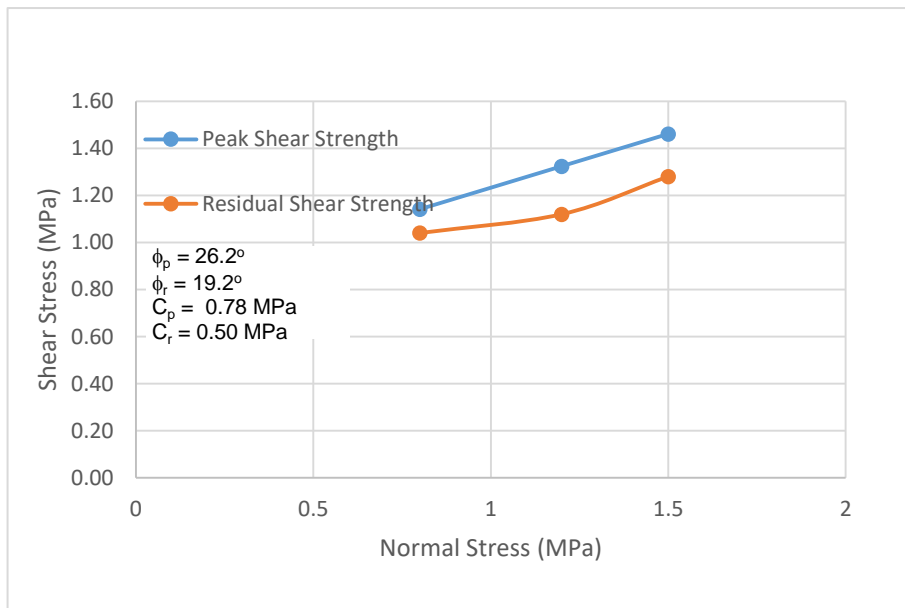


Figure 7.45. Shear stress-normal stress graph (B10-2, $V=10 \times 10^{-4}$ mm/sec)

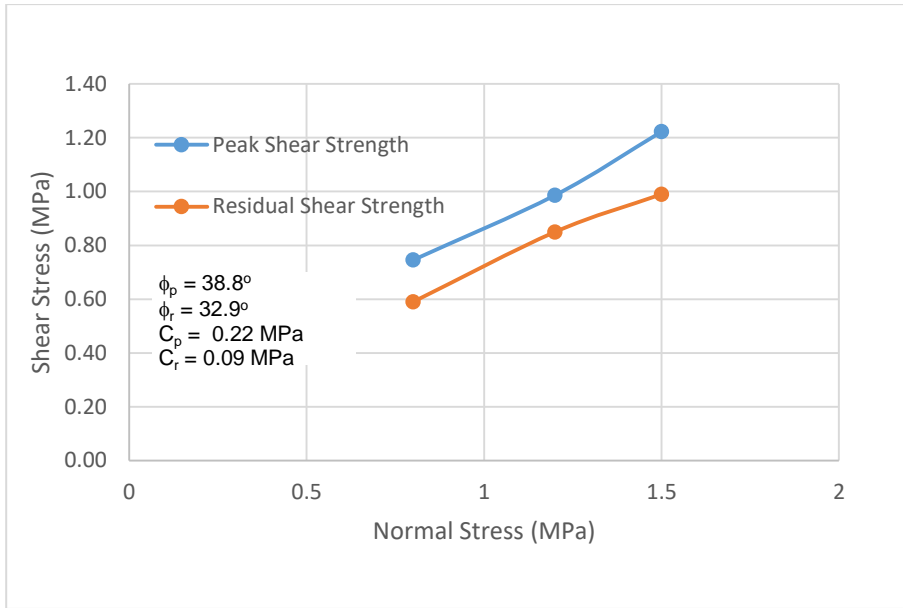


Figure 7.46. Shear stress-normal stress graph (B10-3, $V=10 \times 10^{-4} \text{ mm/sec}$)

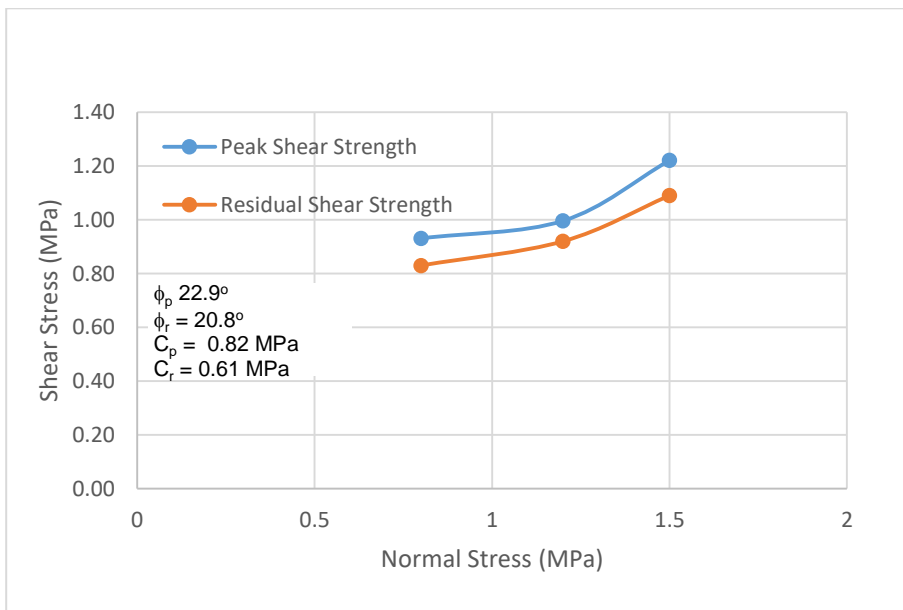


Figure 7.47. Shear stress-normal stress graph (B10-4, $V=10 \times 10^{-4} \text{ mm/sec}$)

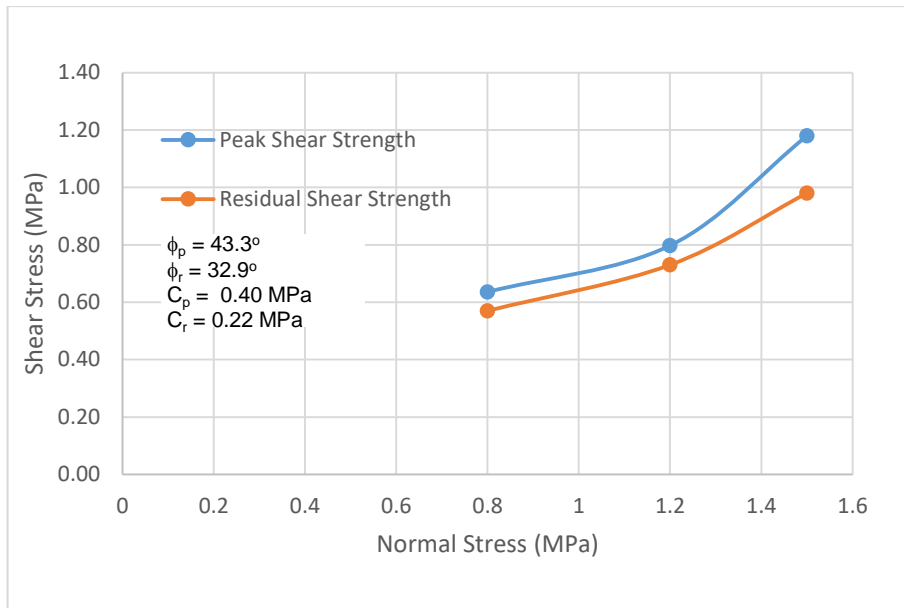


Figure 7.48. Shear stress-normal stress graph (B10-1, $V=7.5 \times 10^{-4}$ mm/sec)

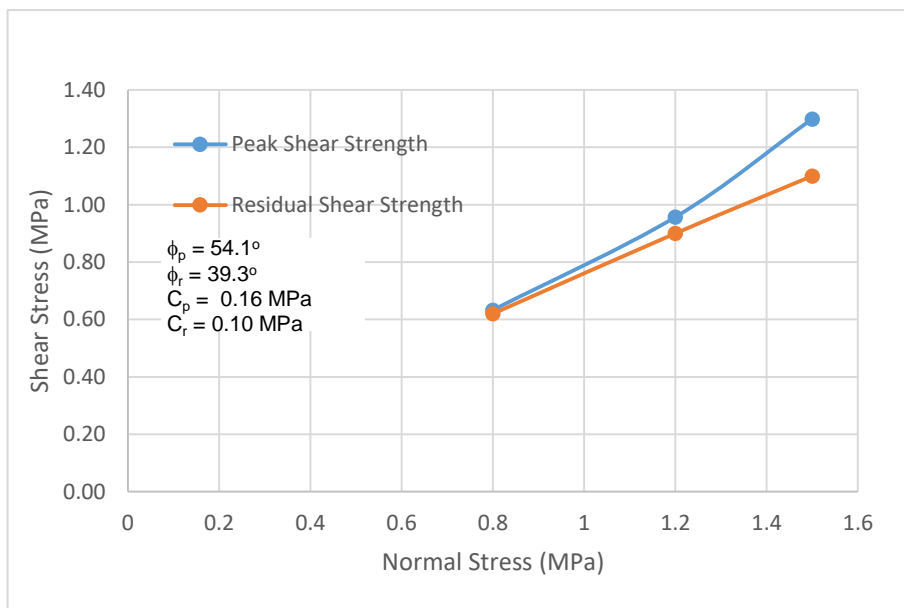


Figure 7.49. Shear stress-normal stress graph (B10-2, $V=7.5 \times 10^{-4}$ mm/sec)

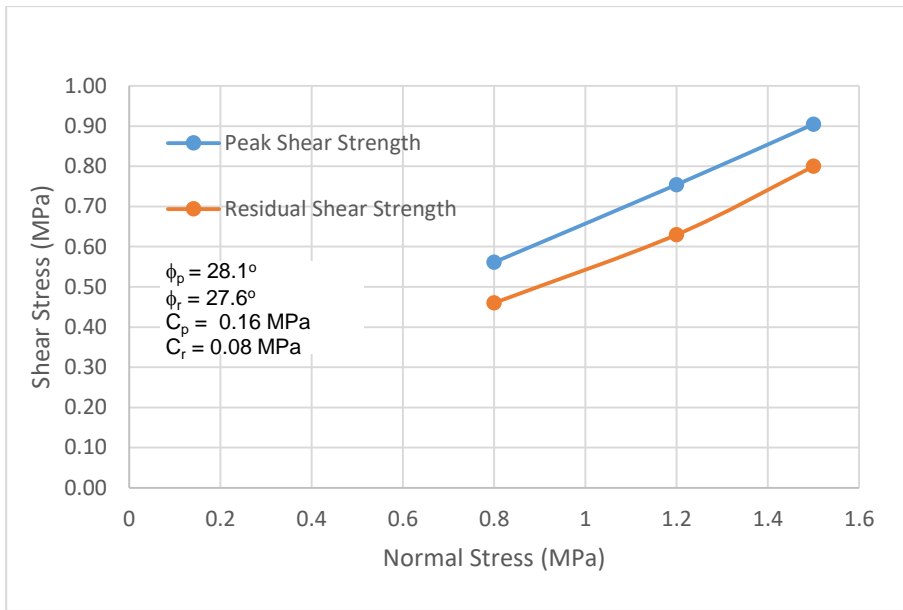


Figure 7.50. Shear stress-normal stress graph (B10-3, $V=7.5 \times 10^{-4}$ mm/sec)

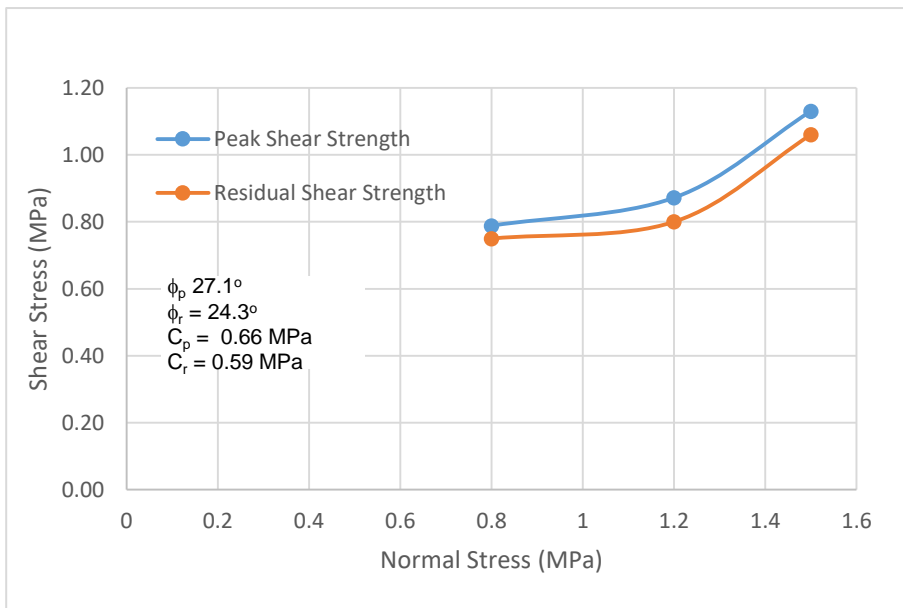


Figure 7.51. Shear stress-normal stress graph (B10-4, $V=7.5 \times 10^{-4}$ mm/sec)

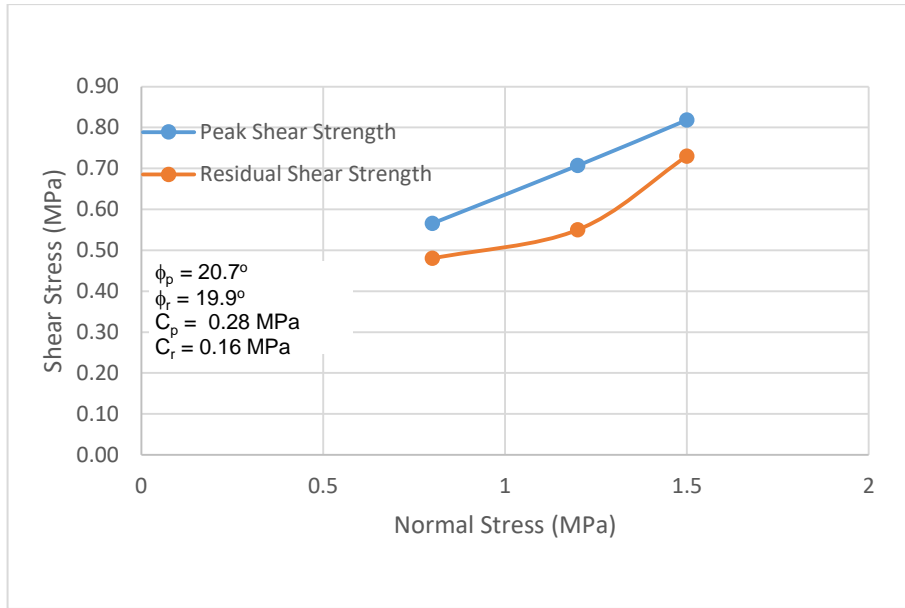


Figure 7.52. Shear stress-normal stress graph (B10-1, $V=5 \times 10^{-4}$ mm/sec)

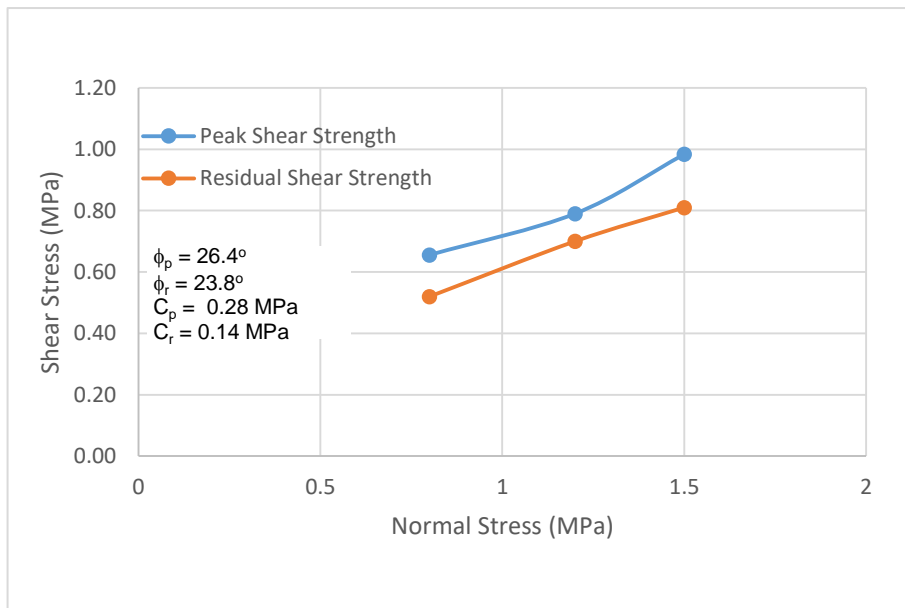


Figure 7.53. Shear stress-normal stress graph (B10-2, $V=5 \times 10^{-4}$ mm/sec)

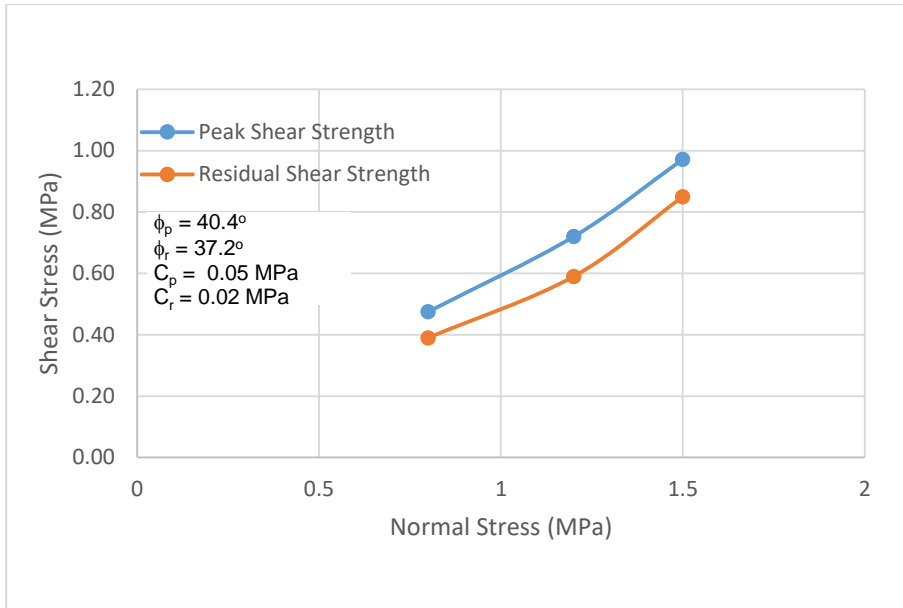


Figure 7.54. Shear stress-normal stress graph (B10-3, $V=5 \times 10^{-4}$ mm/sec)

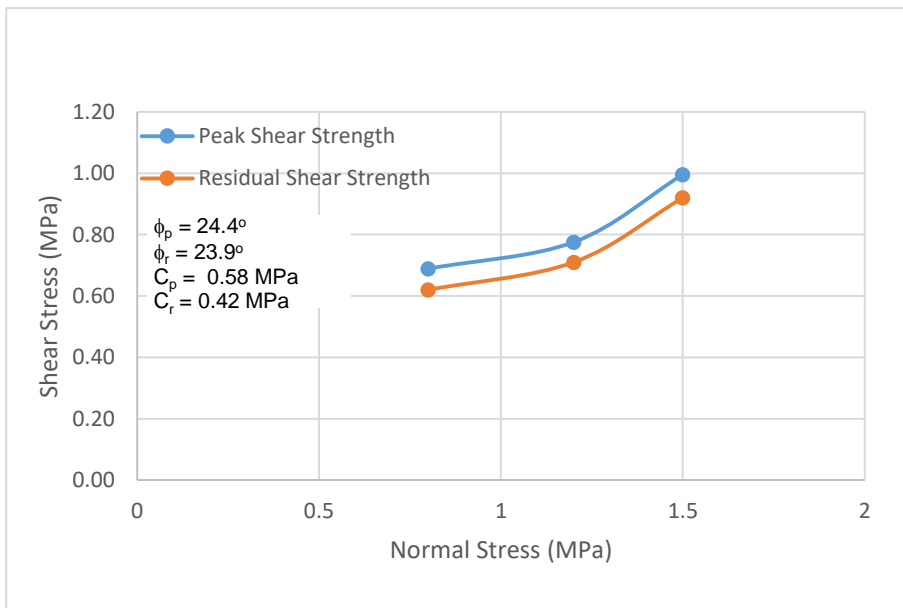


Figure 7.55. Shear stress-normal stress graph (B10-4, $V=5 \times 10^{-4}$ mm/sec)

The peak and residual values of friction angle and cohesion of samples are also given in Table 7.3.

Table 7.3. Friction angles and cohesions

Specimen	Shear Rate (10 ⁻⁴ mm/sec)	Peak		Residual	
		Cohesion (MPa)	Friction Angle (°)	Cohesion (MPa)	Friction Angle (°)
A20	10	0.18	68.7	0.11	54.8
	7.5	0.40	51.9	0.35	43.7
	5	0.63	37.4	0.50	26.1
B20	10	0.21	73.9	0.10	50.5
	7.5	0.10	48.8	0.03	42.4
	5	0.55	44.0	0.30	38.5
B10-1	10	0.80	54.7	0.41	53.8
	7.5	0.40	43.3	0.22	32.9
	5	0.28	20.7	0.16	19.9
B10-2	10	0.78	26.2	0.50	19.2
	7.5	0.16	54.1	0.10	39.3
	5	0.28	26.4	0.14	23.8
B10-3	10	0.22	38.8	0.09	32.9
	7.5	0.16	28.1	0.08	27.6
	5	0.05	40.4	0.02	37.2
B10-4	10	0.82	22.9	0.61	20.8
	7.5	0.66	27.1	0.59	24.3
	5	0.58	24.4	0.42	23.9

The peak and the residual friction angles increase as the roughness level increases. The peak and the residual cohesion values decrease as the roughness level increases. For A20 and B20, the peak and residual friction angles decrease with decreasing shear rate. For small size samples, the values also decrease, however there are a few contradictory results that need to be investigated with further experiments. The peak and the residual cohesion values increase with decreasing shear rate for A20 and B20, however, for B10 samples, the peak and the residual cohesion values generally decrease with decreasing shear rate. The peak and friction angles increase with increasing sample size and the cohesion values decrease with increasing sample size.

7.3. Discussion of Co-Dependency of Roughness and Shear Rate on Shear Strength

In this study, shearing behaviors of A20 and B20 discontinuities are compared in order to understand the effect of roughness, shear rate and co-dependency of these two factors. Also, by comparing the percent changes in shear strengths, change in the effect of roughness characteristics with respect to different shear rates are analyzed.

The surface roughness has a strengthening effect on shearing characteristics of rock discontinuities. The peak shear strength is reached when overridden or failure of individual asperities and undulations are completed. As expected, peak shear strength values are higher at all normal stress levels for B20 which has the higher Z_2 (0.212) and JRC (11.71) values. After reaching the peak value, the shear strength decreases to a residual value where major asperities are failed or overridden and shear displacement takes place at a constant applied force. At this point, since roughness is no longer predominantly present, residual shear strength becomes a material property. Therefore, experimental results showed closer values of residual shear strengths for both discontinuities.

The rock discontinuities show different frictional behaviors under different shear rates. Changes in shearing characteristics are generally caused by stick-slip behavior or position of contact faces. For hard rocks, shear strength of rock discontinuities increases with decreasing shear rate and for softer rocks, shear strength decreases with decreasing shear rate (Crawford and Curran, 1981). ISRM suggested using shear rates between 0.1-0.2 mm/min (1.67×10^{-3} - 3.33×10^{-3} mm/sec) in direct shear test of rock discontinuities (Muralha et al., 2014). Densmore et al. (1998) summarized the previous studies based on calculated rate of bedrock landsliding which is around 10 – 14 mm/year (3.2×10^{-7} – 4.4×10^{-7} mm/sec). In this study, frictional behaviors of rock discontinuity replicas (A20 and B20) are investigated under three different shear rates (10×10^{-4} , 7.5×10^{-4} , 5×10^{-4} mm/sec). Results showed that, effect of shear rate depends on the level of normal stress. For both discontinuity samples, peak and residual values of shear strength decreases with decreasing shear rate at 1.5 MPa normal stress. However, under 0.8 MPa normal stress, shear strength values increases with decreasing shear rates. Under 1.2 MPa normal stress, experiments yielded complex results, therefore more tests are required for indepth understanding. In order to explain the level of normal stress dependence of shear rate effects, normal displacement-shear displacement graphs are examined (Figures 7.56-7.59).

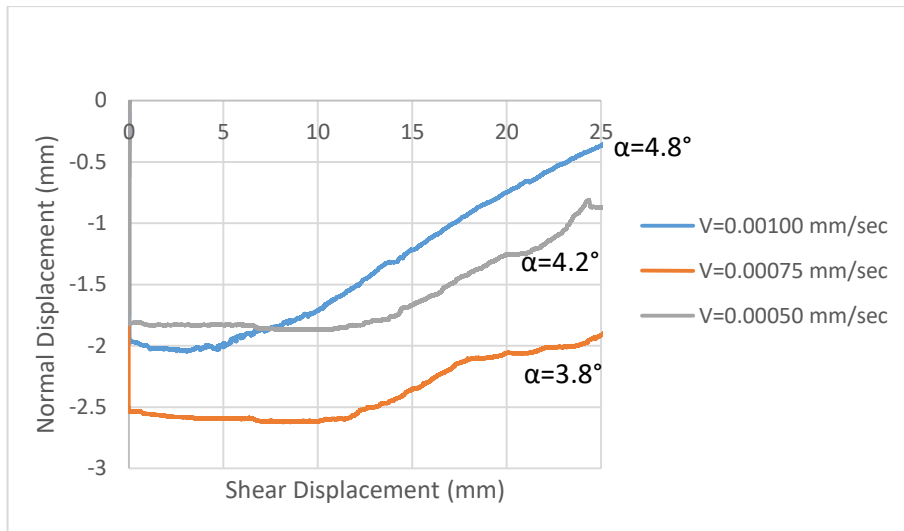


Figure 7.56. Normal displacement-shear displacement graph (A20-N=1.5 MPa)

For A20, under 1.5 MPa normal stress, dilation angles decrease with decreasing shear rate. However, dilation angle at 0.0075 mm/sec shear rate is lower than expected.

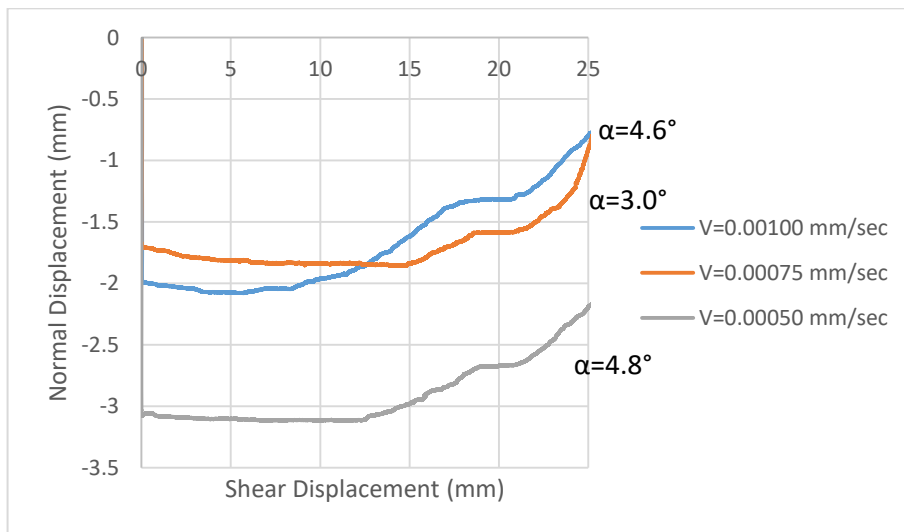


Figure 7.57. Normal displacement-shear displacement graph (A20-N=0.8 MPa)

For A20, under 0.8 MPa normal stress, dilation angles decrease with decreasing shear rate.

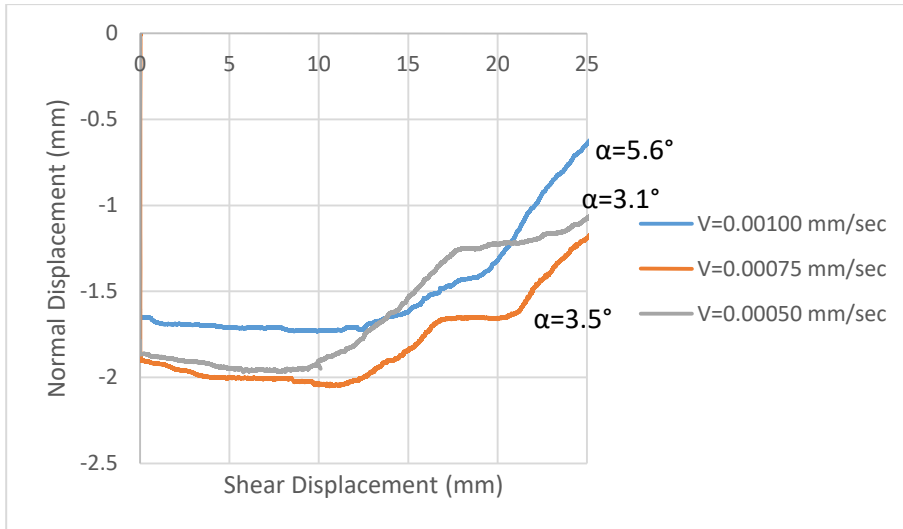


Figure 7.58. Normal displacement-shear displacement graph (B20-N=1.5 MPa)

For B20, under 1.5 MPa normal stress, dilation angles decrease with decreasing shear rate. However, dilation angle at 0.0075 mm/sec shear rate is lower than expected.

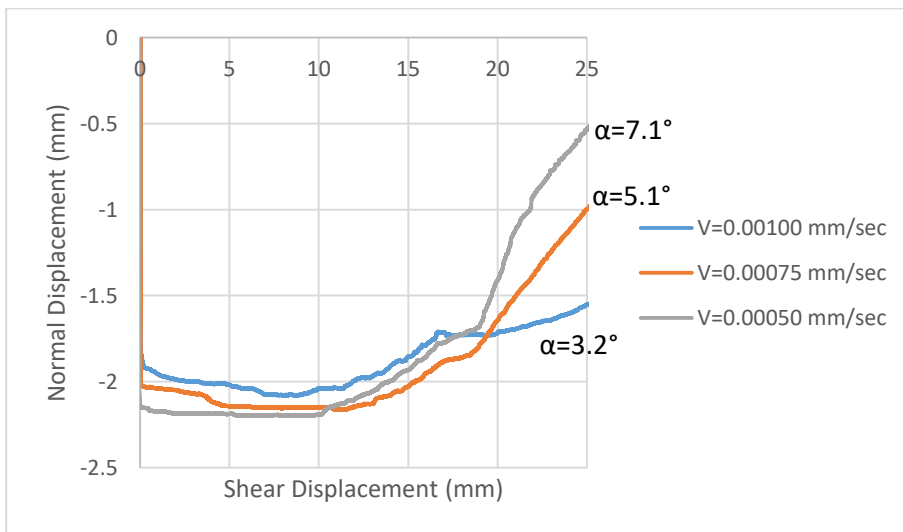


Figure 7.59. Normal displacement-shear displacement graph (B20-N=0.8 MPa)

For B20, under 0.8 MPa normal stress, dilation angles increase with decreasing shear rate.

Under 1.5 MPa normal stress, dilation angles decrease with decreasing shear rate. Consequently, shear strength values decrease. However, under 0.8 MPa normal stress, dilation angles increase with decreasing shear rate which results in an increase of shear strength values.

Co-dependency of shear rate and roughness effects are examined in the Figures 7.60-7.65.

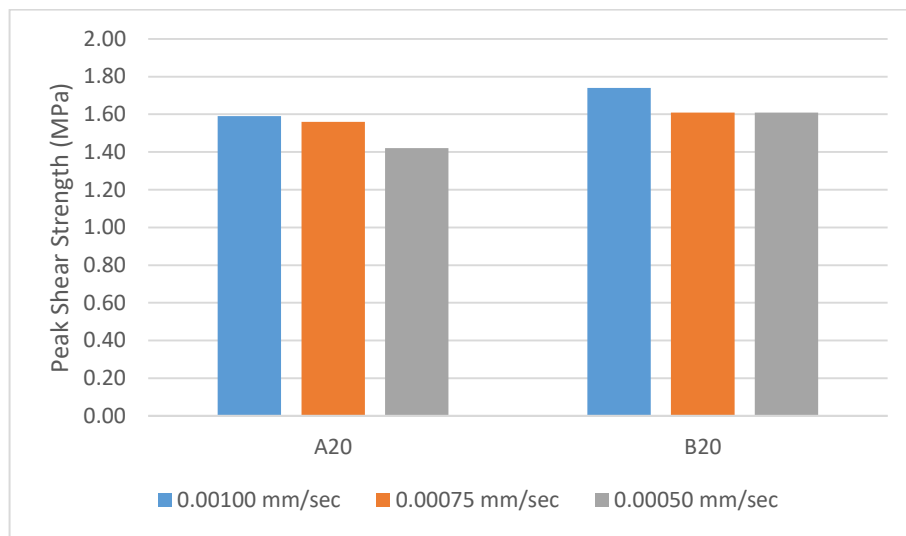


Figure 7.60. Roughness-shear rate effect, A20-B20 peak shear strengths, N=1.5 MPa

Under 1.5 MPa normal stress, decreasing the shear rate, decreases the peak shear strength for both roughness levels.

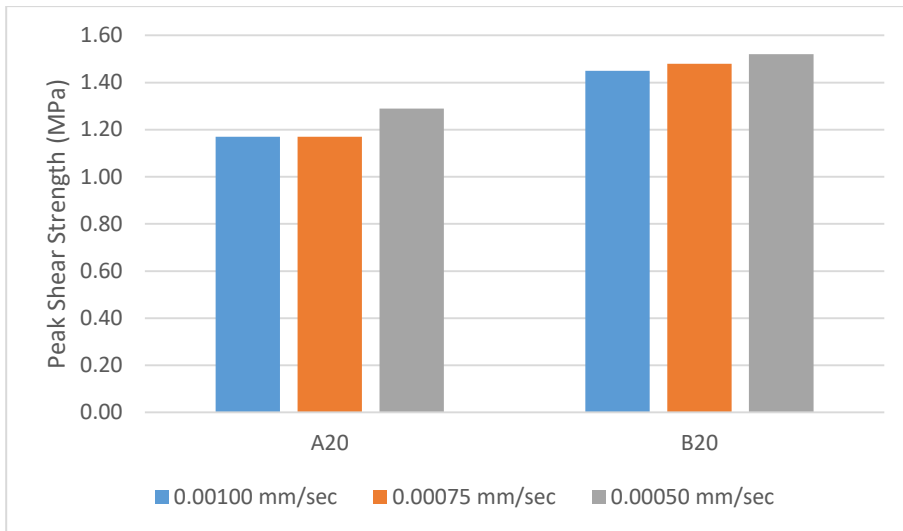


Figure 7.61. Roughness-shear rate effect, A20-B20 peak shear strengths, N=1.2 MPa

Under 1.2 MPa normal stress, decreasing the shear rate, increases the peak shear strength for both roughness levels.

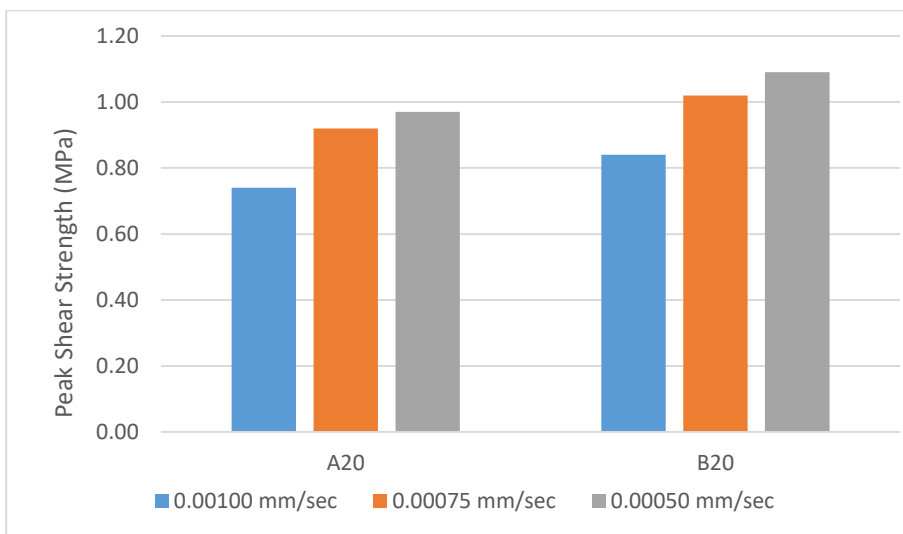


Figure 7.62. Roughness-shear rate effect, A20-B20 peak shear strengths, N=0.8 MPa

Under 0.8 MPa normal stress, decreasing the shear rate, increases the peak shear strength for both roughness levels.

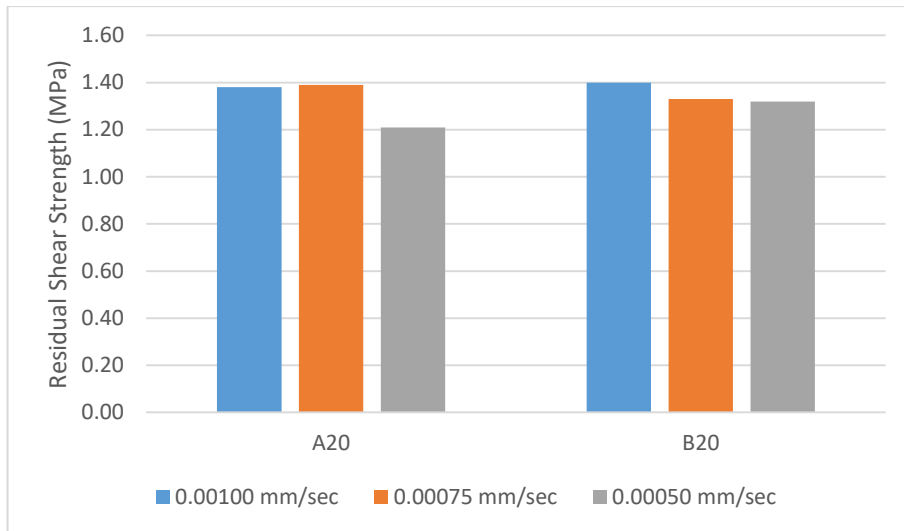


Figure 7.63. Roughness-shear rate effect, A20-B20 residual shear strengths, N=1.5 MPa

Under 1.5 MPa normal stress, decreasing the shear rate, decreases the residual shear strength for both roughness levels.

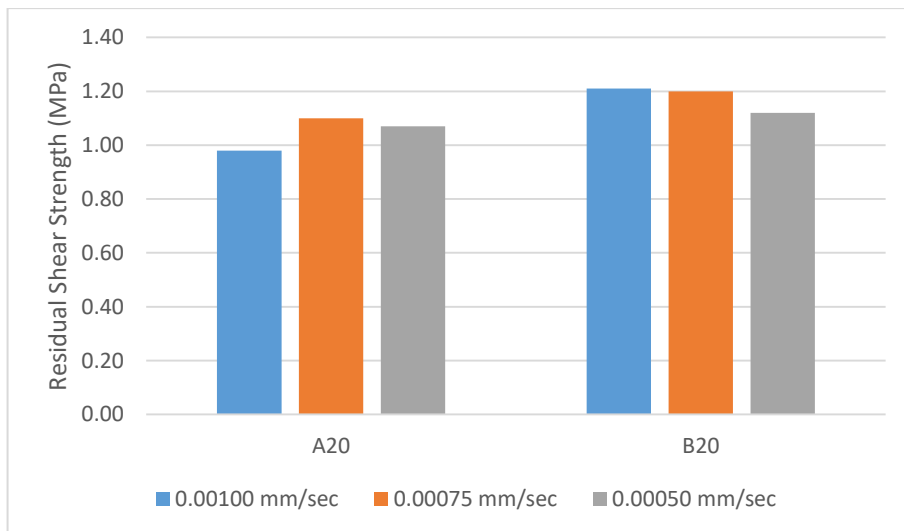


Figure 7.64. Roughness-shear rate effect, A20-B20 residual shear strengths, N=1.2 MPa

Under 1.2 MPa normal stress, decreasing the shear rate, increases the residual shear strength of the planar surface and decreases the residual shear strength of the rough surface.

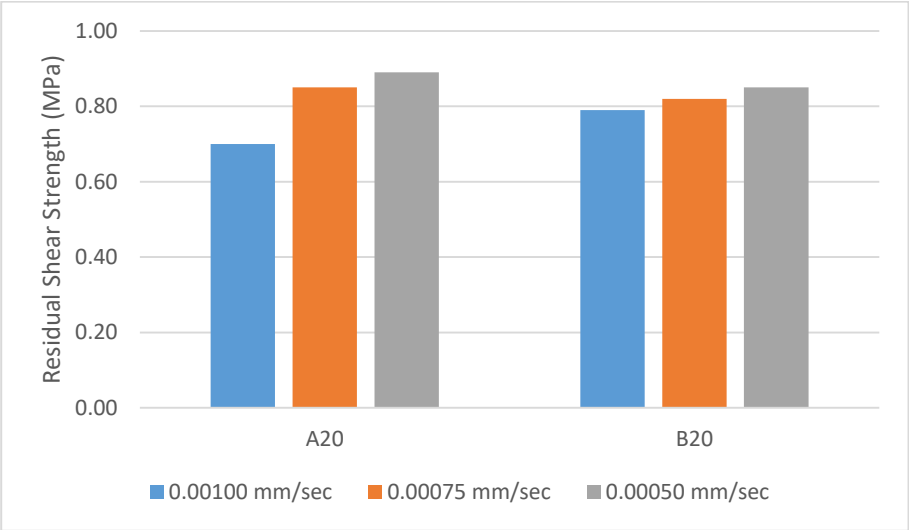


Figure 7.65. Roughness-shear rate effect, A20-B20 residual shear strengths, N=0.8 MPa

Under 0.8 MPa normal stress, decreasing the shear rate, increases the residual shear strength for both roughness levels.

The shear rate effect on peak and residual shear strength is normal stress dependent for both roughness levels. Under 1.5 MPa normal stress, decreasing the shear rate, lowers the peak and the residual shear strength values for both discontinuities. Under 1.2 MPa normal stress, the peak shear strengths increase with the decreasing shear rate. However, residual shear strength of discontinuity A20 increases with the decreasing shear rate whereas that of discontinuity B decreases. This shows that, investigation of shearing behavior under 1.2 MPa shows variant results. Therefore, more experiments with different roughness levels should be conducted, in order to be able to better interpret the behavior under 1.2 MPa normal stress. Under 0.8 MPa normal stress, decreasing shear rate, increases the peak and the residual shear strengths of both discontinuities.

Even though the shear rate effect on shear strength for both discontinuities is on the same direction, magnitude of the effect might be different. Therefore, percent changes in peak and residual shear strength with decreasing shear rate is investigated in Figures 7.66 and 7.67.

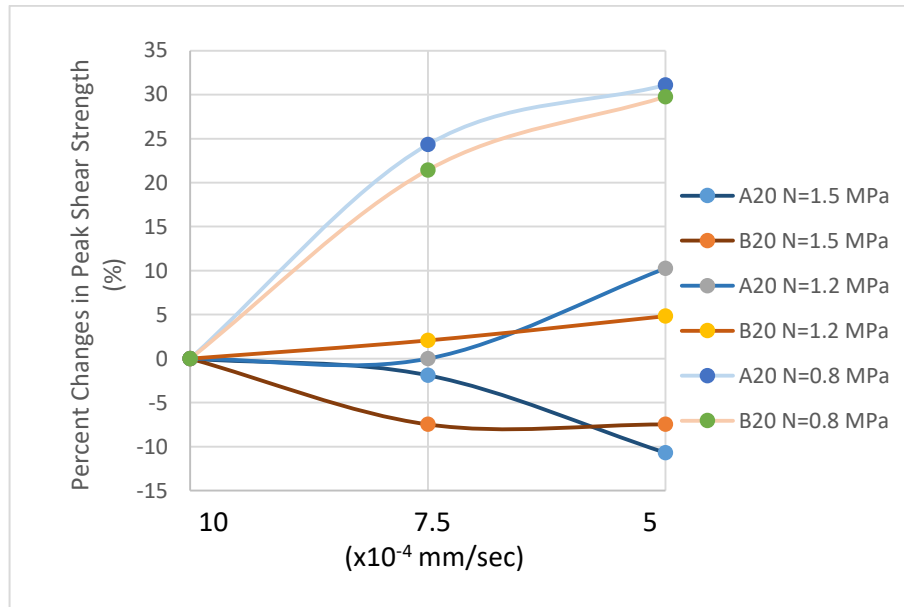


Figure 7.66. Roughness-shear rate effect - Percent changes in peak shear strength

Under 1.5 MPa normal stress, the peak shear strengths of A20 and B20 decreased 11% and 7%, respectively. Under 1.2 MPa normal stress, the peak shear strength of A20 and B20 increased 11% and 5%, respectively. Under 0.8 MPa normal stress, the peak shear strength of A20 and B20 increased 31% and 29%, respectively.

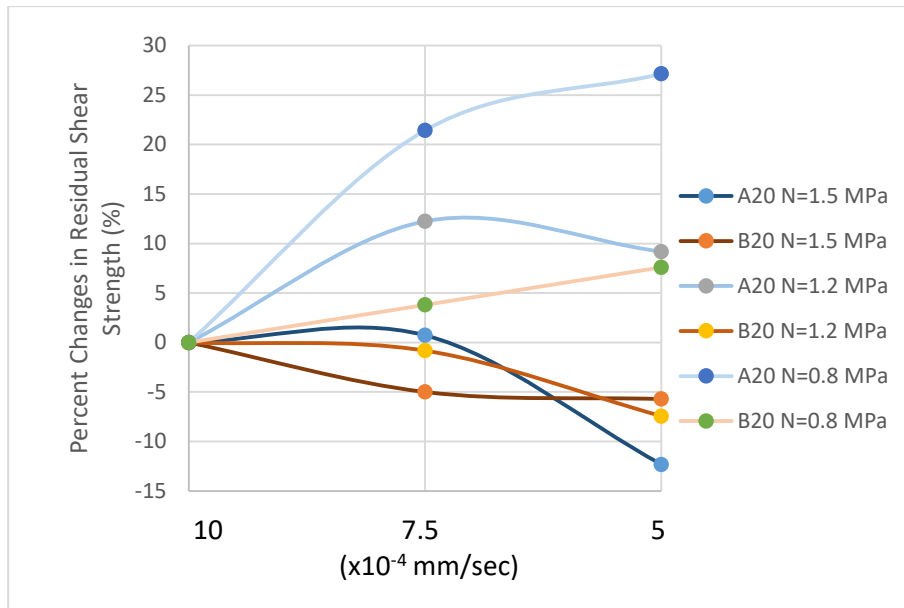


Figure 7.67. Roughness-shear rate effect - Percent changes in residual shear strength

Under 1.5 MPa normal stress, the residual shear strengths of A20 and B20 decreased 12% and 6%, respectively. Under 1.2 MPa normal stress, the residual shear strength of A20 increased 9%, whereas the residual shear strength of B20 decreased 7%. Under 0.8 MPa normal stress, the residual shear strengths A20 and B20 increased 27% and 8%, respectively.

Changes in shear rate cause changes with different magnitudes on the peak and the residual shear strength of rock discontinuities based on their roughness degree. When the shear rate is decreased from 10×10^{-4} mm/sec to 5×10^{-4} mm/sec, greater changes occurred in planar surfaces (A20). Consequently, the shear rate and the roughness effects are co-dependent. In other words, effect of shear rate becomes greater as the degree of roughness decreases.

7.4. Discussion of Co-dependency of Sample Size and Shear Rate on Shear Strength

In this study, effect of specimen size on shear strength of rock discontinuities are studied by conducting direct shearing experiments on 20 cm x 20 cm and 10 cm x 10 cm samples of Discontinuity B.

The size of the specimen has a decisive effect on the roughness level of the discontinuity sample. In small size samples, asperities are the source of the surface irregularity. In large size samples, asperities usually form a smoother surface with large scale undulations. Large scale undulations jump over smaller and steeper asperities, while sampling only larger and more gently inclined asperities. Therefore, longer and gently inclined undulations control the shear behavior of the large size samples, whereas small and steep asperities control the shear behavior of the small size samples. In addition, as explained by Ueng et al. (2010) not only specimen size, but also geometry configuration of the surface is responsible for size effect. Generally roughness increases as the sample size decreases. This phenomenon has been verified by this study as well. Z_2 value of 20 cm x 20 cm sample of the discontinuity B is 0.212 and the average Z_2 value of 10 cm x 10 cm samples of the discontinuity B is 0.384. It's expected that the increases in the degree of roughness would cause an increase in the shear strength. Thus, the expected conclusion would be the increase of the shear strength as the sample size decreases. This conclusion is provided by previous researchers (Bandis et al., 1981; Ueng et al., 2010; Yoshinaka et al., 1991) who conducted direct shear tests on different size specimens. However, in this study, shear strength is found to be decreasing with decreasing sample size.

The shear strength is dependent on the shear displacement rate, in which this effect for 20 cm x 20 samples are explained in the previous section. As a reminder, for large size samples, shear strength values decreases with decreasing shear rate at 1.5 MPa and increases with decreasing shear rate at 0.8 MPa. For small size samples (10 cm x 10 cm), shear strength decreases with decreasing shear rate for all normal stress levels. The behavior is similar to the large size sample's behavior under high normal stress. As the experiments are conducted in a large shear box, applied normal load might be turning into a point load on the discontinuity surface, causing the shearing behavior to be the same at all normal stress levels.

Co-dependency of the shear rate and the sample size effect is investigated in Figures 7.68-7.73. In order to provide a simple comparison between different sizes, average shear strength values of the four B10 samples are calculated and compared with the shear strength values of B20 in Figures 7.74-7.79.

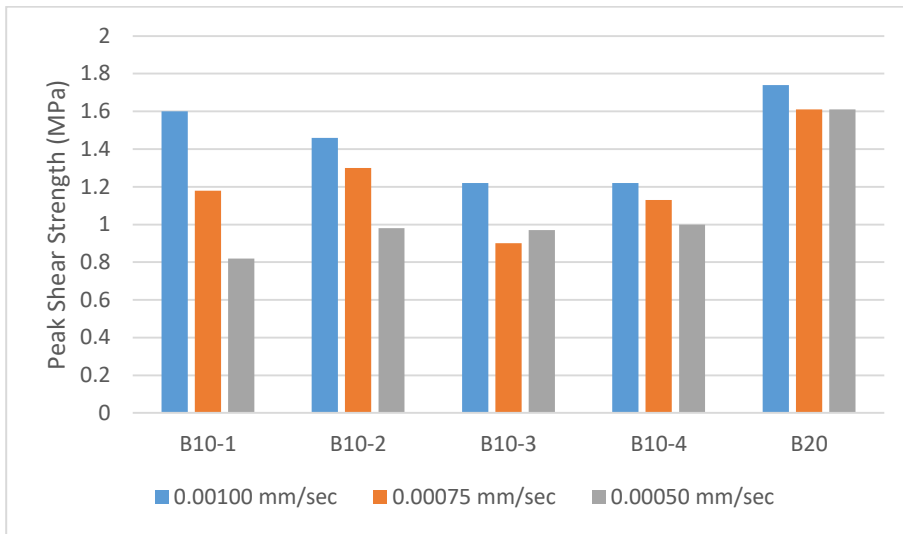


Figure 7.68. Size-shear rate effect, B10-B20 peak shear strengths, N=1.5 MPa

Under 1.5 MPa normal stress, decreasing shear rate, decreases the peak shear strength for both sample sizes. The peak shear strength is higher for the large size samples.

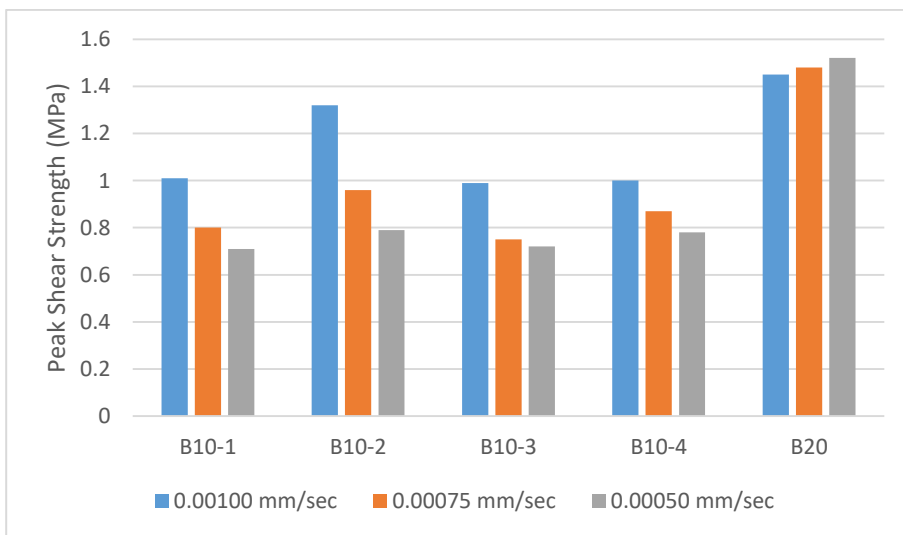


Figure 7.69. Size-shear rate effect, B10-B20 peak shear strengths, N=1.2 Mpa

Under 1.2 MPa normal stress, decreasing shear rate, decreases the peak shear strength for small size samples and increases the peak shear strength of large size samples. The peak shear strength is higher for the large size samples.

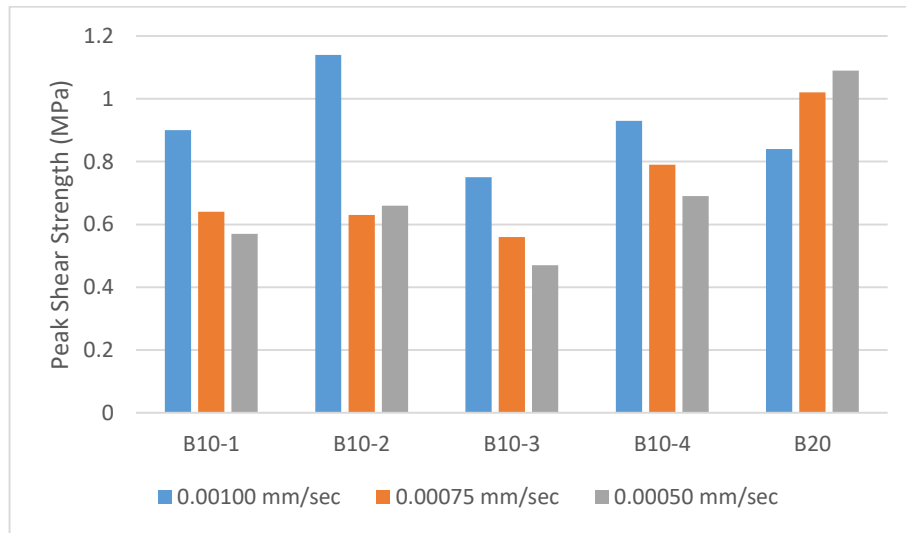


Figure 7.70. Size-shear rate effect, B10-B20 peak shear strengths, N=0.8 MPa

Under 0.8 MPa normal stress, decreasing shear rate, decreases the peak shear strength for small size samples and increases the peak shear strength of large size samples. The peak shear strength is higher for the large size samples.

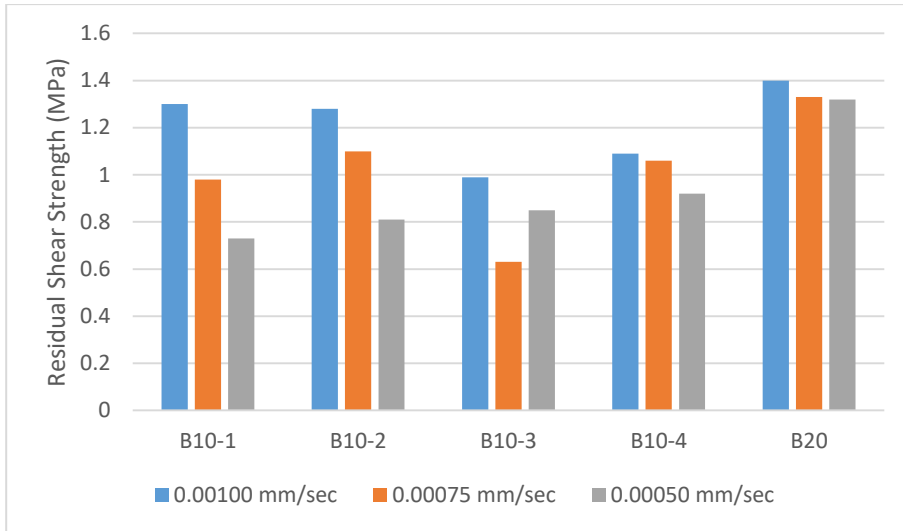


Figure 7.71. Size-shear rate effect, B10-B20 residual shear strengths, N=1.5 Mpa

Under 1.5 MPa normal stress, decreasing shear rate, decreases the residual shear strength for both sample sizes. The residual shear strength is higher for the large size samples.

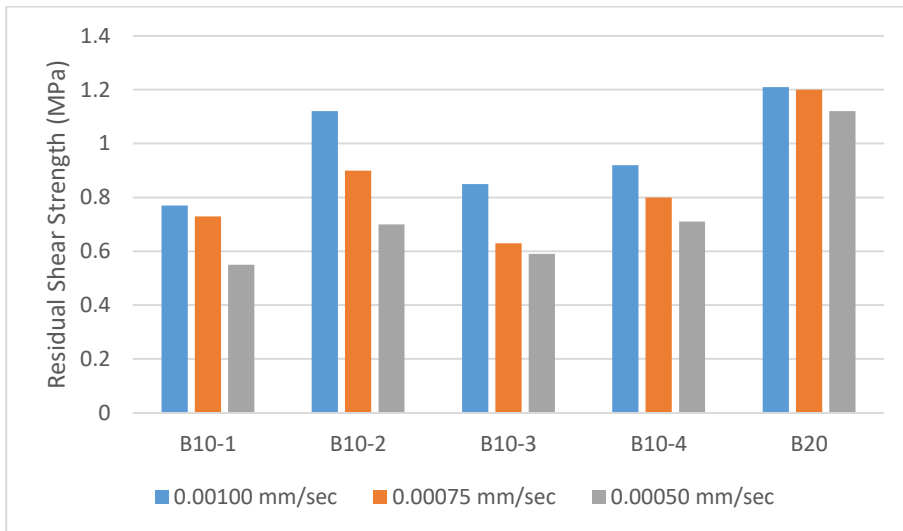


Figure 7.72. Size-shear rate effect, B10-B20 residual shear strengths, N=1.2 MPa

Under 1.2 MPa normal stress, decreasing shear rate, decreases the residual shear strength for both sample sizes. The residual shear strength is higher for the large size samples.

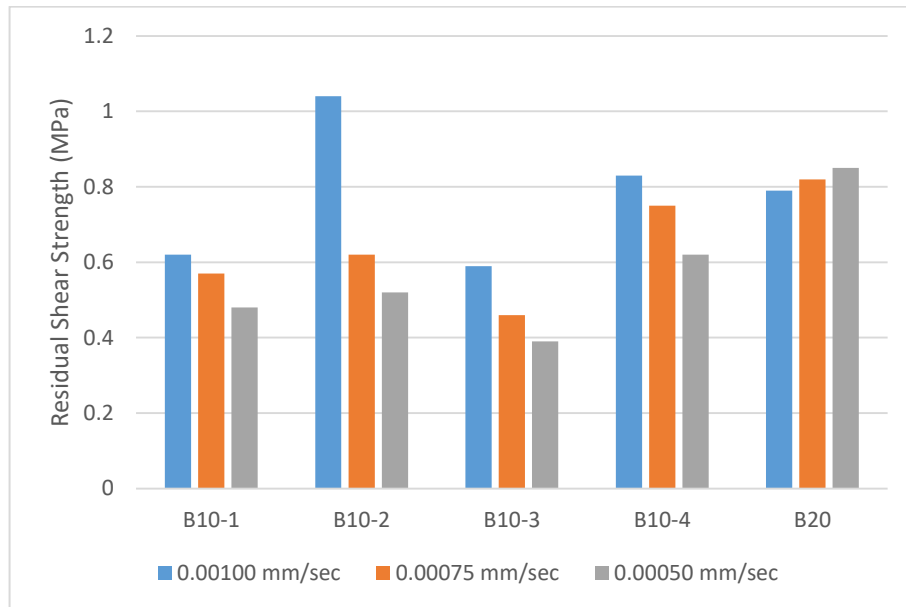


Figure 7.73. Size-shear rate effect, B10-B20 residual shear strengths, N=0.8 Mpa

Under 0.8 MPa normal stress, decreasing shear rate, decreases the residual shear strength for both sample sizes. The residual shear strength is higher for the large size samples except for B10-2 and B10-4 at 0.001 mm/sec shear rate.

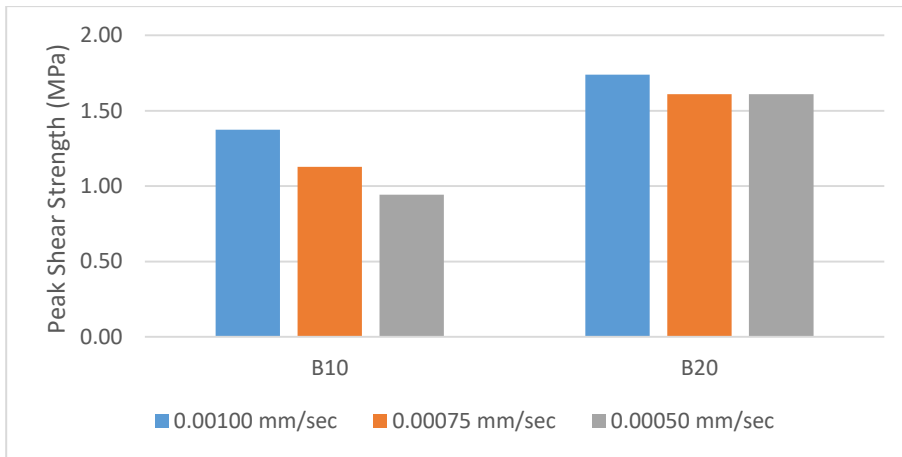


Figure 7.74. Size-shear rate effect, Average B10-B20 peak shear strengths, N=1.5 MPa

Under 1.5 MPa normal stress, decreasing shear rate, decreases the peak shear strength for both sample sizes. The peak shear strength is higher for the large size samples than the average peak shear strength of the small size samples.

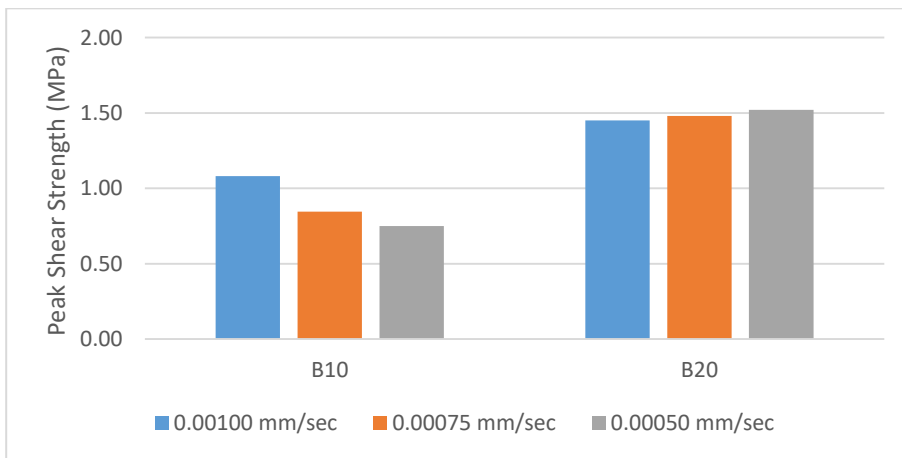


Figure 7.75. Size-shear rate effect, Average B10-B20 peak shear strengths, N=1.2 MPa

Under 1.2 MPa normal stress, decreasing shear rate, decreases the peak shear strength of small size samples and increases the peak shear strength of large size samples. The

peak shear strength is higher for the large size samples than the average peak shear strength of the small size samples.

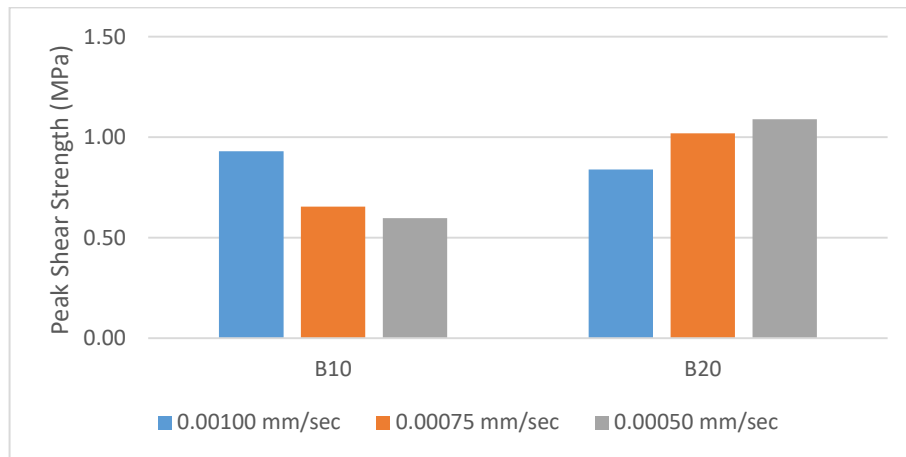


Figure 7.76. Size-shear rate effect, Average B10-B20 peak shear strengths, N=0.8MPa

Under 0.8 MPa normal stress, decreasing shear rate, decreases the peak shear strength of small size samples and increases the peak shear strength of large size samples. The peak shear strength is higher for the large size samples than the average peak shear strength of the small size samples.

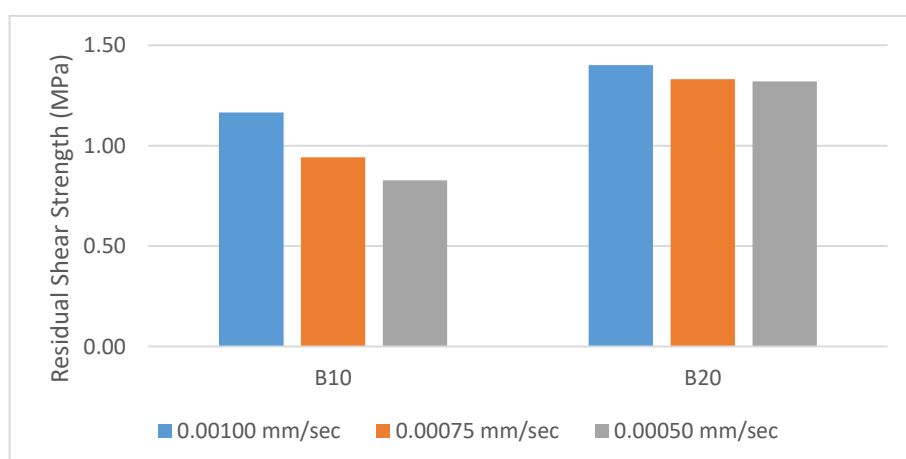


Figure 7.77. Size-shear rate effect, Average B10-B20 residual shear strengths, N=1.5 MPa

Under 1.5 MPa normal stress, decreasing shear rate, decreases the residual shear strength for both sample sizes. The residual shear strength is higher for the large size samples than the average residual shear strength of the small size samples.

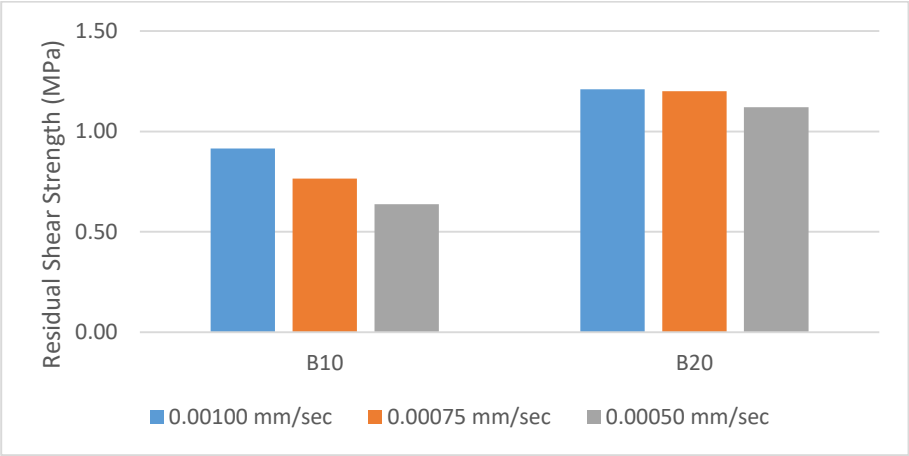


Figure 7.78. Size-shear rate effect, Average B10-B20 residual shear strengths, N=1.2 MPa

Under 1.2 MPa normal stress, decreasing shear rate, decreases the residual shear strength for both sample sizes. The residual shear strength is higher for the large size samples than the average residual shear strength of the small size samples.

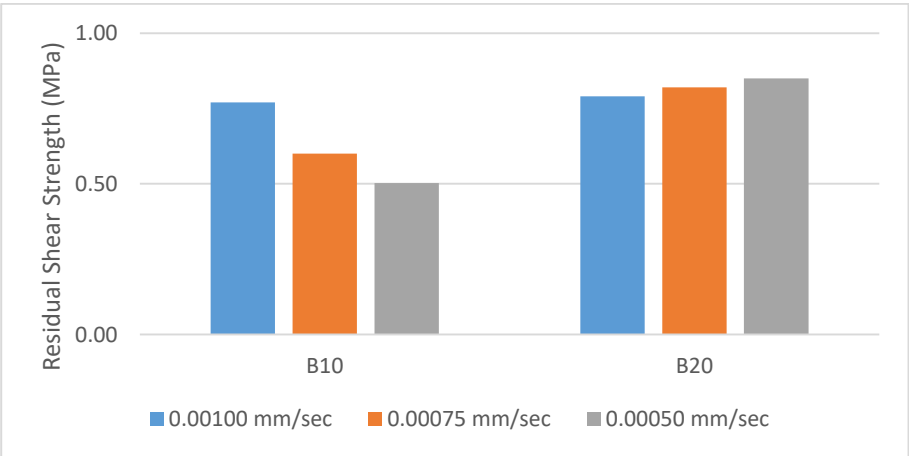


Figure 7.79. Size-shear rate effect, Average B10-B20 residual shear strengths, N=0.8 MPa

Under 0.8 MPa normal stress, decreasing shear rate, decreases the residual shear strength of the small size samples and increases the peak shear strength of the large size samples. The residual shear strength is higher for the large size samples than the average residual shear strength of the small size samples.

The shear rate effect on the shear strength of rock discontinuities is dependent on the sample size. At all normal stress levels, the average peak and the average residual shear strength of four 10 cm x 10 cm B10 samples decreases with decreasing shear rate. However, the peak and the residual shear strength of 20 cm x 20 cm B20 sample decreases with decreasing shear rate under 1.5 MPa whereas they increase with decreasing shear rate under 1.2 and 0.8 MPa. As a result, effect of the shear rate changes direction with decreasing sample size under 1.2 and 0.8 MPa normal stress levels. In addition, at different sample sizes, magnitude of the shear rate effect is different. Percent changes in the peak and the residual shear strengths of B10 and B20 when the shear rate is decreased from 10×10^{-4} to 5×10^{-4} are investigated in Figures 7.80 and 7.81.

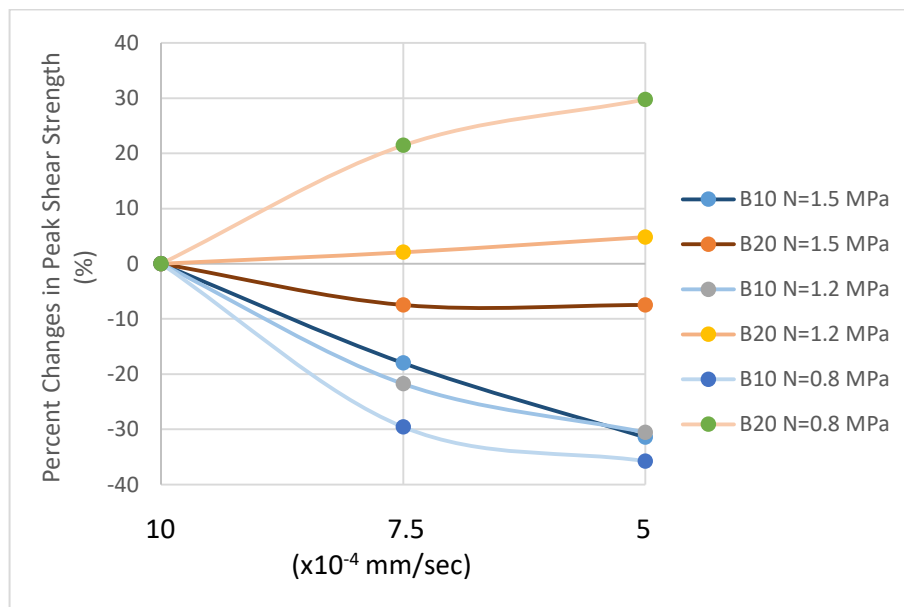


Figure 7.80. Size-shear rate effect – Percent changes in peak shear strength

Under 1.5 MPa normal stress, the peak shear strength of B10 and B20 decreased 31% and 8%, respectively. Under 1.2 MPa normal stress, the peak shear strength of B10 decreased 10% and the peak shear strength of B20 increased 5%. Under 0.8 MPa normal stress, the peak shear strength of B10 decreased 35% and the peak shear strength of B20 increased 30%.

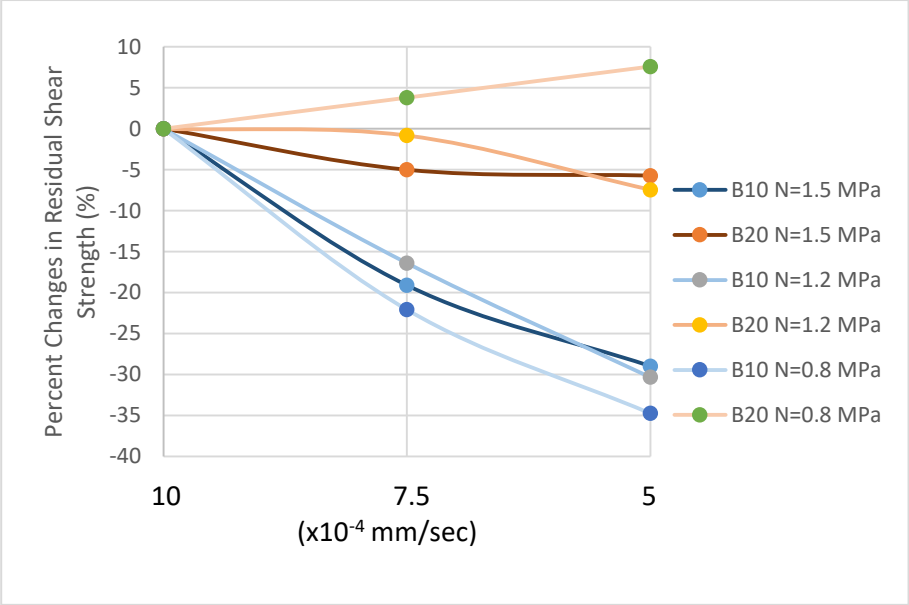


Figure 7.81. Size-shear rate effect - Percent changes in residual shear strength

Under 1.5 MPa normal stress, the residual shear strength of B10 and B20 decreased 28% and 6%, respectively. Under 1.2 MPa normal stress, the residual shear strength of B10 and B20 decreased 30% and 7%, respectively. Under 0.8 MPa normal stress, the residual shear strength of B10 decreased 35% and the residual shear strength of B20 increased 8%.

Changes in shear rate cause changes with different magnitudes and directions on the peak and the residual shear strength of rock discontinuities of different sizes. When the shear rate is decreased from 10x10⁻⁴ mm/sec to 5x10⁻⁴ mm/sec, greater changes occurred in small size samples (B10). Consequently, the shear rate and the sample size effects are co-dependent. In other words, effect of shear rate becomes greater as the sample size decreases.

7.5. Comparison of the Results and the Findings of the Previous Studies

The results derived from this study and that of previous studies by other researchers are summarized in Table 7.4. Last row of Table 7.4 presents the summary of the results of this study. In Table 7.4, positive (+) effect means that, the shear strength increases as the shear rate or sample size increases and negative (-) effect means that, the shear strength decreases as the shear rate or sample size increases.

Normal stresses used for investigation of shear rate and sample size effects are generally in the range of 0.5-2 MPa if direct shear test is employed. Much greater confining pressures are required for other shear testing systems such as triaxial shearing. Normal stress levels used in this study (0.8-1.2-1.5 MPa) are compatible with previous research.

A wide range of rock types, from soft rocks to hard rocks, or other materials such as plaster are tested for investigation of parameter effects in many previous works. Looking at the results of these experiments, it's clear that material type has a fundamental effect on characteristics of shear rate and sample size effects. In this study, concrete is used for direct shear test, whose material properties are similar to sedimentary rocks (e.g. sandstone).

Previous researchers used much higher shear rates in direct shear test than the rates used in this study. Rates are selected as to better reflect the field conditions, since sliding rates are much lower in the field. The past research about the shear rate effect on rock discontinuity shearing behavior, revealed different outcomes. Some of the results indicated increasing shear strength with decreasing shear rates (Crawford and Curran, 1981; Atapour and Mosavi, 2013; Kleepmak et al., 2016), there are other studies showing opposite results (Dieterich, 1972; Schneider, 1977; Crawford and Curran, 1981; Lockner et al., 1986; Li et al., 2012; Atapour and Mosavi, 2013). The results of this study are not completely in the same direction with any of the previous results in the literature. On the contrary, this study revealed that effect of the shear rate depends on the level of normal stress. At high normal stress levels, shear strength increases with increasing shear rate and at low normal stress levels, shear strength decreases with increasing shear rate. In addition, different results encountered in the literature might be caused by the differences in material types.

The sample size effect is generally investigated with 6-30 cm sample lengths in previous works. Although there are some studies that used much greater lengths, indicated size range is seen enough to observe the trend. Effect of sample size on shearing behavior is also an often investigated phenomenon. It's widely known that, shear strength is expected to increase as the sample size decreases and there are studies confirming this (Bandis et al., 1981; Yoshinaka et al., 1991; Ueng et al., 2010). However, there are many other works showing no significant size effect (Hencher et al., 1993; Tatone and Grasselli, 2012; Johansson, 2016). Conversely, this study has indicated a reverse size effect, that's not been encountered in the literature. According to the results of this study, shear strength increases with increasing sample size.

Table 7.4. Results of the Previous Studies

Reference	Test Apparatus	Material Type	Normal Stress	Roughness	Shear Rate	Sample Size	Shear Rate Effect	Sample Size Effect
Atapour and Mosavi, 2013	Direct Shear	Plaster	0.6 - 1.8 MPa	i = 0°, 10°, 20°	0.3 - 30 mm/min	116x100x65 mm	(-)	NA
Atapour and Mosavi, 2013	Direct Shear	Concrete	0.64 - 1.92 MPa	i = 0°, 10°, 20°	0.3 - 30 mm/min	116x100x65 mm	(+)	NA
Schneider, 1977	Direct Shear	Shale	1.9 MPa	Not specified	0.01-200 mm/min	500 cm ²	(+)	NA
Dieterich, 1972	Double-Direct Shear	Sandstone, Graywacke, Red Granite, Quartzite	2 - 85 MPa	Not specified	15 - 10 ⁵ sec. (Stick Intervals)	6x6 cm	(+)	NA
Kleepmak, 2016	Triaxial Shear	Granite, Sandstone, Marl	1 - 18 Mpa (Confining Pressure)	JRC= 13-10-11	10 ⁻⁵ - 10 ⁻² mm/sec	50 x 100 mm ²	(-)	NA
Lockner et al., 1986	Triaxial Shear	Granite	250 Mpa (Confining Pressure)	Not specified	5x10 ⁻⁵ - 5x10 ⁻³ mm/sec	d=19.05 mm	(+)	NA
Olsson, 1974	Triaxial Shear	Limestone	20 - 100 Mpa (Confining Pressure)	Not specified	10 ⁻³ - 10 ⁻⁷ mm/sec	d=2 cm	(0)	NA
Li et al., 2012	Direct Shear	Plaster	1 - 4 MPa	Not specified	0.5 - 50 mm/min	100x200x100 mm	$\tau_p(0)$ $\tau_r(+)$	NA
Crawford and Curran, 1981	Direct Shear	Dolomite	0.625 - 2.5 MPa	Not specified	0.05 - 200 mm/sec	200x200 mm	at low normal stress (+)	NA

(+): Positive effect

(-): Negative effect

(0): Insignificant effect

NA: Not Applicable

Reference	Test Apparatus	Material Type	Normal Stress	Roughness	Shear Rate	Sample Size	Shear Rate Effect	Sample Size Effect
Crawford and Curran, 1981	Direct Shear	Granite	0.625 - 2.5 MPa	Not specified	0.05 - 200 mm/sec	200x200 mm	(0)	NA
Crawford and Curran, 1981	Direct Shear	Syenite, Sandstone	0.625 - 2.5 MPa	Not specified	0.05 - 200 mm/sec	200x200 mm	(-)	NA
Bandis et al., 1981	Direct Shear	A multicomponent brittle material	0.04 - 3.6 MPa	JRC= 6.5 - 7.5 - 10.6 - 16.6	Not specified	6 - 12 - 18 - 36 cm	NA	(-)
Johansson, 2016	Direct Shear	Granite	1 MPa	Not specified	Not specified	6 - 20 cm	NA	(0)
Ueng et al., 2010	Direct Shear	Plaster	0.5 - 2 MPa	JRC= 4~6 - 18~20	0.5 mm/min	7.5 - 30 cm	NA	(-)
Tatone and Grasselli, 2012	Numerical Direct Shear	NA	24.5 kPa	Not specified	4 mm/s	50 - 100 - 200 - 400 mm	NA	(0)
Hencher et al., 1993	Direct Shear	A multicomponent brittle material	24.5 kPa	Not specified	0.4 mm/min	88 - 176 - 354 mm	NA	(0)
Yoshinaka et al., 1991	Direct Shear	Granite	0.5 - 2 MPa	Not specified	Not specified	4 cm - 100 cm	NA	(-)
This Study	Direct Shear	Concrete	0.8 - 1.2 - 1.5 MPa	JRC= 1.9 - 11.7 - 17.0	10x10 ⁻⁴ - 7.5x10 ⁻⁴ - 5x10 ⁻⁴ mm/sec	10 cm - 20 cm	At high normal stress (+) At low normal Stress (-)	(+)

(+): Positive effect

(-): Negative effect

(0): Insignificant effect

NA: Not Applicable

CHAPTER 8

CONCLUSION AND RECOMMENDATIONS

In this thesis, direct shear tests are conducted on rock discontinuity sample replicas, in order to investigate effect of roughness, shear rate, sample size and dependency of these parameters on each other.

1. In order to evaluate the accuracy of the proposed methodology of replicating discontinuity samples, Z_2 values of 3D models, PLA moulds and concrete test specimens are compared. For a planar surface (A20), success rate of the methodology is around 90%, while for a rougher surface (B20), success rate of the methodology is around 79%. Also, as the sample size gets smaller success rate increases even though the roughness is higher in small samples.
2. The direct shear tests are conducted under three different constant normal load levels and with three different shear rate (10×10^{-4} , 7.5×10^{-4} , 5×10^{-4} mm/sec). In order to assess roughness-shear rate effect, tests are performed on A20 and B20 discontinuities. Z_2 values of the discontinuities are 0.115 and 0.212 respectively. As expected, peak and residual values of shear strength increase with increasing surface roughness. One significant outcome of these experiments is the normal stress dependence of shear rate effect. Results showed that, under high normal stress (1.5 MPa), the shear strength decreases with the decreasing shear rate. However, under low normal stress (0.8 MPa), the shear strength increases with the decreasing shear rate. The result is justified by the differences in dilation angles between two normal stress levels.
3. The shear rate effect arises from the contact area between discontinuity surfaces. At lower shear rates, the contact between surfaces will be higher, resulting from

the creep of asperities. Similarly, at higher shear rates asperity interlocking decreases. Also, Wang and Scholz (1994) argued that an increase in shear rate causes an increase in dilation, which results in a change in contact area, thus effecting shear strength (Atapour and Mosavi, 2013). This concept explains the material's shear behavior that is observed at low normal stress levels. At 0.8 MPa normal stress, as the shear rate decreases, the contact area between the surfaces increases which results an increase in shear strength. However, at high normal stress levels, crushing of asperities becomes the dominant mode of displacement, rather than creep of asperities. As Atapour and Mosavi (2013) stated, crushing strength of asperities increases with increasing loading rate. Since, loading rate on asperities increases with increasing shear rate, crushing strength of asperities are also increases. Therefore, at 1.5 MPa normal stress, material shows a different behavior than former.

4. Co-dependency of the shear rate and the roughness characteristics is investigated by comparing the percent changes in the peak and the residual shear strength values. Experimental results showed that planar surfaces are affected more than rough surfaces by the changes in the shear rate. An explanation might be related to the magnitude of change in contact area as shear rate changes for different roughness levels. According to this explanation, as shear rate change, contact area of planar surfaces change more significantly. Therefore, changes in shear strength becomes more significant for planar discontinuities.

Results of this study revealed that shear rate effect may change its direction and magnitude depending on the level of normal stress. However, in the ISRM's suggested method for direct shear test of the rock discontinuities, a small range of shear rates (0.1 – 0.2 mm/min) is suggested for all normal stress conditions. Therefore, the shear rates proposed by the ISRM may require reinvestigation and revision with respect to applied normal stress levels.

5. In the second part of the direct shear test, experiments are conducted on small size samples (B10-1, B10-2, B10-3, B10-4) to investigate sample size effect and co-dependency between the sample size and the shear rate. Z_2 values of the B10 samples are between 0.36 and 0.42. Results showed that shear strengths decrease

with decreasing sample size, even though the roughness increases in the small samples.

6. In order to propose an explanation to the size effect, size dependency of basic friction angle is studied. The basic friction angle is one of the two components of peak friction angle along with the dilation angle. Therefore, it has a direct effect on the shear strength. Basic friction angles are roughly measured with a simple hand-made tool, since the tilting device is not available. Because of the simplicity of the method, exact values of basic friction angles could not be determined. However, it's observed that the basic friction angle of the 20 cm x 20 cm specimen is higher than the basic friction angle of 10 cm x 10 cm specimen, and the difference between them is estimated to be around 8-12°. Therefore, the size effect on the basic friction angle can be considered to be the cause of higher shear strength values for the large size samples. In addition, since the experiments are conducted in a large shear box (30 cm x 30 cm), error margin is expected to be higher for the smaller sample sizes. Therefore, experimental results for 10 cm x 10 cm samples might have significant errors, which would cause in lower shear strength values for the small size samples.
7. General trend of the sample size effect encountered in this study, might be explained by the differences in geometrical configuration between the 20 cm x 20 cm and the 10 cm x 10 cm samples. Geometrical characteristics of the smaller samples could be different from that of the larger samples. Damaged areas of the asperities could show differences, leading to decrease of the shear strength for the small size samples. In addition, surface match between upper and lower blocks for the large samples may not be as accurate as the match for the small samples, which may cause some degree of scatter for results (Ueng et al., 2010).
8. The jointwall compressive strength (JCS) is known to be accountable for scale effect (Bandis et al., 1981). The samples used in this study, show a weak correlation between size and JCS (B20: 22.4, B10-1:21.5, B10-2: 22.1, B10-3:20.0, B10-4:18.4). As the sample size decreases, JCS exhibits a small decrease. The change in the JCS value may propose a partial explanation for the decrease of the shear strength with the sample size.

9. Co-dependency of the shear rate and the sample size is investigated by comparing the percent changes in the peak and the residual shear strength values of the small and the large size samples. It's observed that the effect of the shear rate is greater for the small size samples. An explanation may come from the contact area between upper and lower surfaces. Since the experiments are conducted in a large shear box, effect of normal stress can be more perceivable along the discontinuity surface of a smaller sample. Thus, asperities become more strongly interlocked, causing an increase in the effective contact area. Also, the smaller samples have a better chance of having 100% accurate surface match, thereby having more contact area. As previously explained in this study, shear rate and contact area are correlated. Having more effective contact area causes the effects of shear rate to become more significant.

Following recommendations can be made for future studies;

1. Results of this study revealed that shear rate effect may change its direction and magnitude depending on the level of normal stress. However, in the ISRM's suggested method for direct shear test of the rock discontinuities, a small range of shear rates (0.1 – 0.2 mm/min) is suggested for all normal stress conditions. Therefore, the shear rates proposed by the ISRM might be revised with respect to applied normal stress levels with further investigation of normal stress dependence of the shear rate.
2. Direct shear tests can be repeated on the same specimen with different normal load levels. Conducting the experiments on the previously tested and deformed surface under a lower normal load and comparing the result with that of the fresh surface can be useful for evaluating the necessity of sample replication in the direct shear tests.
3. In discontinuity sample replication, particle size distribution of the sand used in the cement mixture can be significant for the material property of the concrete and the roughness of the sample surface. Therefore, investigation of the effect of the particle size distribution of the sand, could be useful to obtain concrete materials that show material properties similar to different rocks. In addition, the

investigation could reveal a new way to increase the success of the sample replication methodology by better representation of the roughness degree.

To conclude, in this thesis, a rock discontinuity sample replication methodology is developed and the effect of roughness characteristics, the shear rate and the sample size on the shear strength are investigated by laboratory works. The proposed methodology of specimen replication is proved to be successful enough to be applied in different studies. Also, the co-dependency of the shearing rate effect with the roughness effect and the sample size effect is investigated. The significance of these results can be extended in a future study to develop a methodology for laboratory to field scale simulation of time to slope failure analysis.

REFERENCES

- Agisoft LLC. (2016). Agisoft photoscan user manual: professional edition, version 1.2. Retrieved from http://www.agisoft.com/pdf/photoscan-pro_1_2_en.pdf.
- Ahn, D. & Kweon, J. H. & Kwon, S. & Song, J. & Lee, S. (2009). Representation of surface roughness in fused deposition modelling. *Journal of Materials Processing Technology*, 209 (15-16), 5593-5600.
- Atapour, H. & Moosavi, M. (2013). The influence of shearing velocity on shear behavior of artificial joints. *Rock Mechanics and Rock Engineering*, 47(5), 1745-1761.
- Bandis, S. (1979). Experimental studies on shear strength-size relationships and deformation characteristics of rock discontinuities. University of Leeds, Ph.D. thesis.
- Bandis, S. & Lumsden, A. C. & Barton, N. (1981). Experimental studies of scale effects on the shear behaviour of rock joints. *International Journal of Rock Mechanics & Mining Sciences & Geomechanics Abstracts*, 18, 1-21.
- Barton, N. R. (1971). A relationship between joint roughness and joint shear strength.
- Barton, N. (1973). Review of new shear strength criterion for rock joints. *Engineering Geology*, 7, 287-332.
- Barton, N. & Bandis, S. (1980). Some effects of scale on the shear strength of joints. *International Journal of Rock Mechanics & Mining Sciences & Geomechanics Abstracts*, 17, 69-73.
- Barton, N. & Bandis, S. (1982). Effects of block size on the shear behavior of jointed rock. *American Rock Mechanics Association*.

- Barton, N. & Choubey, V. (1977). The shear strength of rock joints in theory and practice. *Rock Mechanics*, 10, 1-54.
- Belem, T. & Homand-Etienne, F. & Souley, M. (2000). Quantitative parameters for rock joint surface roughness. *Rock Mechanics and Rock Engineering*, 33(4), 217-242.
- Bowden, R. K. & Curran, J. H. (1984). Time-dependent behaviour of joints in shale. *Rock Mechanics*, 32(1).
- Crawford, A. M. & Curran, J. H. (1981). The influence of shear velocity on the frictional resistance of rock discontinuities. *International Journal of Rock Mechanics & Mining Sciences & Geomechanics Abstracts*, 18, 505-515.
- Crawford, A. M. & Curran, J. H. (1986). A displacement discontinuity approach to modelling the creep behaviour of rock and its discontinuities. *International Journal for Numerical and Analytical Methods in Geomechanics*, 7(2), 245-268.
- Densmore, A. L. & Ellis, M. A. & Anderson, R. S. (1998). Landsliding and the evolution of normal-fault-bounded mountains. *Journal of Geophysical Research*, 103(15), 203-219.
- Dieterich, J. H. (1972). Time-dependent friction in rocks. *Journal of Geophysical Research*, 77(20), 3690-3697.
- El-Soudani, S. M. (1978). Profilometric analysis of fractures. *Metallography*, 11(3), 247-336.
- Environmental Systems Research Institute (ESRI). (2015). ArcGIS 10.4 Desktop Help.
- Fardin, N. & Stephansson, O. & Jing, L. (2001). The scale dependence of rock joint surface roughness. *International Journal of Rock Mechanics & Mining Sciences*, 38, 659-669.

- Fardin, N. & Feng, Q. & Stephansson, O. (2004). Application of a new in situ 3D laser scanner to study the scale effect on the rock joint surface roughness. *International journal of rock mechanics & Mining Sciences*(41), 329-335.
- Fereshtenejad, S. & Song, J. (2016). Fundamental study on applicability of powder-based 3d printer for physical modelling in rock mechanics. *Rock Mechanics and Rock Engineering*, 49(6), 2065-2074.
- Firpo, G. & Salvini, R. & Francioni, M. & Ranjith, P. G. (2011). Use of digital photogrammetry in rocky slope stability analysis by distinct elements numerical methods. *International Journal of Rock Mechanics & Mining Sciences*, 48, 1045-1054.
- Ge, Y. & Kulatilake, P. H. S. W. & Tang, H. & Xiong, C. (2014). Investigation of natural rock joint roughness. *Computers and Geotechnics*, 55, 290-305.
- Gercek, H. (2007). Poisson's ratio values for rocks. *International Journal of Rock Mechanics and Mining Sciences*, 44 (1), 1-13.
- Grasselli, G. & Wirth, J. & Egger, P. (2002). Quantitative three-dimensional description of a rough surface and parameter evolution with shearing. *International Journal of Rock Mechanics & Mining Sciences*, 39, 789-800.
- Haneberg, W. C. (2007). Directional roughness profiles from three dimensional photogrammetric or laser scanner point clouds. In Eberhardt E., Stead D., Morrison T. (Eds.), *Rock Mechanics: Meeting Society's Challenges and Demands: Proceedings, 1st Canada-US Rock Mechanics Symposium*, Vancouver, 27-31 May 2007, pp 101-106.
- Haneberg, W. C. (2008). Using close range terrestrial digital photogrammetry for 3-d rock slope modelling and discontinuity mapping in the United States. *Bulletin of Engineering Geology and the Environment*, 67(4), 457-469.
- Hencher, S. R. & Toy, J. P. & Lumsden, A. C. (1993). Scale dependent shear strength of rock joints. *Scale Effects in Rock Masses*.

- Hoek, E. (2007). *Practical rock engineering*. Retrieved from <https://www.rocsience.com/documents/hoek/corner/Practical-Rock-Engineering-Full-Text.pdf>.
- Hong, E. S. & Lee, J. S. & Lee, I. M. (2008). Underestimation of roughness in rough rock joints. *International Journal for Numerical and Analytical Methods In Geomechanics*, 32, 1385-1403.
- International Society for Rock Mechanics Commission on Standardization of Laboratory and Field Tests. (1978). Suggested methods for the quantitative description of discontinuities in rock masses. *International Journal of Rock Mechanics and Mining Sciences & Geomechanics Abstracts*, 15, 319-368.
- Jafari, M. K. & Pellet, F. & Boulon, M. & Hosseini K. A. (2004). Experimental study of mechanical behaviour of rock joints under cyclic loading. *Rock Mechanics and Rock Engineering*, 37(1), 3-23.
- Jang, H. S. & Kang, S. S. & Jang, B. A. (2014). Determination of joint roughness coefficients using roughness parameters. *Rock Mechanics and Rock Engineering*, 47(6), 2061-2073.
- Jiang, Y. & Li, B. & Tanabashi, Y. (2006). Estimating the relation between surface roughness and mechanical properties of rock joints. *International Journal of Rock Mechanics & Mining Sciences*, 43, 837-846.
- Jiang, C. & Zhao, G. (2014). A preliminary study of 3d printing on rock mechanics. *Rock Mechanics and Rock Engineering*, 48(3), 1041-1050.
- Jiang, Q. & Feng, X. & Gong, Y. & Song, L. & Ran, S. & Cui, J. (2016). Reverse modelling of natural rock joints using 3d scanning and 3d printing. *Computers and Geotechnics*, 73, 210-220.
- Johansson, F. (2016). Influence of scale and matedness on the peak shear strength of fresh, unweathered rock joints. *International Journal of Rock Mechanics and Mining Sciences*, 82, 36-47.
- Kanji, M. A. (2014). Critical issues in soft rocks. *Journal of Rock Mechanics and Geotechnical Engineering*, 6, 186-195.

- Kimura, T. & Ikusada, K. & Esaki, T. (1993). Surface roughness and shear behavior of rock joints. In R. Sousa & Grossmann (Eds.), *International Society of Rock Mechanics Symposium–Eurock’93* (583-590). Balkema: Rotterdam.
- Klempmek, M. & Khamrat, S. & Thongrapha, T. & Fuenkajorn, K. (2016). Displacement velocity effects on rock fracture shear strengths. *Journal of Structural Geology*, 90, 48-60.
- Kliche, C. A. (1991). *The effect of rock discontinuity surface roughness on shear strength* (Doctoral dissertation). University of Arizona, Tucson, USA.
- Kulatilake, P. H. S. W. & Balasingam, P. & Park, J. & Morgan, R. (2006). Natural rock joint roughness quantification through fractal techniques. *Geotechnical and Geological Engineering*, 24, 1181-1202.
- Lajtai, E.Z. & Gadi, A. M. (1989). Friction on a granite to granite interface. *Rock Mechanics and Rock Engineering*, 22(1), 25-49.
- Li, B. & Jiang, Y. & Wang, G. (2012). Evaluation of shear velocity dependency of rock fractures by using repeated shear tests. In Qian & Zhou (eds.), *Harmonising Rock Engineering and the Environment*. Paper presented at ISRM, Beijing, China (pp. 699-702). London: Taylor & Francis Group.
- Li, Y. & Huang, R. (2015). Relationship between joint roughness coefficient and fractal dimension of rock fracture surfaces. *International Journal of Rock Mechanics & Mining Sciences*, 75, 15-22.
- Li, Y. & Zhang, Y. (2015). Quantitative estimation of joint roughness coefficient using statistical parameters. *International Journal of Rock Mechanics & Mining Sciences*, 77, 27-35.
- Linder, W. (2003). *Digital Photogrammetry—Theory and Applications*. Heidelberg: Springer.
- Lockner, D. A. & Summers, R. & Byerlee, J. D. (1986). Effects of temperature and sliding rate on frictional strength of granite. *Pure and Applied Geophysics*, 124(3), 445-469.

- Malan, D. F. (1998). An investigation into the identification and modelling of time-dependent behaviour of deep level excavations in hard rock (PhD Thesis). University of Witwatersrand, Johannesburg, South Africa.
- Miller, R. P. (1965). Engineering classification and index properties for intact rock (PhD Thesis). University of Illinois, United States of America.
- Muralha, J. & Grasselli, G. & Tatone, B. & Blümel, M. & Chryssanthakis, P. & Yujing, J. (2014). ISRM suggested method for laboratory determination of the shear strength of rock joints: revised version. *Rock Mechanics & Rock Engineering*, 47, 291-302.
- Odling, N. E. (1994). Natural fracture profiles, fractal dimension and joint roughness coefficients. *Rock Mechanics and Rock Engineering*, 27(3), 135-153.
- Ohnishi, Y. & Nishiyama, S. & Yano, T. & Matsuyama, H. & Amano, K. (2006). A study of the application of digital photogrammetry to slope monitoring systems. *International Journal of Rock Mechanics & Mining Sciences*, 43, 756-766.
- Olsson, W. A. (1974). Effects of temperature, pressure and displacement rate on the frictional characteristics of a limestone. *International Journal of Rock Mechanics & Mining Sciences & Geomechanics Abstracts*, 11, 267-278.
- Patton, F.D. (1966). Multiple modes of shear failure in rock. *International Society for Rock Mechanics*.
- Perras, M. A. & Diederichs, M.A. (2014). A review of tensile strength of rock: Concepts and testing. *Geotechnical and Geological Engineering*, 32 (2), 526-546.
- Reeves, M. J. (1985). Rock surface roughness and frictional strength. *International Journal of Rock Mechanics & Mining Sciences*, 22(6), 429-442.
- Roosta, P. M. & Sadaghiani, M. H. & Pak, A. & Saleh, Y. (2006). Rock joint modeling using a visco-plastic multilaminate model at constant normal load condition. *Geotechnical & Geological Engineering*, 24, 1449-1468.

- Schneider, H. (1977). The time dependence of friction in rocks. *Bulletin of International Association of Engineering Geology*, 16, 235-239.
- Sfondrini, G., & Sterlacchini, S. (1996). Influence of joint roughness on discontinuity shear strength. In Barla (Ed.), *International Society of Rock Mechanics Symposium–Eurock'96* (135-142). Balkema: Rotterdam.
- Sharma, P. V. (1997). *Environmental and engineering geophysics*. Cambridge: Cambridge University Press.
- Stimpson, B. (1970). Modelling materials for engineering rock mechanics. *International Journal of Rock Mechanics & Geomechanics Abstracts*, 7(1), 77-121.
- Tatone, B. S. A. & Grasselli, G. (2009). A method to evaluate the three-dimensional roughness of fracture surfaces in brittle geomaterials. *Review of Scientific Instruments*, 80(2).
- Tatone, B. S. A. & Grasselli, G. (2010). A new 2d discontinuity roughness parameter and its correlation with jrc. *International Journal of Rock Mechanics & Mining Sciences*, 47, 1391-1400.
- Tatone, B. S. A. & Grasselli, G. (2012). Modeling direct shear tests with fem/dem: investigation of discontinuity shear strength scale effect as an emergent characteristic. *American Rock Mechanics Association*.
- Tatone, B. S. A. & Grasselli, G. (2013). An investigation of discontinuity roughness scale dependency using high-resolution surface measurements. *Rock Mechanics and Rock Engineering*, 46(4), 657-681.
- Tse, R., & Cruden, D. M. (1979). Estimating joint roughness coefficients. *International Journal of Rock Mechanics and Mining Sciences & Geomechanics Abstracts*, 16, 303-307.
- Ueng, T. Z. & Jou, Y. J. & Peng, I. H. (2010). Scale effect on shear strength of computer-aided-manufactured joints. *Journal of Geoengineering*, 5(2), 29-37.

- Ünal, M. & Yakar, M. & Yıldız, F. (2012). Discontinuity surface roughness measurement techniques and the evaluation of digital photogrammetric method. *International Society for Photogrammetry and Remote Sensing*. Melbourne.
- Wang, W. & Scholz, C. H. (1994). Micromechanics of the velocity and normal stress dependence of rock friction. *Pure Applied Geophysics*, 143, 303-315.
- Xu, H. F. & Zhao, P. S. & Li, C. & Tong, Q. (2012). Predicting joint roughness coefficients using fractal dimension of rock joint profiles. *Applied Mechanics and Materials*, Vols. 170-173, pp. 443-448.
- Yang, Z. & Taghichian, A. & Li, W. (2010). Effect of asperity order on the shear response of three-dimensional joints by focusing on damage area. *International Journal of Rock Mechanics & Mining Sciences*, 47, 1012-1026.
- Yang, Z. Y. & Lo, S. C. & Di, C. C. (2001). Reassessing the joint roughness coefficient (jrc) estimation using z_2 . *Rock Mechanics and Rock Engineering*, 34(3), 243-251.
- Yoshinaka, R. & Yoshida, J. & Shimizu, T. & Arai, H. & Arisaka, S. (1991). Scale effect in shear strength and deformability of rock joints. *International Society of Rock Mechanics*.
- Yu, X., & Vayssade, B. (1991). Joint profiles and their roughness parameters. *International Journal of Rock Mechanics and Mining Sciences & Geomechanics Abstracts*, 28(4), 333-336.
- Zhang, G. & Karakus, M. & Tang, H. & Ge, Y. & Zhang, L. (2014). A new method estimating the 2d joint roughness coefficient for discontinuity surfaces in rock masses. *International Journal of Rock Mechanics & Mining Sciences*, 72, 191-198.

APPENDICES

APPENDIX A

PHOTOGRAPHS OF THE SPECIMENS AFTER THE EXPERIMENTS



Figure A.1. A20-N0.8-V0.001



Figure A.2. A20-N0.8-V0.0005



Figure A.3. A20-N0.8-V0.00075



Figure A.4. A20-N1.2-V0.001



Figure A.5. A20-N1.2-V0.0005



Figure A.6. A20-N1.2-V0.00075



Figure A.7. A20-N1.5-V0.001



Figure A.8. A20-N1.5-V0.0005



Figure A.9. A20-N1.5-V0.00075



Figure A.10. B20-N0.8-V0.001



Figure A.11. B20-N0.8-V0.0005



Figure A.12. B20-N0.8-V0.00075



Figure A.13. B20-N1.2-V0.001



Figure A.14. B20-N1.2-V0.0005



Figure A.15. B20-N1.2-V0.00075



Figure A.16. B20-N1.5-V0.001



Figure A.17. B20-N1.5-V0.0005



Figure A.18. B20-N1.5-V0.00075



Figure A.19. B10/1-N0.8-V0.001



Figure A.20. B10/1-N0.8-V0.0005



Figure A.21. B10/1-N0.8-V0.00075



Figure A.22. B10/1-N1.2-V0.001



Figure A.23. B10/1-N1.2-V0.0005



Figure A.24. B10/1-N1.2-V0.00075



Figure A.25. B10/1-N1.5-V0.001



Figure A.26. B10/1-N1.5-V0.0005



Figure A.27. B10/1-N1.5-V0.00075

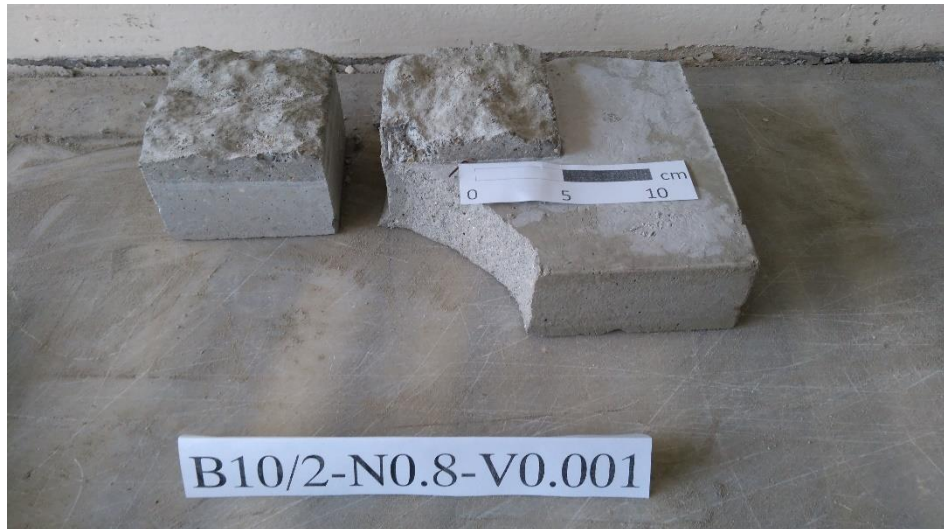


Figure A.28. B10/2-N0.8-V0.001



Figure A.29. B10/2-N0.8-V0.0005



Figure A.30. B10/2-N0.8-V0.00075



Figure A.31. B10/2-N1.2-V0.001



Figure A.32. B10/2-N1.2-V0.0005



Figure A.33. B10/2-N1.2-V0.00075



Figure A.34. B10/2-N1.5-V0.001



Figure A.35. B10/2-N1.5-V0.0005

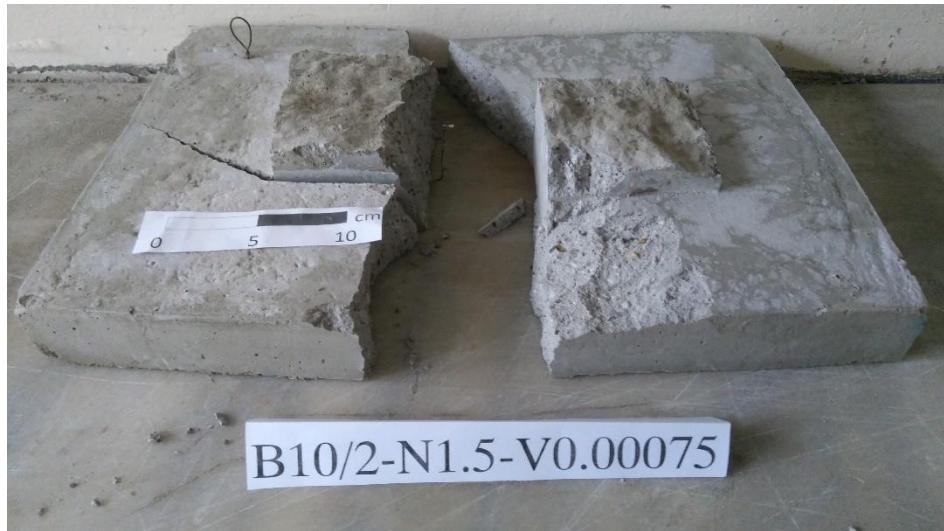


Figure A.36. B10/2-N1.5-V0.00075



Figure A.37. B10/3-N0.8-V0.001



Figure A.38. B10/3-N0.8-V0.0005

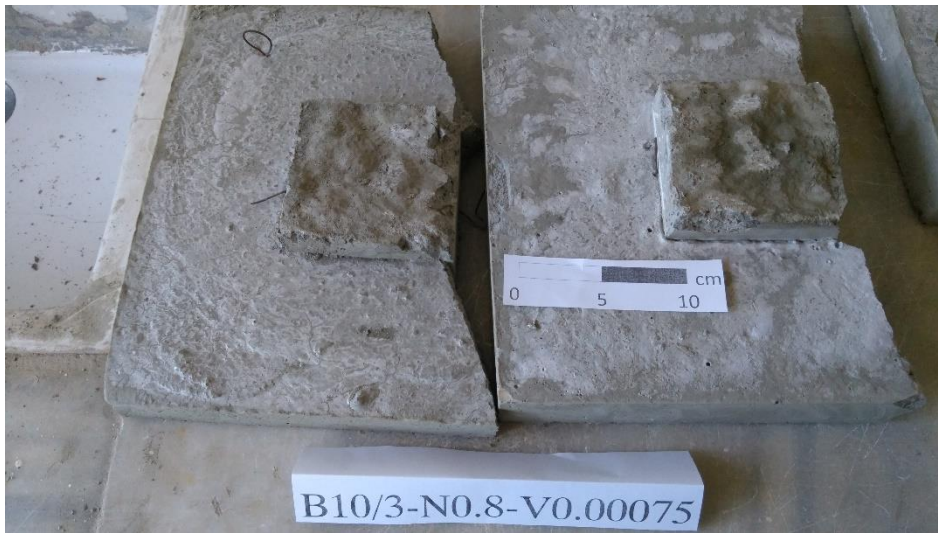


Figure A.39. B10/3-N0.8-V0.00075



Figure A.40. B10/3-N1.2-V0.001

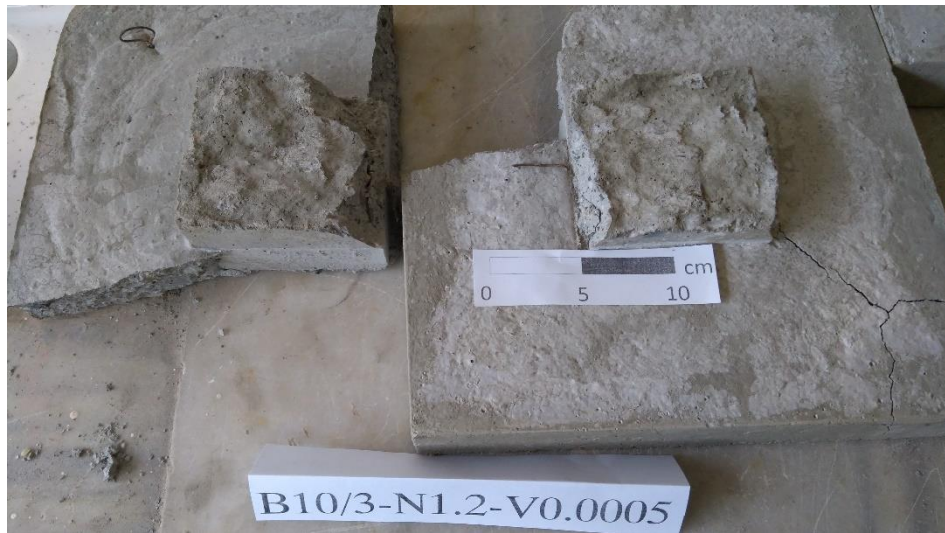


Figure A.41. B10/3-N1.2-V0.0005



Figure A.42. B10/3-N1.2-V0.00075



Figure A.43. B10/3-N1.5-V0.001

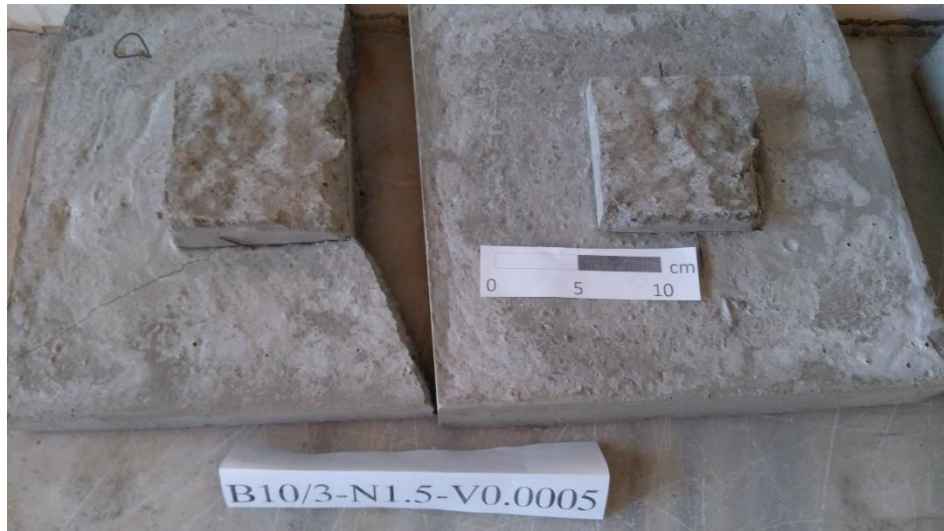


Figure A.44. B10/3-N1.5-V0.0005



Figure 6. B10/3-N1.5-V0.00075

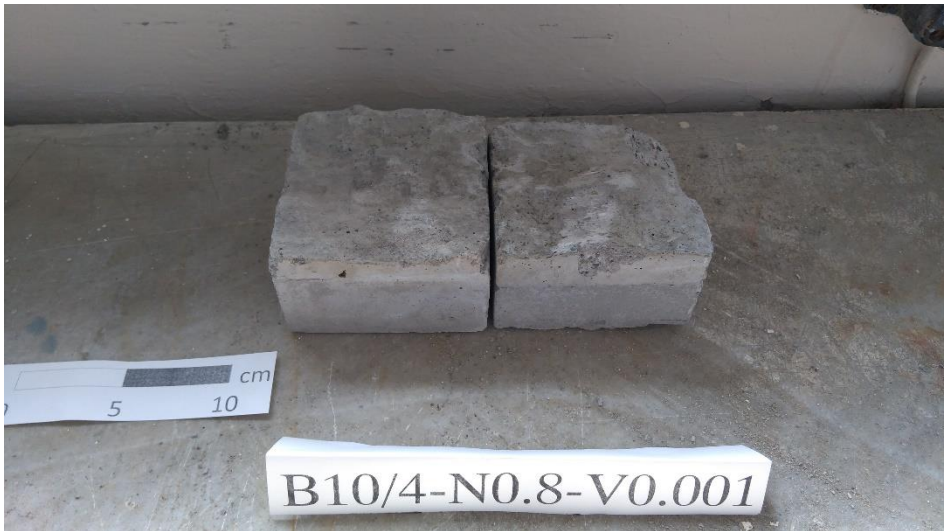


Figure A.46. B10/4-N0.8-V0.001



Figure A.47. B10/4-N0.8-V0.0005



Figure A.48. B10/4-N0.8-V0.00075



Figure A.49. B10/4-N1.2-V0.001

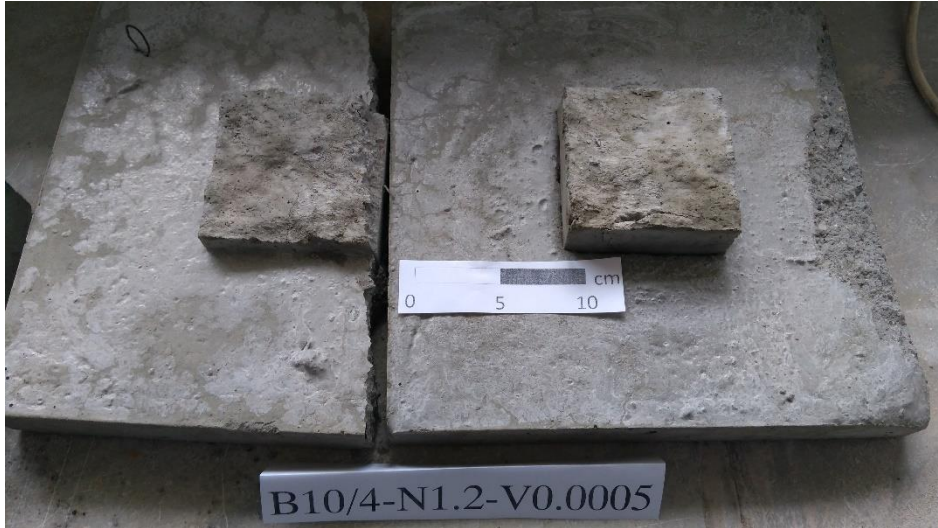


Figure A.50. B10/4-N1.2-V0.0005



Figure A.51. B10/4-N1.2-V0.00075



Figure A.52. B10/4-N1.5-V0.001



Figure A.53. B10/4-N1.5-V0.0005



Figure A.54. B10/4-N1.5-V0.00075

APPENDIX B

ORIGINAL PLOTS OF THE TEST RESULTS

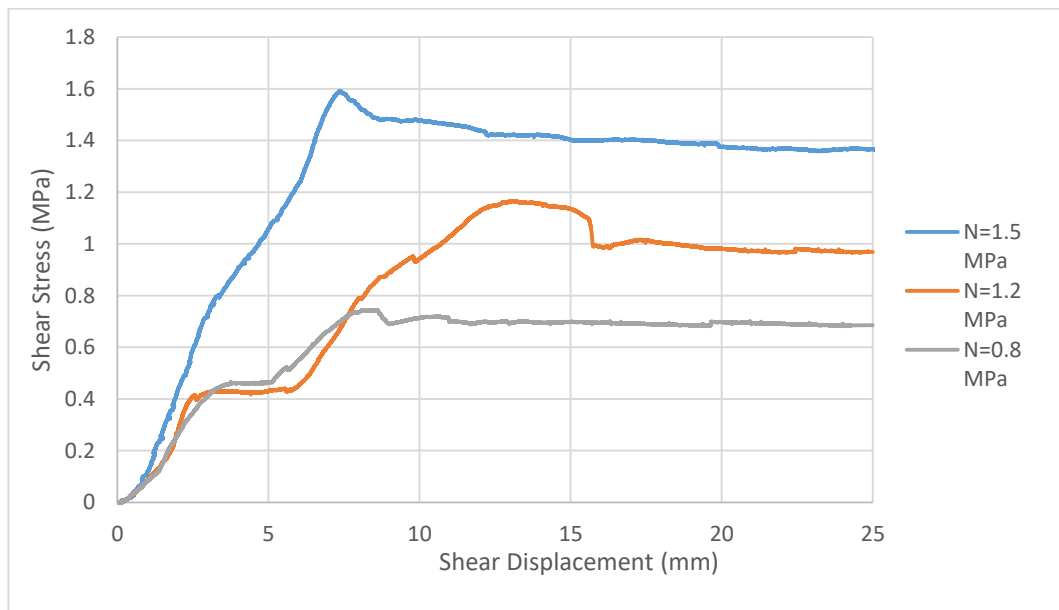


Figure B.1 Original test result (A20-V=0.001 mm/sec)

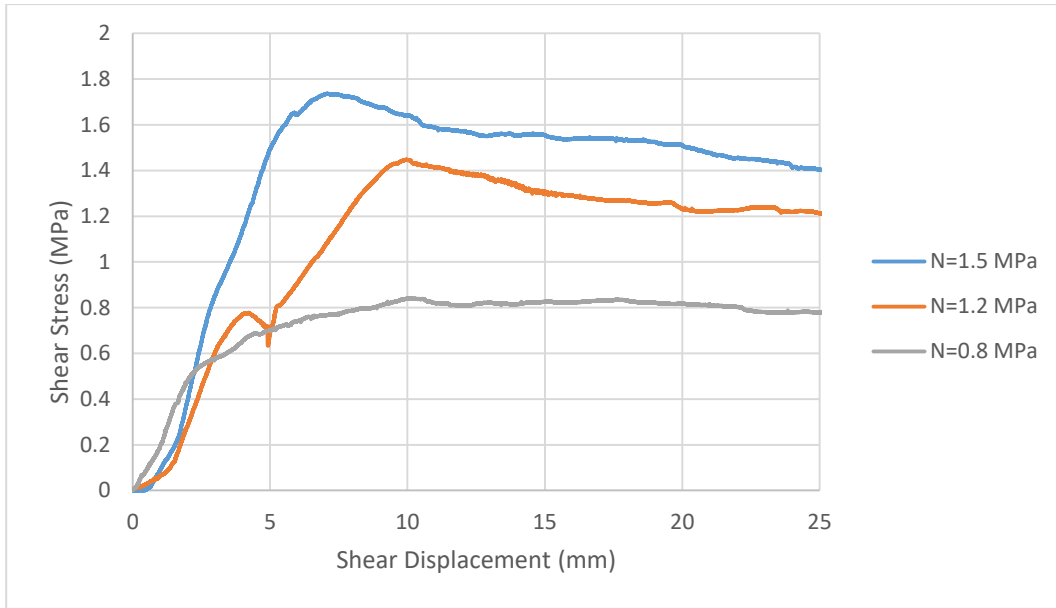


Figure B.2. Original test result (B20-V=0.001 mm/sec)

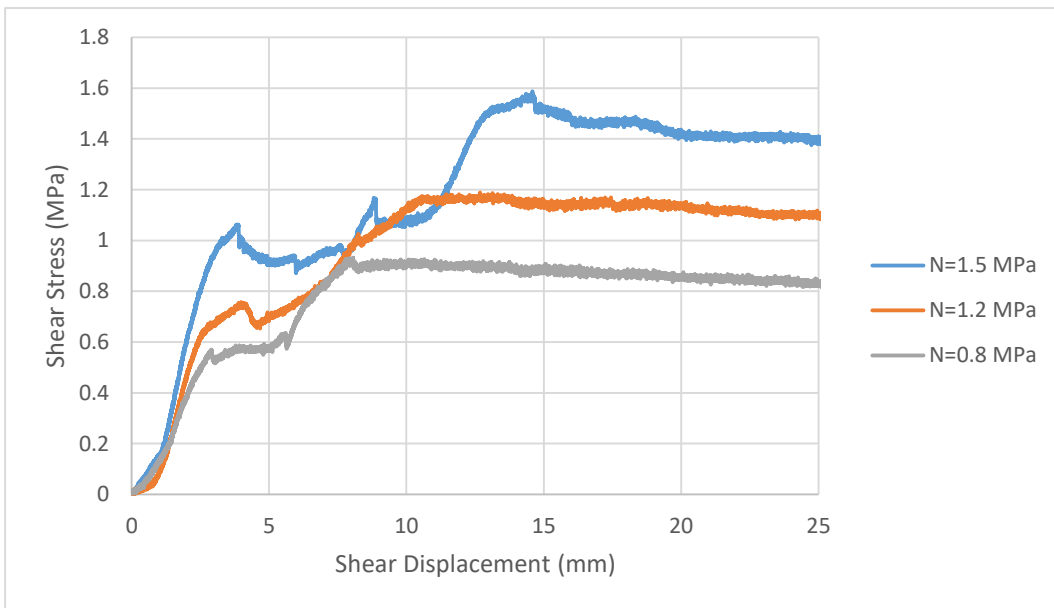


Figure B.3. Original test result (A20-V=0.00075 mm/sec)

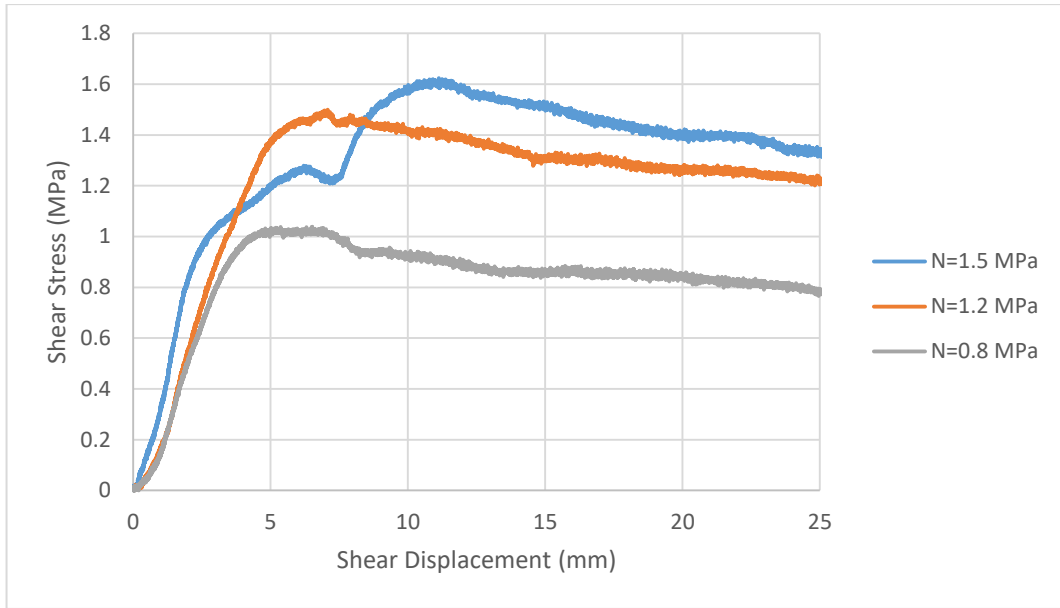


Figure B.4. Original test result (B20-V=0.00075 mm/sec)

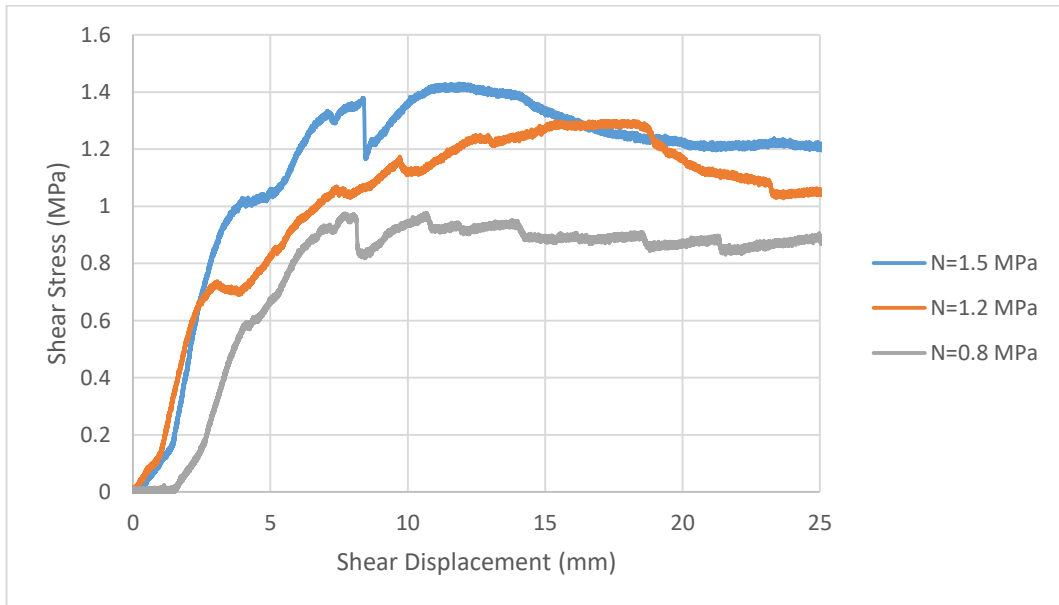


Figure B.5. Original test result (A20-V=0.0005 mm/sec)

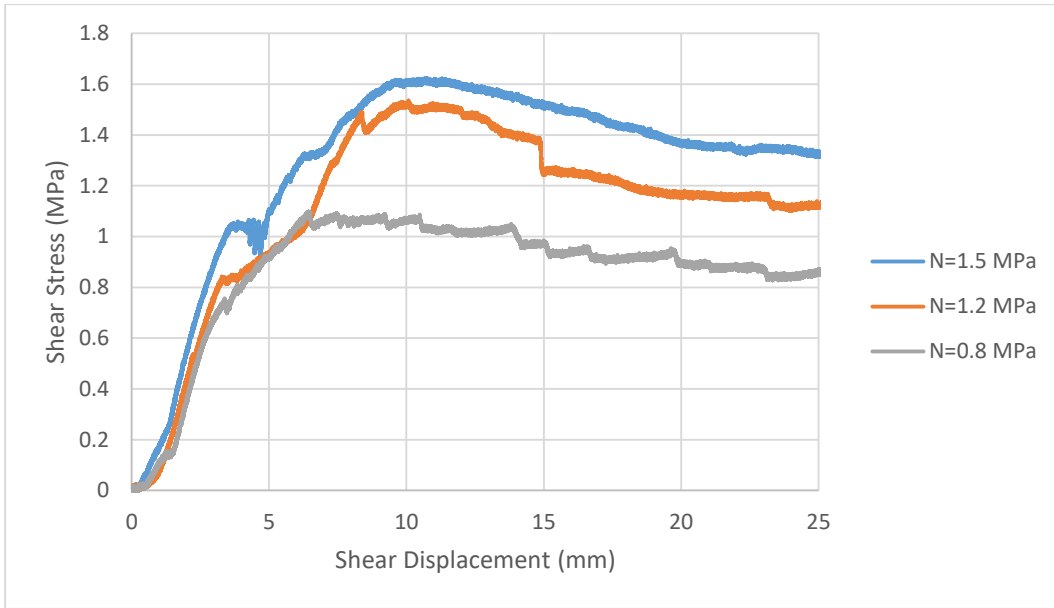


Figure B.6. Original test result (B20-V=0.0005 mm/sec)

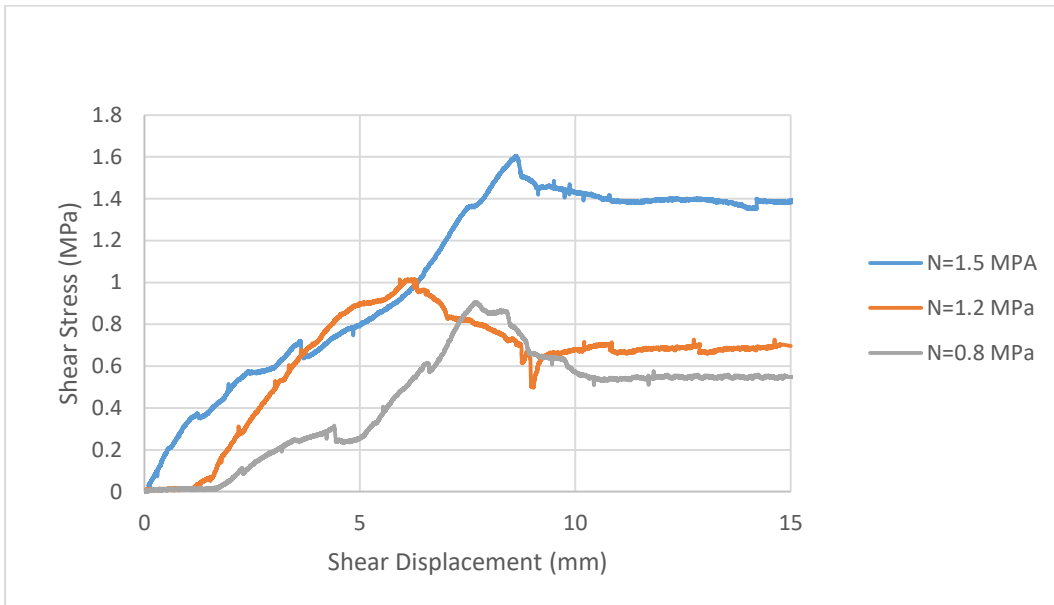


Figure B.7. Original test result (B10/1-V=0.001 mm/sec)

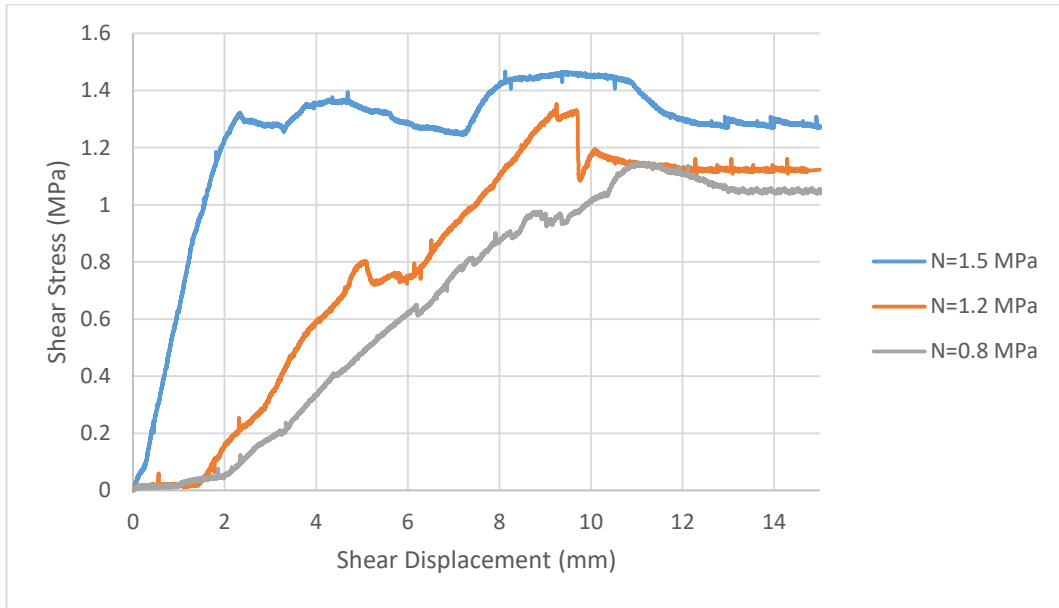


Figure B.8. Original test result (B10/2-V=0.001 mm/sec)

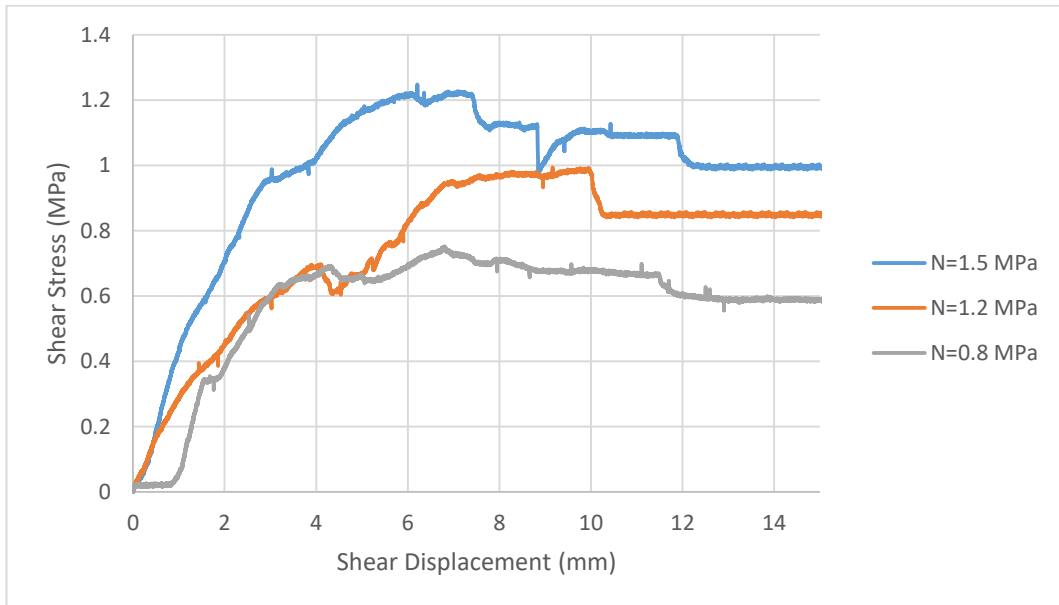


Figure B.9. Original test result (B10/3-V=0.001 mm/sec)

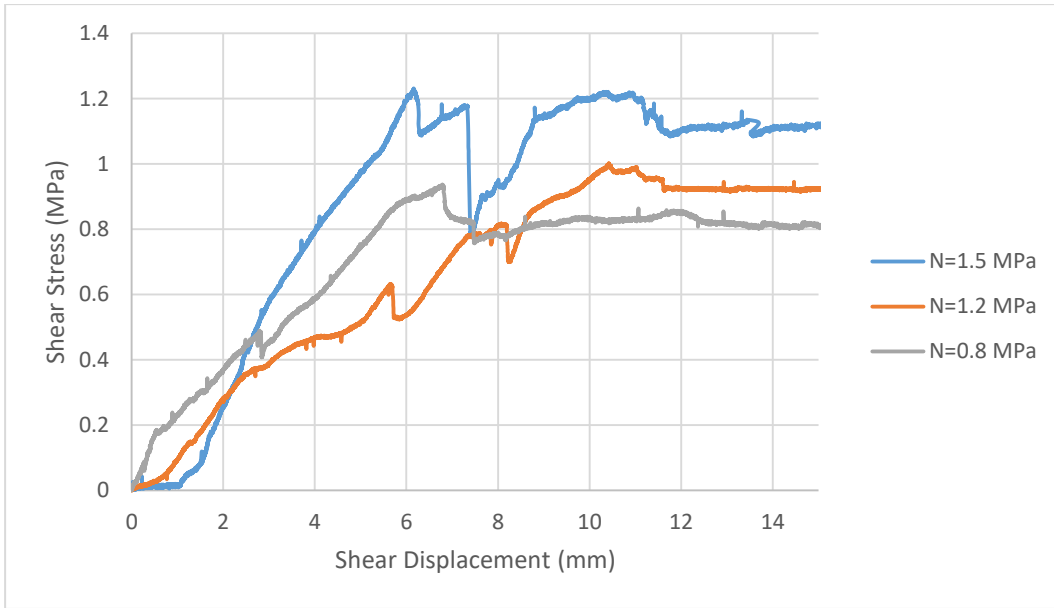


Figure B.10. Original test result (B10/4-V=0.001 mm/sec)

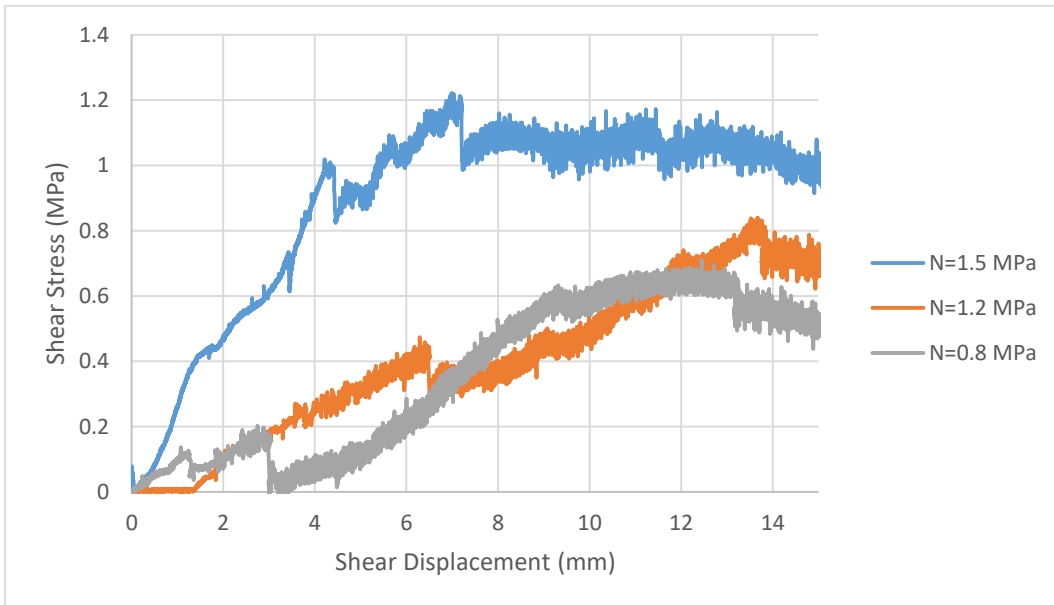


Figure B.11. Original test result (B10/1-V=0.00075 mm/sec)

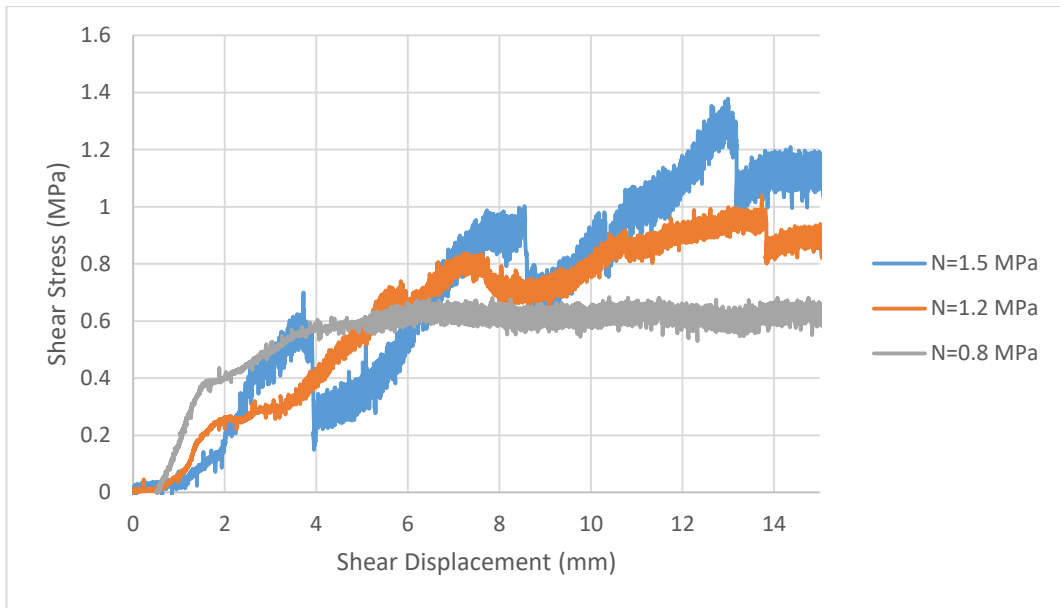


Figure B.12. Original test result (B10/2-V=0.00075 mm/sec)

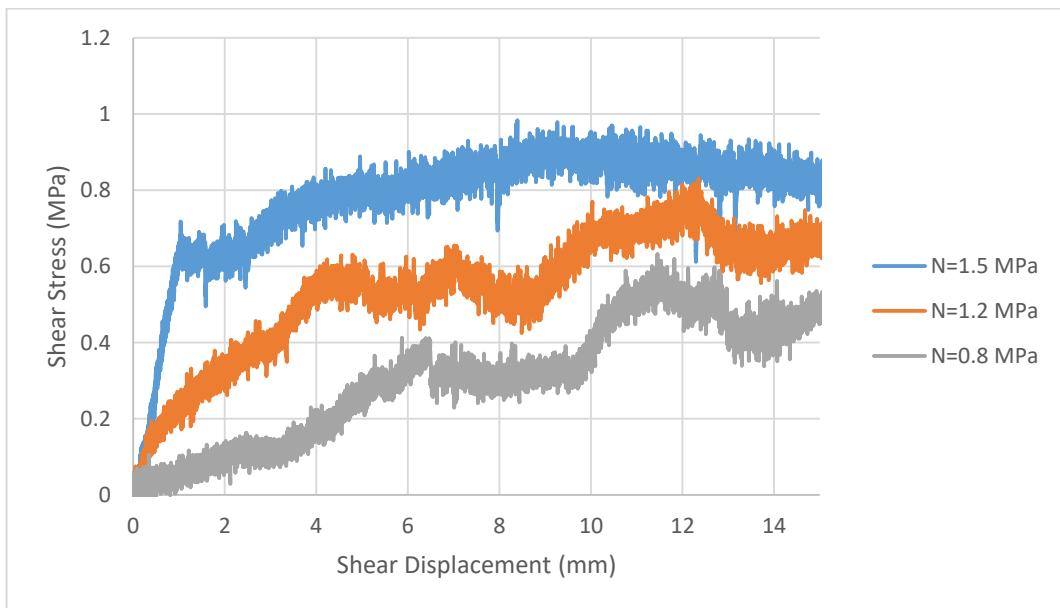


Figure B.13. Original test result (B10/3-V=0.00075 mm/sec)

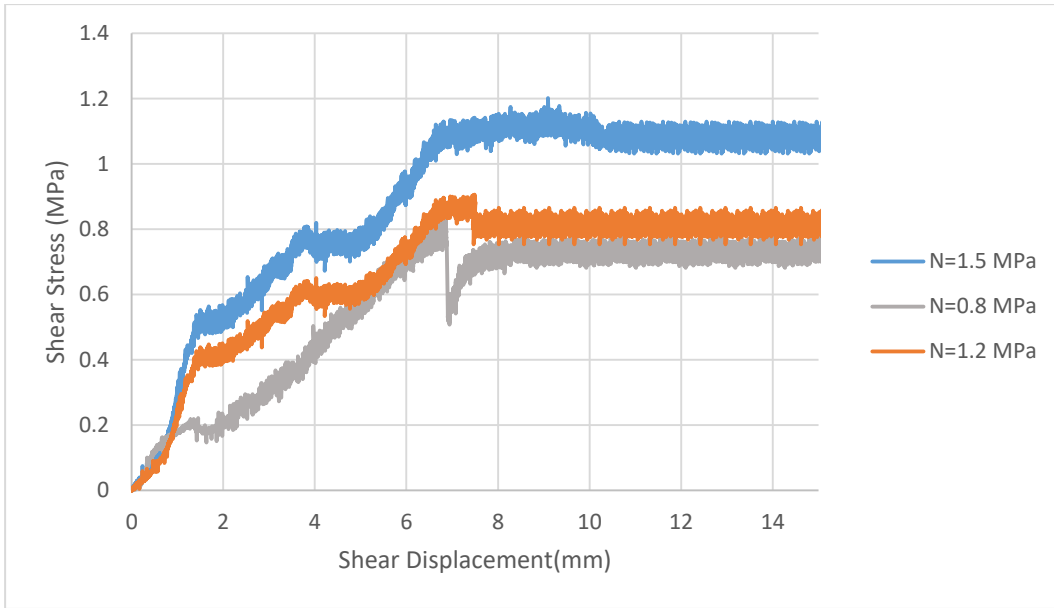


Figure B.14. Original test result (B10/4-V=0.00075 mm/sec)

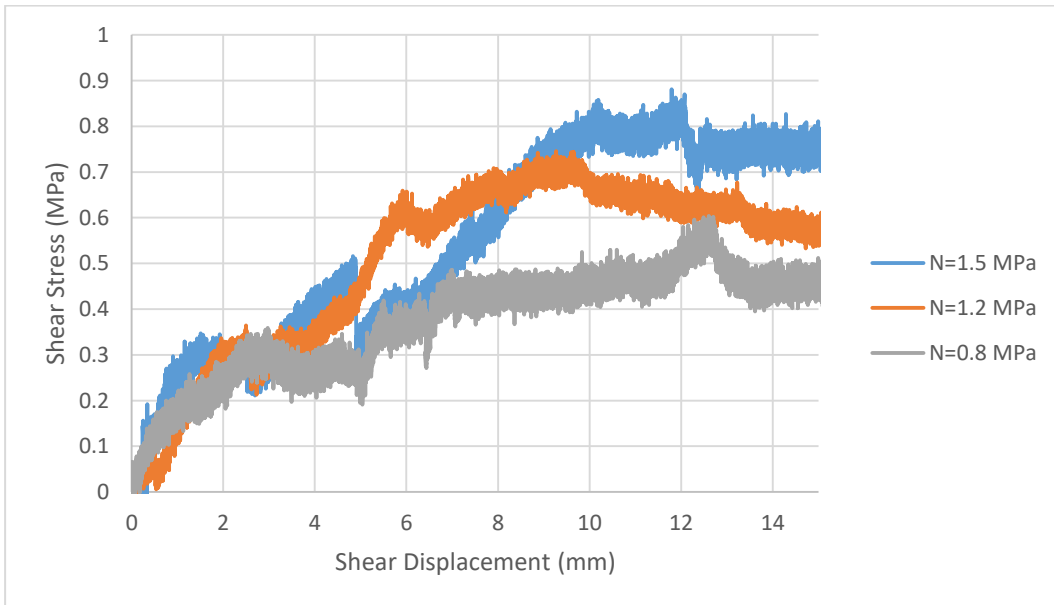


Figure B.15. Original test result (B10/1-V=0.0005 mm/sec)

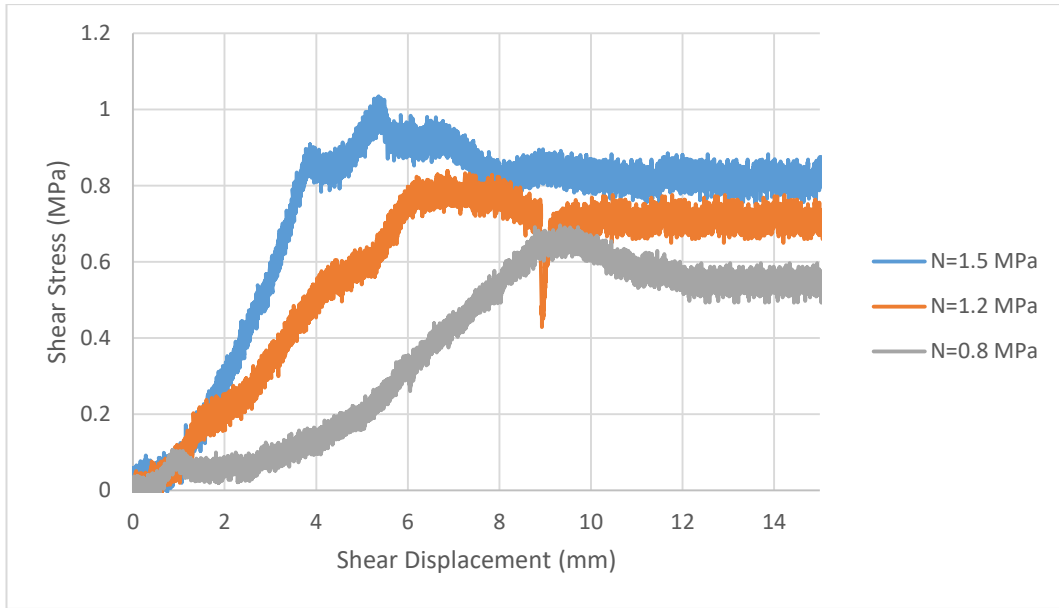


Figure B.16. Original test result (B10/2-V=0.0005 mm/sec)

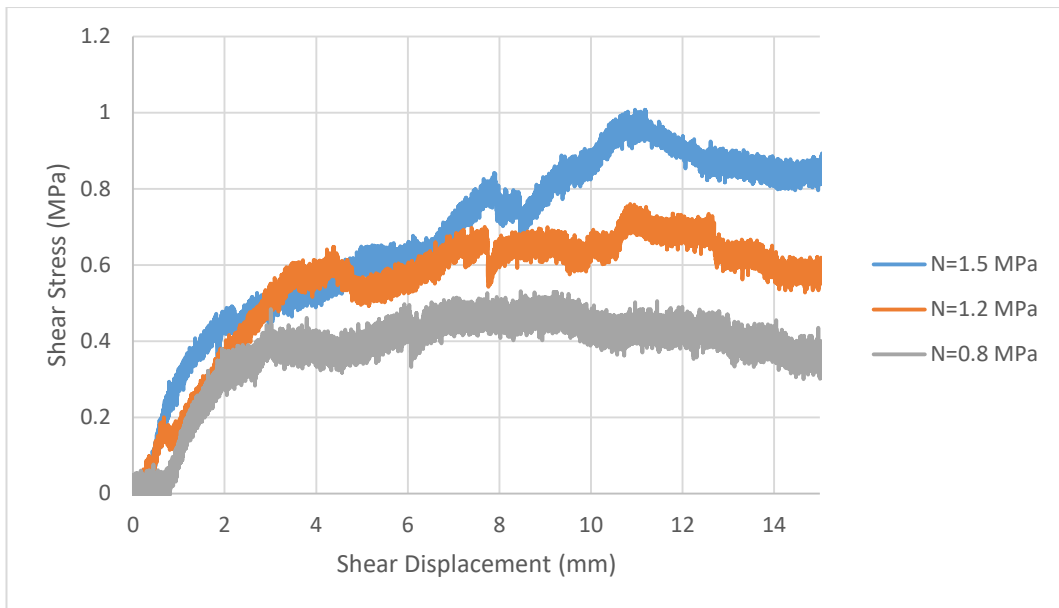


Figure B.17. Original test result (B10/3-V=0.0005 mm/sec)

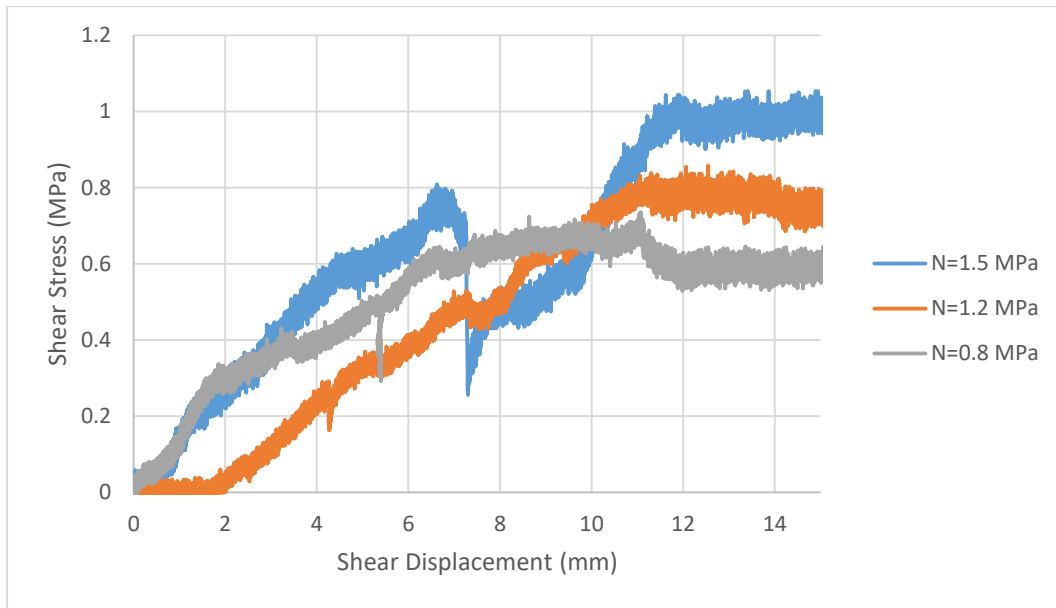


Figure B.18. Original test result (B10/4-V=0.0005 mm/sec)